Characterization of [Ni(cyclam)]@CB[8] as an Outer-Sphere Redox Agent

A Thesis

Submitted to the Graduate Faculty

in Partial Fulfillment of the Requirements

for the Degree of

Master of Science

in the Department of Chemistry

Faculty of Science

University of Prince Edward Island

Saskia L.A. Hart

Charlottetown, P. E. I.

July, 2008

Your file Votre référence
ISBN: 978-0-494-49854-5
Our file Notre référence
ISBN: 978-0-494-49854-5

SIGNATURE PAGES

iii-iv

REMOVED

TABLE OF CONTENTS

In Loving Memory

Dr. Robert Haines

For my supervisor and friend,
Dr. Robert Haines –
A man whose smile and
warm personality has enriched the
lives of many.

You've taught me to
live life to the fullest
And so, ***so*** much more.

Anita Elsinga

For my mother,
Anita Elsinga –
A woman whose gentle,
loving, and giving spirit
continues to inspire me.

My greatest and my
truest fan, the best
mother a girl could ask for.

I will miss you always.

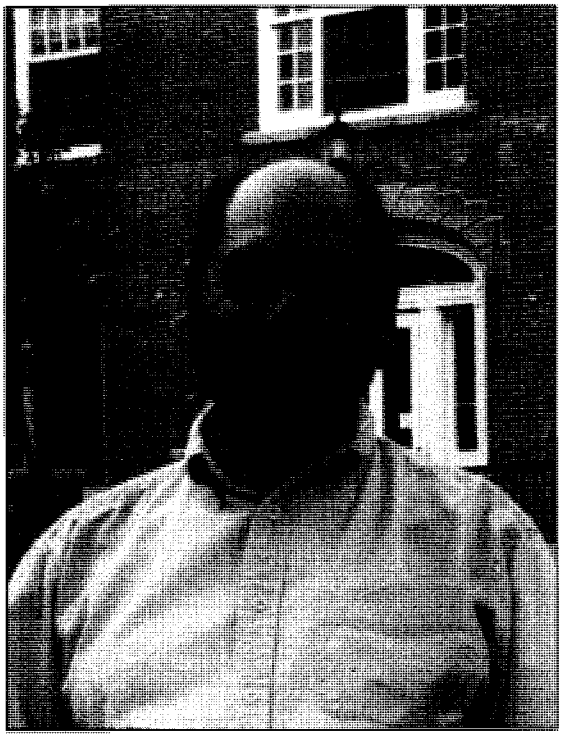

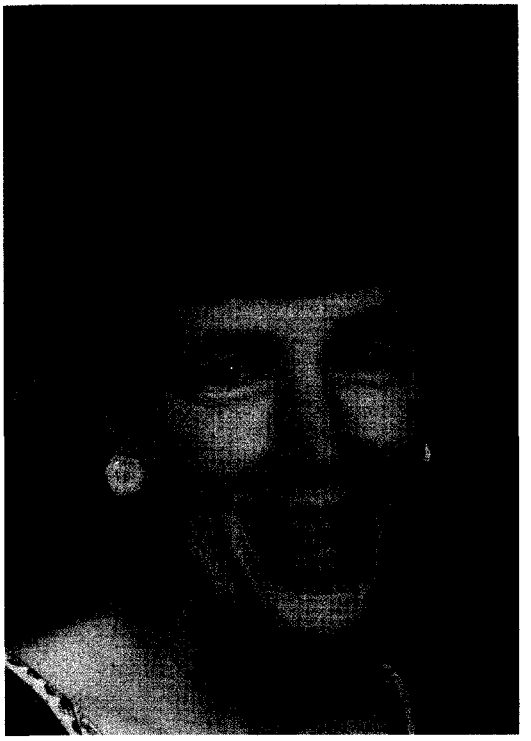

Acknowledgements

It is a great man, and only a great man, whose inspiring words and contagious curiousity can reach beyond a grave. It is to this great man, Dr. Robert Haines, that I owe this present work. The flash of excitement in his eyes gave me the confidence to start working on the project, the encouraging comments he sent my way gave me the endurance to continue when the outlook looked dim, and the desire to honour his memory gave me the willingness to continue on without him. This thesis is for him.

There are others to whom I am indebted for the completion of this work. I thank my husband, Nelson, for his patience, love, and continual support. Special thanks to Dr. Brian Wagner, who took me on as a student and guided me through the completion of this project. Your constant encouragement and support gave me the strength to push through. Thank you for always making time for me. I am also indebted to Mrs. Dawna Lund, whose tireless efforts to keep the stopped-flow machine in working order were essential for the completion of my project. I could not have finished without your time and dedication. Erika Weeks, you were always there on the days that I thought I couldn't finish to tell me that you thought I could. I would like to thank Dr. Andreas Decken, who not only provided me with the X-ray crystal structures, but went the extra mile, assisting me with their proper documentation.

I sincerely thank the members of my supervisory committee – Dr. Russell Kerr and Dr. Rabin Bissessur – who provided me with feedback and were always there for moral support when needed. I would like to acknowledge the entire UPEI Chemistry Department, who constantly encouraged me to reach high and to dream big.

Thank you.

Glossary of Abbreviations

CB[8] ----------	Cucurbit[8]uril
Cyclam ----------	1, 4, 8, 11 – Tetraazacyclotetradecane
Cyclen ----------	1,4,7,10-Tetrazacyclododecane
L^1 ----------	1,4,8,11-Tetrabenzyl-1,4,8,11-tetraazacyclotetradecane
L^2 ----------	1,4,8,11-Tetrakis(1-methylnaphthalend)-1,4,8,11-tetraazacyclotetradecane
L^3 ----------	1,4,8,11-Tetrakis(9-methylanthracene)-1,4,8,11-tetraazacyclotetradecane
Tacn ----------	1,4,7-Triazacyclononane
Tet-a ----------	Meso-5,5,7,12,12,14-Hexamethyl-1,4,8,11-tetraazacylotetradecane
Tet-b ----------	Rac-5,5,7,12,12,14-Hexamethyl-1,4,8,11-tetraazacylotetradecane

Abstract

Long-range electron transfer reactions play a key role in the life-giving processes of photosynthesis and respiration; however, much is still unknown about electron transfer occurring over extended distances. The focus of this project is to design and study synthetic systems in which electron transfer will be forced to take place over larger than normal distances due to steric bulk surrounding a redox active metal centre. Two approaches are followed – 1) complexing bulky pendant arm macrocycles with redox active metals and 2) encapsulating a redox active metal macrocycle within a bulky host molecule – cucurbit[8]uril.

The metal pendant arm macrocycles proved to be insoluble in aqueous solutions, excluding them from kinetic studies. The inclusion complex, [Ni(cyclam)]@CB[8], however, is water-soluble at the low concentrations needed for kinetic analysis. Furthermore, the inclusion complex is readily oxidized to the nickel(III) form by the oxidant hexaaquacobalt(III). Upon oxidation, the $[Ni^{III}(cyclam)]$@CB[8] complex can be used as an oxidant for the benzenediols, hydroquinone and catechol. The results of the above kinetic studies can be directly compared to previous studies involving free Ni^{II}(cyclam) as the reductant/oxidant. In this way, the steric effect of the bulky cucurbit[8]uril ring on the rate of electron transfer can be directly accounted for. The results indicate that encapsulation of the Ni(II) macrocycle within cucurbit[8]uril results in a factor of 2 decrease in the rates of electron transfer as compared to that of the free Ni(II) macrocycle. This indicates that steric bulk has a significant effect on the rate of electron transfer, as expected.

A novel "one-pot" synthesis of the inclusion complex [Ni(cyclam)]@CB[8], as well as the crystal structure of [Cu(cyclam)]@CB[8], showing cyclam in the rare trans-I configuration, will also be reported.

Chapter 1 – Introduction

Our world is high-tech. We talk of nanowires, sending ionic liquid mirrors into space, and fabricating new and improved robots. We can transplant hearts, build new knees, and fix the smallest skin blemishes with a laser. In light of these impressive discoveries, it is somewhat surprising that details surrounding some of the most fundamental life processes continue to elude us. High on the list of "unknowns" is the mechanism by which electrons are transported in the life-giving processes of respiration and photosynthesis. Biological electron transfer reactions occur over extremely large distances – oftentimes as great as 1 – 3 nm.[1] Do the electrons "hop" through empty space? Are they transported *via* a tunneling mechanism? How are electrons moved over such large distances at the incredibly high rates required for biological systems? The hypotheses are many and varied, and these questions remain largely unanswered.[1]

Perhaps the greatest hindrance to studies of electron transport in biological systems is the sheer complexity of these systems. The enzymes involved in electron transport are huge molecules with many active sites and are impossible to synthesize in the lab. The development of simplified systems that could act as models for the more complicated biological systems may provide some insights into the effect of steric bulk on long-range electron transfer processes. This project focuses on the design and study of such systems. Bulky pendant arm macrocycles and the host macromolecule cucurbit[8]uril will be employed to mimic the steric bulk of an enzyme. The kinetics of electron transfer reactions between a redox agent and a redox active metal centre "buried" within these sterically bulky systems will then be monitored to note the effect of steric bulk on the rate of electron transfer. These kinetic studies will also allow for the

elucidation of the reaction mechanisms and the derivation of full rate laws. Since kinetic theories are central to this present work, a brief overview of this field of study will be useful and is given below.

It should be noted that the synthetic systems studied in this work can be only loosely compared to biological systems. Biological systems are significantly more complex, and electron transfer reactions are expected to take place by more complicated mechanisms than can be simulated by the simple outer sphere electron transfer reactions studied in this work. For this reason, this study is performed principally to study the effect of steric bulk on electron transfer rates; mechanisms of biological electron transfer reactions are beyond the scope of this project.

1.1. Kinetics

Derived from the Greek word for motion, the word *kinetic* has been adopted into the English language as a reference to any type of motion. Kinetic energy is the energy possessed by an object in motion; kinesiology is the study of moving parts (with reference to the human body). Chemists refer to kinetics as describing an area of chemistry that is concerned with the study of rates and mechanisms of reactions. In a very broad sense, chemical kinetics is the study of how and how quickly molecules move from reactant states to product states.[2]

The origin of chemical kinetics can be traced to 1850, when a physicist by the name of L. F. Wilhelmy published "The Law of Acid Action on Cane-Sugar."[3] In this work, Wilhelmy proposed a relationship between reactant concentration (cane sugar) and the rate at which it hydrolyzes. This relationship was further studied by two Swedish

scientists, C. M. Guldberg and P. Waage,[4] who in 1879 introduced the fundamental law of mass action, in which reactions of the type:

$$aA + bB \leftrightarrow cC + dD$$

were shown to proceed until an equilibrium (K) was reached. The equilibrium could be described by the equation:

$$K = \frac{k^+}{k^-} = \frac{[C]^c[D]^d}{[A]^a[B]^b}$$

Where A, B, C, D = active masses

a, b, c, d = reactant stoichiometries

k^+ and k^- = affinity constants

This law holds true to the present day, with active masses now being referred to as reagent concentrations and k^+ and k^- as rate constants.

In 1884, the first book dealing with kinetic topics was published by J. Van't Hoff.[3] The publication of this work was quickly followed by the establishment of another fundamental kinetic law – the Arrhenius Law, which, building on a theory first proposed by J. Van't Hoff, relates the rate of a reaction to temperature *via* the equation:[2]

$k = Aexp(-E/RT)$

where E = activation energy of reacting molecules

exp(-E/RT) = fraction of active collisions

Significant contributions to kinetic theory were made by a man named Henry Eyring (1901 – 1981).[5] In 1931, in collaboration with Michael Polanyi, Eyring

successfully quantified the potential energy corresponding to the formation and breaking of the hydrogen bond in molecular hydrogen. Four years later, Eyring proposed the transition-state theory. (This theory was also concurrently proposed by two other scientists, Michael Polanyi and M. G. Evans.) According to this theory, a reactant must pass through a transition state of maximum potential energy (Gibb's free energy) known as the activated complex. The forward reaction is controlled by $\Delta G\dagger_1°$, and the reverse reaction by $\Delta G\dagger_{-1}°$. The transition state theory is summarized by the following equation:[5]

$$k = \frac{k_B T}{h} e^{\Delta\dagger S°/R} e^{-\Delta\dagger H°/RT}$$

Where k_B = the Boltzmann constant

h = Planck's constant

Importantly, the equation can be rewritten in the form below, which allows the determination of the activation enthalpy ($\Delta H\dagger$) and acitivation entropy ($\Delta S\dagger$) for the reaction under study.

$$\ln (k/T) = \ln(k_B/h) + \Delta S\dagger/R - \Delta H\dagger/RT$$

Since these early discoveries, the field of chemical kinetics has advanced considerably. Kinetic studies have progressed from measuring the rates of simple reactions (those that follow elementary steps or a series of elementary steps) to more complicated reactions (those that involve consecutive or parallel reactions). The

elucidation of reaction rates and mechanisms requires the monitoring of a change in the reactant or product concentrations over a given time interval. The change can be monitored *via* various detection methods, such as vibrational spectrophotometry, pulse radiolysis, UV-visible spectrophotometry, nuclear magnetic resonance (NMR), or even conductivity, to name but a few. The only necessity is that the detector response must vary proportionally with reactant or product concentrations.[6]

A common method used to observe changing reactant concentrations, and the method of choice for this work, is through absorbance changes monitored *via* UV-visible spectrophotometry. Beer's law, $A = c\varepsilon\ell$, where A = absorbance, c = concentration, ε = molar absorptivity, and ℓ = path length, allows the absorbance measurements to be directly correlated to the concentration of the reactant or product. Absorbance changes are easily monitored *via* UV-visible spectroscopy; however, traditional spectrophotometers are only able to measure the kinetics of slow reactions (on the order of seconds to hours) as the experimentalist must mix the solutions before the absorbance changes can be monitored, and fast reactions would be complete within the time of mixing.

For these fast reactions, several techniques have been developed, such as the relaxation method (for reactions complete within a timescale of microseconds to milliseconds), and the stopped-flow method (for reactions complete within a timescale of milliseconds to seconds).[6] Relaxation methods require the reaction to be completed and at equilibrium before any kinetic measurements are taken; the equilibrium is then disrupted by either a sudden change in pressure (P-jump) or a sudden change in temperature (T-

jump). It is the rate of "relaxation" of the system to its new equilibrium state that is monitored and subsequently related to the corresponding rate constants.[2]

Stopped-flow methods are suitable for reactions having slightly longer reaction times (half-lives of 10 ms to ~60 s)[6] than those monitored *via* relaxation techniques (half-lives as low as ~ 10 μs) and is the method employed throughout this work. In stopped-flow spectrophotometry, the reactants are introduced to a mixer *via* pressurized plungers. The flow of the reactants is abruptly stopped once they pass from the mixer to an optical cell, and absorbance changes at specific wavelengths are monitored by a computer.[6] The dead time (time from the initial mixing of the reactants to the first absorbance reading) for stopped-flow techniques is usually ~ 1-5 milliseconds.[6] Under the conditions normally employed in kinetic studies (pseudo-first-order), this dead time does not affect the kinetic results; in pseudo-first-order reactions initial absorbance measurements are not needed, only the *change* in concentration with time is important.[6]

The data gathered from extensive kinetic studies often provides valuable insights into important processes, such as the rate of drug decomposition[7] or the rate of metal ion remediation in heavy-metal waste water treatments.[8] In this present work, the kinetics governing electron transfer reactions will be of primary interest. Interest in reactions of this type is strong (several thousand publications in the last 50 years)[1] and has been largely driven by their fundamental role in biological life-giving processes, as mentioned previously.

1.1.1. Kinetics of Electron Transfer Reactions

Electron transfer reactions occur when an oxidizing agent comes into contact with a reducing agent. The electron is transferred *via* one of two possible mechanisms – an inner-sphere or an outer-sphere mechanism. The principle difference between these two mechanisms lies in the fact that an inner-sphere mechanism requires the electron to travel through a bridging ligand, while an outer-sphere reaction involves an electron transfer through space.[1]

Inner-Sphere Mechanism:

This mechanism requires one redox agent to have a bridging ligand and the other redox agent to have either an unsaturated coordination sphere or an exchangeable (labile) ligand. The mechanism involves the formation of a bridging intermediate, through which the electron travels *via* resonance or chemical transferal pathways.[9] Electron transfer *via* an inner-sphere mechanism is a multi-step process involving a) the association of the redox agents in a common solvent shell, b) the formation of an intermediate involving a bridging ligand, c) electron transfer, and d) transfer of the bridging ligand/subsequent dissociation of the redox agents[1] (See Scheme 1.1). Analysis of inner-sphere electron transfer reactions is complex because bond-breaking/forming is involved.

a) $LM_1^{III} + M_2^{II} \longrightarrow M_1^{III}L,M_2^{II}$

b) $M_1^{III}L,M_2^{II} \longrightarrow M_1^{III}—L—M_2^{II}$

c) $M_1^{III}—L—M_2^{II} \longrightarrow M_1^{II}—L—M_2^{III}$

d) $M_1^{II}—L—M_2^{III} \longrightarrow M_1^{II} + LM_2^{III}$

Scheme 1.1. Sample reaction mechanism for an inner-sphere reaction.

Outer-Sphere Mechanism:

This mechanism is more common and is the mechanism studied in the present work. To ensure an outer-sphere electron transfer process, the reducing and oxidizing agents must be chosen so that neither species contains a ligand that might act as a bridge. Also, neither reactant can be prone to undergoing substitution reactions. Two coordinatively saturated redox agents are prime components for studying outer-sphere electron transfer reactions.[9] The mechanism of the reaction can be broken into three distinct steps. In the first step, represented by the formation constant for an outer-sphere adduct (K_o), the two species diffuse together so that they share the same outer solvent shell. In the second step, the electron undergoes an intermolecular transfer from one agent to the other (k_{et}). The last step involves the diffusion of the two species away from each other.[9] (See Scheme 1.2)

$$Ni^{II}(tacn)_2 + [Fe(CN)_6]^{2-} \overset{K_o}{\rightleftharpoons} \{Ni^{II}(tacn)_2 \ , \ [Fe(CN)_6]^{2-}\}$$

$$\{Ni^{II}(tacn)_2 \ , \ [Fe(CN)_6]^{2-}\} \xrightarrow{k_{et}} \{Ni^{III}(tacn)_2 \ , \ [Fe(CN)_6]^{3-}\}$$

$$\{Ni^{III}(tacn)_2 \ , \ [Fe(CN)_6]^{3-}\} \xrightarrow{k_{diff}} Ni^{III}(tacn)_2 + [Fe(CN)_6]^{3-}$$

Scheme 1.2. Sample reaction mechanism for an outer-sphere electron transfer reaction.

1.1.2. Long Distance Electron Transfer Processes

Of particular interest to this work is the study of electron transfer processes occurring over extended distances. A literature search of long-distance electron transfer processes will inevitably take the reader deep into the realm of biochemistry, where redox agents are often located deep within the steric encumbrance of large biological molecules. Due to its relatively simple composition, cytochrome c, a protein in the electron transfer chain, has been the subject of many studies. In 1996, the Davidson group[10] examined the rate of electron transfer between a copper metalloprotein and the heme group of cytochrome c-55li; the Körner group[11] and the Sykes group[12] have also been actively involved in studying the redox chemistry of cytochrome c. The objective of these studies has not been to simply evaluate rate constants, but more importantly, to gain an understanding of the mechanism of biological long-distance electron transfer, which, according to Clark, is "still only sketchily understood."[13]

More applicable to this particular project are studies focusing on long-distance electron transfer in non-biological systems. Surprisingly, there are relatively few examples of such systems in the literature. In 2001 the Fukuzumi group[14] enforced a long-distance, outer-sphere electron transfer reaction by encapsulating an iron complex $\{Fe(bpy)_3\}^{3+}$ within the cavity of a Y-type zeolite. Close approach of the reducing agent, ferrocene, was prevented by the steric bulk of the zeolite, and the rate of reaction was reported to take days. In 1999, the Macartney group[15] reported decreased oxidation rates of several bisferrocenyl complexes upon inclusion in the host molecule ß-cyclodextrin. The decreased rate constants were attributed to the steric bulk of the ß-cyclodextrin and/or to the increased reduction potential of the included bisferrocenyl complexes. In

2006 and 2007, two redox systems incorporating the bulky macrocyclic cavitand cucurbit[7]uril were studied, also by the Macartney group.[16,17] These systems are described fully in Section 1.3.3.

To expand upon the literature dealing with long-range electron transfer processes, as well as to create a simplified model for complicated biological systems, it is necessary to isolate a redox agent within a kinetically inert, yet sterically bulky system. One approach to this problem would be to bind a redox active metal centre to a macrocycle modified with bulky pendant arms. The pendant arm substituents would provide steric bulk, preventing the close approach of redox agents and forcing the electron transfer to occur over larger than normal distances. Macrocycles are relatively recent additions to the field of chemistry, and a brief description of these cyclic molecules is warranted.

1.2. Macrocycles

By simple definition, a macrocycle is a cyclic ring composed of nine or more atoms, with at least three of the ring atoms having lone pairs of electrons.[18] The field of macrocyclic chemistry is a case of man catching up to nature; macrocycles have always been a crucial and abundant part of the natural world. Life as we know it would be impossible without the macrocyclic heme complex of hemoglobin transporting life-giving oxygen to the body's cells. Photosynthesis, another life-giving process, relies on the photochemical reactions occurring within chlorophyll *a*, a macrocyclic magnesium complex (see Figure 1.1).

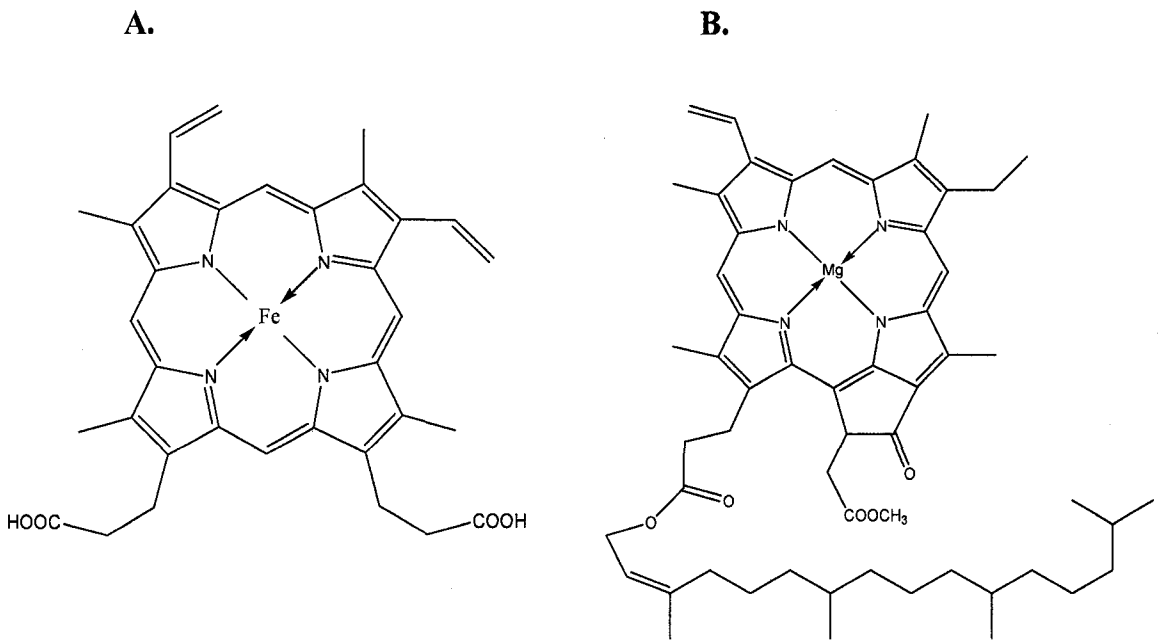

Figure 1.1. Structural representations of Heme B (A) and chlorophyll *a* (B)

The field of macrocyclic chemistry had humble beginnings. The first synthetic macrocycle was actually discovered by mistake! The iron atoms of an iron-walled reaction vessel reacted with the reactants phthalic anhydride and ammonia to yield a bright blue iron phthalocyanine complex in addition to the expected phthalimide (see Figure 1.2).[18]

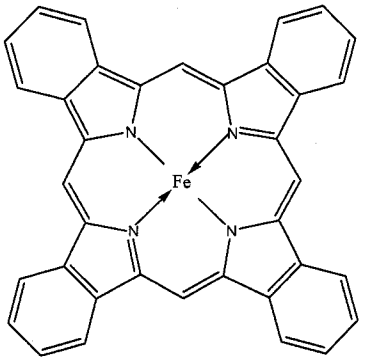

Figure 1.2. Structural representation of iron (II) phthalocyanine

Later, Curtis successfully isolated the nickel complexes of *meso*- and *rac*-5,5,7,12,12,14-hexamethyl-1,4,8,11-tetraazacyclotetradecane, or tet-a and tet-b, respectively (Figure 1.3).[19] This pioneering work paved the way for an explosion of interest in these cyclic ligands. In 1969, Cabbiness and Margerum[20] reported that copper reacts with tet-a to form a complex with a stability constant that is much greater than the corresponding complex formed upon reaction with a comparable open-chained ligand. In fact, the increase in the stability constant was so great, the authors argued, that the *chelate effect* did not adequately describe the dramatic increase in stability; a new term, the *macrocyclic effect*, was warranted. In 1974, the macrocyclic effect was deemed responsible for a similar observation in another system. Hinz and Margerum found the nickel complex with the macrocyclic ligand cyclam, $Ni(cyclam)^{2+}$ to be a million times more stable than its complex with an open-chained tetramine.[21]

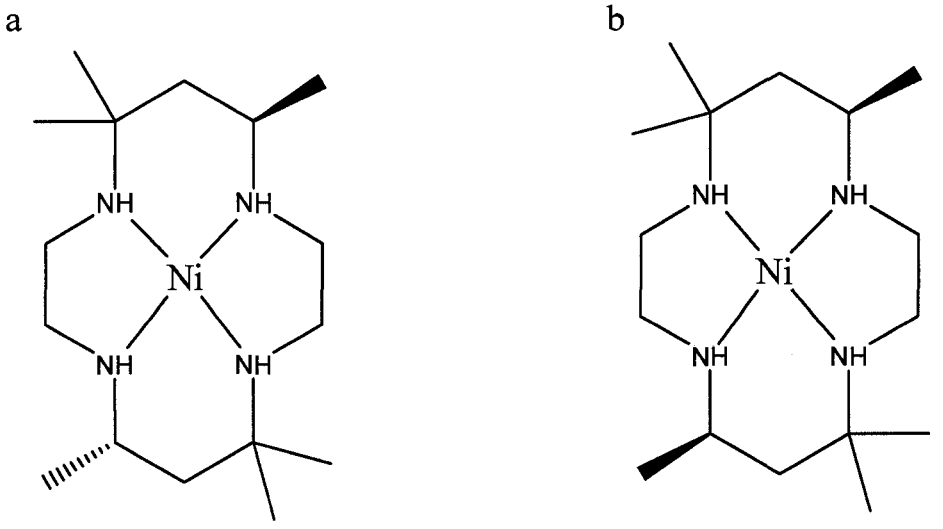

Figure 1.3. Structural representations of Ni(tet-a) (a) and Ni(tet-b) (b)

The macrocyclic effect became a subject of intense study in the following years, and it was found that the phenomenon could be explained both in terms of kinetics and thermodynamics. From a thermodynamic point of view, the macrocyclic effect is a function of the increased thermodynamic stability of the metallated product. The formation of this stable product drives the equilibrium forward, favouring the production of the metal complexes. From a kinetic point of view, the macrocyclic effect is a function of the fact that the metal centre provides a chelation centre for the ligands in solution, thus pre-organizing them in solution and providing a kinetically favorable pathway for the formation of the macrocyclic complexes.[18]

Perhaps no macrocycle has been the subject of more studies than 1, 4, 8, 11-tetraazacyclotetradecane (cyclam) (see Figure 1.4). First reports of its synthesis in the early to mid 1900's were either very complicated or very inefficient, resulting in low percent yields.[22,23] Interest in the macrocyclic ligand received a substantial boost with the work of E. K. Barefield,[24] who in 1972 announced a simplified synthetic technique involving the use of nickel as a templating agent. Percentage yields of the cyclam product were significantly higher than those reported *via* earlier methods.

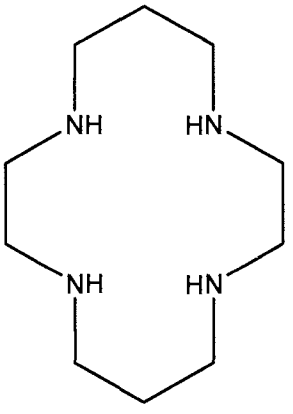

Figure 1.4. Structural representation of 1, 4, 8, 11-tetraazacyclotetradecane (cyclam)

The fourteen-membered cyclic ring system of cyclam with its four nitrogen donor atoms provides a unique coordination environment for transition metal ions. A molecular mechanics and crystallographic study launched by Hancock *et al.* in 1984[25] gave ideal metal-nitrogen bond lengths of 2.05Å and 2.29Å for the trans-III and trans-I isomers respectively, beautifully suiting this macrocycle for complexation with metals such as copper, nickel, cobalt and zinc.

The popularity of cyclam and its metallated complexes – a popularity that remains strong to this present day – is not unwarranted. The cyclam ring is reasonably flexible, allowing complexation with many different metal centres in many different oxidation states. In addition, the four nitrogen moieties within the ring can easily undergo nucleophillic addition reactions to form an almost unlimited number of substituted cyclam derivatives. Thirdly, the metal complexes of cyclam are unusually stable both kinetically and thermodynamically, a fact which is especially important when considering their use in biological systems.[26]

As mentioned previously, the secondary nitrogen atoms of the cyclam ring predispose the macrocyclic ligand to facile substitution reactions. Derivatives of cyclam having substituents at the nitrogen atoms are often referred to as "pendant arm" cyclam macrocycles. The introduction of pendant arms can add important functional groups to the macrocycle, suiting it for a particular function. In some cases, the additional pendant arms can coordinate to the metal centres, stabilizing unique oxidation states, or allowing the metal complex to take up an unusual isomeric configuration, as reported in 2007 by Soneta *et al.* for the formation of the extremely unusual trans-IV conformer of a nickel complex with a pendant arm cyclam derivative.[27] In other recent studies, the effect of

pendant arm substituents on the formation kinetics of the metallated complex[28] and on the redox potential of the metal centre was investigated.[29]

The physico-chemical properties of cyclam beautifully suit it for this particular project. It can be synthesized simply and cost-effectively. Its cavity size is a perfect fit for the redox active metal centres, copper and nickel, and its nitrogen donor atoms are easily substituted *via* nucleophillic displacement. Sterically bulky pendant arms can be chosen, so that the redox active metal centre is effectively shielded from the close approach of oxidants or reductants. For these reasons, the cyclam macrocycle will be the object of experiments involving bulky pendant arm macrocycles in this present work.

A second method for initiating long-distance electron transport in biomimetic systems can be envisioned. Supramolecular host/guest systems, in which a guest is encapsulated within a host molecule, have been extensively studied in recent years. Perhaps the most popular host system is the cyclodextrin family, consisting of α-, ß-, and γ-cyclodextrin. As noted previously, ß-cyclodextrin has already been used to study the effect of steric bulk on the rate of electron transfer.[15] However, cyclodextrins bear slight positive charges in their internal cavities, and are therefore not effective host molecules for positively charged redox active metal centres.[30]

A new family of host molecules – the cucurbit[n]urils – has recently emerged. Contrary to the cyclodextrins, these macrocyclic cavitands have slightly negatively-charged inner cavities – suiting these macrocycles for the encapsulation of positively charged metal complexes.[30] It can be imagined that the steric bulk of the cucurbituril ring may enforce long-distance electron transfer, which is the key objective of this work.

1.3. Cucurbiturils

Cucurbituril first entered the scientific world as a white crystalline powder in the laboratory of Behrend *et al.*[31] The year was 1905, and, due to the lack of modern technology, the powder remained largely uncharacterized. Nicknamed Behrend's polymer in honor of its discoverer, the substance was found to complex with various metal salts, but further experimentation was limited due to the uncertainty surrounding its structure. It remained for Mock *et al.*[32] to elucidate the hexameric structure of 6 glycoluril units and 12 methylene bridges in 1981 (Figure 1.6). Inspired by the pumpkin–like shape of this macrocycle, the group renamed the substance cucurbituril, after the Latin name for the pumpkin or gourd family (*cucurbitacee*).[30]

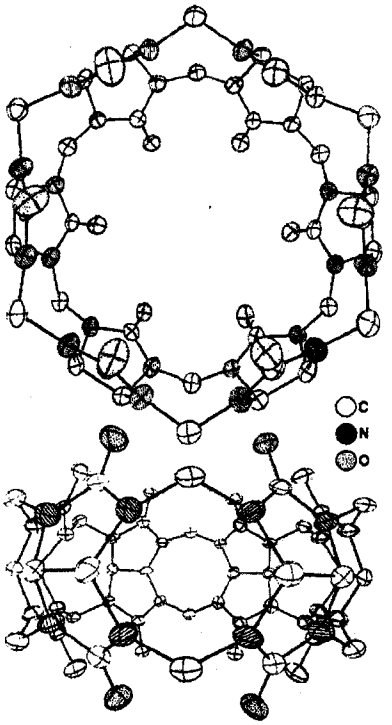

Figure 1.6. Early crystallographic image of cucurbituril from top down and side on. Image reproduced from reference 32.

Interest in the macrocyclic structure waned after this major discovery, probably due to its extremely poor solubility in all solvents other than concentrated aqueous acids and salt solutions; however, in the year 2000, Kim *et al.*[33] announced that the hexameric macrocycle was only one of a series of cyclic curcurbituril species. The Kim group broadened the cucurbituril family with the addition of pentameric, heptameric, and octameric cucurbiturils (see Figure 1.7).

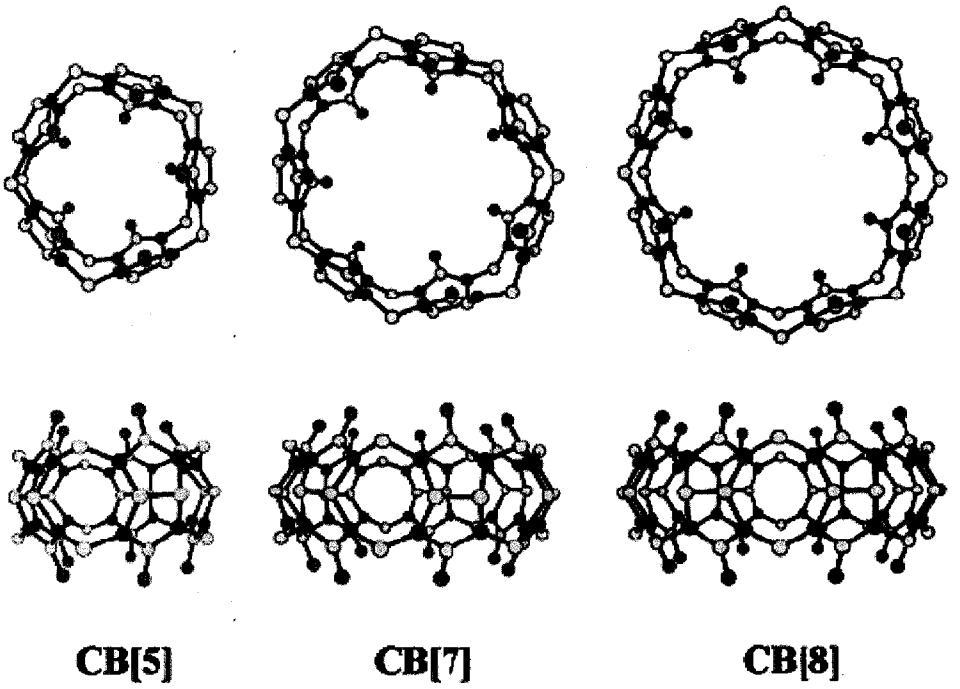

Figure 1.7. X-ray crystal structures of CB[5], CB[6], and CB[8]. Image reproduced from reference 34.

To avoid confusion, the original cucurbituril was named cucurbit[6]uril, or CB[6] for short, with the new species being named cucurbit[5]uril (CB[5]), cucurbit[7]uril (CB[7]), and cucurbit[8]uril (CB[8]), respectively. Not long after, in 2003, the Day group[34] was successful in isolating a CB[10] complex encapsulating CB[5]. The free CB[10] was attained by Isaacs *et al.*[35] in 2005.

1.3.1. Synthesis and Physico-Chemical Properties of the Cucurbit[n]uril Family

The suite of cucurbiturils results from a condensation reaction between glycoluril and formaldehyde in strongly acidic solutions. Day *et al.*[36] have undertaken a detailed study in an attempt to tune the synthetic methodology to the formation of specific cucurbit[n]urils. In general, a broader range of cucurbiturils are synthesized if lower reaction temperatures are used. The initial product from every synthesis is composed of the entire suite of cucurbiturils, and careful separation *via* fractional crystallization and dissolution is necessary to obtain the desired cucurbit[n]uril. A European patent filed by Kim *et al.* describes various methods for the synthesis of particular cucurbiturils and is now available to the public.[37]

Cucurbiturils possess some interesting physico-chemical properties. Microscopic analogues of barrels or pumpkins, the interior cavity is hydrophobic and slightly negatively charged, while the top and bottom rims are composed of polar carbonyl moieties. Cavity and portal sizes depend on the number of glycoluril repeating units present, and are summarized in the following table:[33]

	CB[5]	CB[6]	CB[7]	CB[8]
Portal diameter (Å)	2.4	3.9	6.9	6.9
Cavity diameter (Å)	4.4	5.8	7.3	8.8
Cavity volume (Å^3)	82	164	279	479
Outer diameter (Å)	13.1	14.4	16.0	17.5
Height (Å)	9.1	9.1	9.1	9.1

Table 1.1. Molecular dimensions of cucurbit[*n*]urils (n = 5-8). Table reproduced from reference 33.

The cucurbiturils share one unfortunate characteristic – extremely poor solubility. Of the cucurbiturils, CB[5] and CB[7] are the most soluble, with solubilities of 20 – 30 mM in water. CB[6] and CB[8] have almost negligible solubilities, measuring only 0.018 mM and <0.01 mM respectively.[30] Strong acidic aqueous solutions are capable of solubilizing all members of the cucurbituril family; dissolution in acidic solutions is thought to result from hydrogen bond interactions between the carbonyl moieties on the portals and the acidic solvent hydrogens. As reported long ago by the Behrend group,[31] cucurbiturils have a high affinity for metal salts; alkali metal ions are thus also used to solubilize cucurbiturils.[38,39]

1.3.2. Cucurbit[8]uril

Cucurbit[8]uril, the focus of this project, is a larger analogue of the more common CB[6]. Its portal diameter is 6.9 Å, as compared to the smaller portal diameter of CB[6] (3.9 Å). In addition, the inner cavity diameter of CB[8] is approximately 3 Å bigger than

that of CB[6] (8.8 Å as compared to 5.8 Å). The solubility of cucurbit[8]uril in water is yet to be determined, but it is believed to be < 0.01 mM.[30]

1.3.3. Cucurbit[8]uril as a Host Molecule

The crystal structure of cucurbit[8]uril was published in 2000 by the Kim group.[33] Since then, publications detailing the host/guest chemistry of this macrocycle have inundated the literature.[40, 41, 42,43] Like the smaller cucurbit[n]urils, positively charged, hydrophobic guests have been found to form inclusion complexes with CB[8]. However, unlike the smaller homologues, CB[8] is capable of binding larger guests, or even binding two guests at once to form 2:1 (guest@host) inclusion complexes.

Cucurbit[8]uril was chosen for this project because its large cavity size is suitable for the encapsulation of transition metal macrocycles. There is some precedent for the encapsulation of inorganic guests within cucurbit[8]uril. In 2006, the Day and Collins group[44,45] successfully encapsulated di- and tri-nuclear anti-cancer platinum complexes within the cavities of cucurbit[7]uril and cucurbit[8]uril (see Figure 1.9).

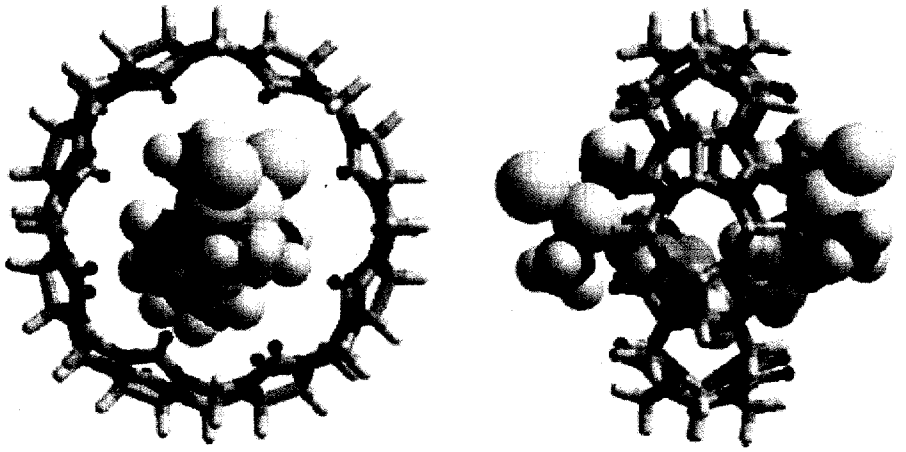

Figure 1.9. Encapsulation of a di-nuclear platinum complex in CB[8]. Image reproduced from reference 44.

In 2001, the Kim group published an exciting paper entitled, "Macrocycles within Macrocycles: Cyclen, Cyclam, and Their Transition Metal Complexes Encapsulated in Cucurbit[8]uril."[46] Inspired by the large cavity size of CB[8], the group reacted the macrocyclic CB[8] species with the protonated forms of the smaller macrocycles, cyclam and cyclen, to yield the inclusion complexes cyclam@CB[8] and cyclen@CB[8]. To extend these results even further, the inclusion complexes were then reacted with an excess of $Cu(NO_3)_2$ and $Zn(NO_3)_2$ to metallate the 1:1 inclusion complexes. Inclusion within the cavity of CB[8] was found to stabilize the metal centre, as an electrochemical study comparing the reduction potential (Cu^{II} to Cu^{I}) of free $[Cu(cyclen)(NO_3)_2]$ species and that of the $\{[Cu(cyclen)]@CB[8]\}(NO_3)_2$ inclusion complex showed an increased reduction potential for the encapsulated species.

The work was continued by the Fedin group, who, in addition to reporting the synthesis of several new inclusion complexes[47] (including the Ni^{II}cyclam analogue of the Cu^{II}cyclam inclusion complex reported previously by Kim *et al.*) went on to develop a new synthetic strategy for the inclusion of other hydrophobic guests within the cavity of CB[8].[48] The strategy involved a two-step process – 1) solubilizing the CB[8] by including the complex *trans*- $[Ni(en)_2(H_2O)_2]$ within the cavity and 2) using an excess of a more hydrophobic guest to replace the previous guest species, forming a more thermodynamically stable 2:1 complex. The preliminary inclusion of *trans*-$[Ni(en)_2(H_2O)_2]$ was found to be crucial to the success of the reaction, as the uncomplexed CB[8] is virtually insoluble in water and is therefore unreactive.

The [Ni(cyclam)]@CB[8] system is particularly relevant to this work. The nickel(II) cation is easily oxidized to the nickel(III) state, and the encapsulation of the

nickel cyclam complex within cucurbit[8]uril could act as a mimic of a biological system, with the cucurbit[8]uril ring being reminiscent of a more complicated biological enzyme. As Kim notes, ". . .such systems are potentially useful as catalysts with high specificity as a result of the unique microenvironment around the transition metal ion *which is reminiscent of metalloenzymes*."[46] Electron transfer reactions involving this sterically hindered redox active nickel centre should occur over larger than normal distances and may lend insight into the effect of steric bulk on electron transfer rates; however, such a study has never been undertaken. In fact, there are strikingly few reports in the literature dealing with kinetic aspects of cucurbituril inclusion complexes. To date, it would appear that only the cucurbit[7]uril inclusion complexes have been studied with reference to kinetics.

1.3.4. Kinetic Studies Involving CB[n] Inclusion Complexes

In 2006, the Macartney group reported the inclusion of (E)-1-ferrocenyl-2-(1-methyl-4-pyridinium)ethylene cation within the cavity of cucurbit[7]uril.[16] Though much of the report centered on exploring the stabilizing affect of the host macrocycle, protecting the guest from photoisomerization, the group did report the kinetics of oxidation using $Co(dipic)^{2-}$as the oxidizing agent. It was found that inclusion within the host macrocycle notably decreased the rate of oxidation, with the free (E)-$FcMPE^{+}$ having a rate constant (k_o) of $(2.1\pm 0.1) \times 10^4\ M^{-1}s^{-1}$and the encapsulated (E)-$FcMPE^{+}$ having a rate constant (k_{CB}) of $(1.6 \pm 0.1) \times 10^2\ M^{-1}s^{-1}$. It was reported that the reduced oxidation rate of the encapsulated species reflects both the increased distance between the redox partners due to the steric bulk of the cucurbituril ring, and the increased reduction potential of the inclusion complex.

A year later, the Macartney group reported the inclusion of another ferrocenium derivative, (trimethylammonio)methylferrocene, within the cavity of cucurbit[7]uril, focusing particularly on elucidating the electron self-exchange rate constants for both the free $FcTMA^{2+/+}$ couple and the complexed $\{FcTMA@CB[7]\}^{2+/+}$ couple.[17] With respect to oxidation *via* the $Co(dipic)^{2-}$ species, this system proved to behave similarly to the previously studied (E)-$FcMPE^{+}$ inclusion complex.

1.4. Objectives for Present Work

It is the overall goal of this particular project to study electron transfer reactions occurring over large distances. To do this, it is necessary to design a system in which the redox active metal centre is protected from the close approach of another redox active metal centre. Two approaches are taken, 1) isolating the metal centre within the cavity of a series of sterically bulky pendant arm macrocycles, and 2) isolating the metal centre within the steric encumbrance of the macrocyclic cavitand cucurbit[8]uril.

Both approaches involve "burying" a redox active metal centre within a sterically bulky system. These systems will be reminiscent of the more complicated biological metalloenzymes, with one distinct advantage – the model systems are considerably simpler and can be easily synthesized in the lab and studied by conventional kinetic techniques such as stopped-flow spectrophotometry.

1.4.1. Pendant Arm Macrocyclic Complexes

A series of pendant arm macrocycles has been synthesized previously by Haines and Zhang.[49] It is expected that these macrocycles, N-alkylated derivatives of cyclam, will complex with transition metal ions such as copper and nickel. In solution, it is

expected that the pendant arms will rotate freely, effectively sweeping out a large radius around the complexed metal centre and shielding it from close interaction with other redox active metal centres introduced to the system. Due to the enforced separation of the redox active pairs, it is expected that electron transfer will occur over large distances, and the rates of electron transfer will be monitored *via* stopped-flow techniques.

1.4.2. Metal Complexes within the Cavity of Cucurbit[8]uril

As previously mentioned, cucurbit[8]uril is ideally suited for the encapsulation of metal-based complexes within its cavity. As an octameric ring system with portal diameters almost 2 Å smaller than the diameter of the internal cavity, cucurbit[8]uril would act as a steric hindrance to the close approach of a redox-active species. Long-distance electron transfer conditions would therefore be enforced.

The encapsulation of Ni^{II}cyclam within the cavity of cucurbit[8]uril has already been reported,[46] though it has not been the subject of any kinetic studies. It is a primary focus of this work to perform such a study, and to compare results with previous studies involving the same reactions with free Ni^{II}(cyclam). In this way, it will be possible to directly account for the effect of the sterically bulky cucurbit[8]uril ring on the rate of electron transfer.

Of further interest will be the inclusion of other macrocyclic species inside the cavity of cucurbit[8]uril, such as nickel complexes of 1,4,7-triazacyclononane (tacn). The redox properties of encapsulated $Ni^{II}(tacn)_2$ can then be compared to those of the free $Ni^{II}(tacn)_2$ complex, providing a preliminary assessment for the effect of the sterically bulky cucurbit[8]uril ring on electron transfer rates.

It is hoped that this project will provide insight regarding the effect of steric bulk on long-distance electron transfer reaction rates. This insight is valuable, as biological electron transfer reactions often involve sterically bulky enzymes.

Chapter 2 – Experimental

2.1 Reagents Used

All chemicals were used as received. Chemical sources and their respective purities have been tabulated in Table 2.1.

Chemical	Source	Purity
Aqueous ammonia	Caledon Laboratories, Ltd.	n/a
Ammonium chloride	Fisher Scientific Company	Crystalline/Certified ACS
Benzyl chloride	Aldrich Chemical Company	99%
Cobalt chloride hexahydrate	BDH, Inc.	97%
Cobalt nitrate hexahydrate	Analar	98%
Copper nitrate trihydrate	Baker	Meets ACS Standards
Copper perchlorate hexahydrate	Aldrich Chemical Company	98%
Formaldeyhyde (37% weight)	Aldrich Chemical Company	n/a
Glycoluril	Aldrich Chemical Company	n/a
Glyoxal (40% weight)	Aldrich Chemical Company	n/a
Nickel chloride hexahydrate	Aldrich Chemical Company	Reagent Plus
Nickel nitrate hexahydrate	Aldrich Chemical Company	Crystalline
Nickel perchlorate hexahydrate	Aldrich Chemical Company	Crystalline
Hydrogen peroxide (30%)	Honeywell Riedel-deHaën	n/a
Sodium borohydride	Aldrich Chemical Company	≥98.5%

Sodium cyanide	Aldrich Chemical Company	97%
Sodium hydrogen carbonate	BDH, Inc.	Meets ACS Standards
Sodium hydroxide	Aldrich Chemical Company	97+%
Sodium sulfate	Aldrich Chemical Company	99+%
1,5,8,12-tetraazadodecane	Strem Chemicals, Inc.	Min. 95%
1,4,7-triazacyclononane trihydrochloride	Aldrich Chemical Company	97%

Table 2.1. List of chemicals used, as well as their respective sources and purities

CAUTION:

It is important to note that metal perchlorates are potentially explosive, and must never be heated in the dry state. Extreme care should be exercised when handling these compounds.

It is also important to note that cyanide is extremely toxic and should be handled with extreme care. Adequate ventilation, eye protection, and appropriate gloves should be used at all times.

2.2. Synthetic Procedures

*2.2.1. 1,4,8,11-Tetrabenzyl-1,4,8,11-tetraazacyclotetradecane: **L**^{1}*

Cyclam derivatives bearing bulky pendant arms ($L^1 - L^3$) have previously been synthesized by Haines and Zhang.[49] The synthesis of L^1 was repeated according to their methodology. All other ligands were used as previously synthesized.

Sodium hydroxide (1.50 g, 37.5 mmol) was dissolved in water (80 mL). Cyclam (1,4,8,11-tetraazacyclotetradecane) (1.01g, 5.04 mmol) was added to the solution and dissolved with stirring. Separately, a solution of benzyl chloride in $CHCl_3$ was made by adding benzyl chloride (2.31 mL, 50.3 mmol) to $CHCl_3$ (8 mL). The benzyl chloride solution was then added to the cyclam solution dropwise and allowed to stir for 24 hours. The organic phase was separated, dried with anhydrous sodium sulfate, and the solvent removed *via* rotary evaporation. The impure L^1 was collected and recrystallized from 50 mL of chloroform and methanol (60:40 ratio, respectively) to yield white crystals of L^1 (1.47 g, 51.9%)

2.2.2 $[Cu^{II}(L^1)(MeCN)](ClO_4)_2$: ***CuL^1***

L^1 (0.264 g, 0.470 mmol) was dissolved in 25 mL of $CHCl_3$ to yield a colourless solution. Separately, $Cu(ClO_4)_2 \cdot 6H_2O$ (0.176 g, 0.474 mmol) was dissolved in 25 mL of EtOH to yield a clear, light blue solution. The two solutions were then added together and refluxed for 2 hours. The emerald green precipitate was collected *via* vacuum filtration and washed twice with ice-cold chloroform, yielding 0.364 g (120 %). (The product can be assumed to be wet.)

2.2.3. $[Cu^{II}(L^2)](ClO_4)_2$ and $[Cu^{II}(L^3)(MeCN)](ClO_4)_2$: ***$CuL^2$*** *and* ***$CuL^3$***

CuL^2 and CuL^3 were synthesized following the same procedure as described for $[Cu^{II}(L^1)(OH_2)](ClO_4)_2$. The yield for CuL^3 was 0.148 g (80.6%).

2.2.4. Attempted Synthesis of ***NiL***^{1}

To a 25 mL solution of EtOH and $NiCl_2 \cdot 6H_2O$ (0.100 g, 0.420 mmol) was added 0.120 g of L^1 (0.0210 mmole). The pale green/yellow solution was refluxed for twenty minutes, during which time the solution turned bright yellow in colour. The reaction mixture was filtered to collect the pale green nickel (II) hydroxide precipitate; however, upon rotary evaporation to encourage the precipitation of the nickel complex, more nickel (II) hydroxide precipitated. It can be assumed that the nickel complex is formed in solution, but is unstable and can not be isolated in the solid state. Attempts with $L^2 - L^3$ yielded similar results.

2.2.5. Cucurbit[8]uril

Cucurbit[8]uril (CB[8]) was prepared according to a standard literature method.[37] A 20 mL solution of 9 M sulfuric acid was heated with stirring to 70.0 °C in a paraffin oil bath. When the solution temperature reached 70.0 °C, 5.68 g (40.0 mmol) of glycoluril was added slowly. As the glycoluril dissolved, the solution turned pale yellow in colour. After stirring for ½ hour, the temperature was raised to 75.0 °C, and 7 mL of formaldehyde (37% weight) was added dropwise. A reflux condenser was attached and the solution was allowed to stir at 75.0 °C for a 24 hour period. After 24 hours, 100 mL of distilled water was added to the clear dark yellow/orange solution to yield a white precipitate. The solution was then placed in the fridge for 36 hours. Impure cream-coloured CB[8] was collected *via* vacuum filtration through a fine sintered glass crucible. The CB[8] was then swirled in a 2 M sodium sulfate solution (50 mL). The insoluble off-white powder was again collected *via* vacuum filtration and recrystallized from 6 M

sulfuric acid. After storage at ~5°C for five days, colourless crystals of CB[8] were collected (0.566 g; 0.336 mmol), giving a yield of 8.52 %.

2.2.6. 1,4,8,11-Tetraazacyclotetradecane: ***Cyclam***

Cyclam was prepared according a modified literature procedure.[49] To 400 mL of water was added nickel (II) nitrate hexahydrate (43.9 g, 0.151 mol). The forest-green solution was stirred until the nickel (II) nitrate hexahydrate was completely dissolved. At this point, 1,5,8,12-tetraazadodecane (26.1 g, 0.150 mol) was added dropwise. Upon addition, the solution turned dark purple in colour. The solution was then cooled in an ice bath to 5 °C, and 22.5 mL of glyoxal (40% weight) was added dropwise. The solution was left standing at room temperature for four hours.

After standing, the solution was again cooled to 5 °C, and, over a one hour time period, sodium borohydride (11.5 g, 0.304 mol) was carefully added. After addition of sodium borohydride, the solution was allowed to warm to room temperature before being heated at 90 °C for 15 minutes. Hot filtration removed a tar-like black precipitate from the solution. The filtrate (clear, dark orange in colour) was poured into a 2 L round bottom flask, and stirred while 29.0 grams (0.600 mol) of sodium cyanide were added. A condenser was attached, and the solution was refluxed for 2 hours.

The solution was removed from the heat and allowed to cool to room temperature, and sodium hydroxide (15.5 g, 0.388 mol) was added. After the sodium hydroxide had dissolved, excess water was removed *via* rotary evaporation until only a slurry remained. Chloroform (100 mL) was added, and the solid was collected *via* vacuum filtration and washed two times with 100 mL portions of chloroform. The filtrate was then collected in

a large separatory funnel and the water layer removed and washed with five 50 mL portions of chloroform. The chloroform extracts from the washings were combined with the original chloroform extract, dried with anhydrous sodium sulfate, poured into a large round bottom flask, and evaporated to dryness *via* rotary evaporation. The impure yellow cyclam was recrystallized from 800 mL of chlorobenzene to yield a white crystalline product, which was collected *via* vacuum filtration and washed with diethyl ether (50 mL), yielding 10.1 g of cyclam (33.5%).

2.2.7. 1,4,8,11-Tetraazacyclotetradecane • 4HCl: ***Protonated Cyclam***

To 10 mL of 1.2 M hydrochloric acid was added 0.416 g (2.08 mmol) of cyclam. The cyclam dissolved rapidly to yield a clear, yellowish solution. Precipitation of the protonated cyclam was accomplished through the addition of 100 mL of ethanol. Iridescent flakes of protonated cyclam were collected *via* vacuum filtration, yielding 0.746 g (104%) (Product probably retained some hydrochloric acid.) Product used without further purification.

2.2.8. Inclusion Complex of Cyclam@CB[8] • 4HCl

The inclusion complex of cyclam@CB[8] • 4 HCl was synthesized according to the method of Kim *et al.*[46] Cyclam tetrahydrochloride (0.746 g, 1.25 mmol) was dissolved in 10 mL of water. To this solution was added CB[8] (0.334 g, 0.199 mmol). The solution was allowed to reflux for two hours, during which time the CB[8] completely dissolved. Upon cooling to room temperature, no precipitate formed, and the pH was tested to reveal a high acidity.* A 0.4 M solution of NaOH was added dropwise

until the solution was neutralized, and the formation of a white precipitate was noted. The product was collected *via* vacuum filtration and washed first with water and then with methanol to yield 0.241 g (59.8%).

* It is thought that the protonated cyclam retained some hydrochloric acid. A more thorough washing following its synthesis is suggested.

2.2.9. Inclusion complex of {[Ni(cyclam)]@CB[8]}$(NO_3)_2$

The inclusion complex of {[Ni(cyclam)]@CB[8]}$(NO_3)_2$ was synthesized according to the method of Kim *et al.*[46] To cyclam@CB[8] • 4HCl (0.241 g, 0.119 mmol) was added a 10 mL aqueous solution of nickel (II) nitrate hexahydrate (0.235 g, 0.808 mmol). The solution was allowed to reflux for two hours, during which time the colour changed from pale green to bright yellow. After two hours, an additional 5 mL of water was added in order to ensure the complete dissolution of the product. When the solution was clear, it was removed from the heat. Upon cooling to room temperature, bright yellow crystals of {[Ni(cyclam)]@CB[8]}$(NO_3)_2$ precipitated, yielding 0.202 g (80.3%).

2.2.10. Ni^{II}(cyclam)Cl_2

Cyclam, (1.020 g; 5.092 mmol) was dissolved in 20 mL of methanol in a 50 mL round bottom flask. To this solution was added 1.210 g (5.090 mmol) nickel (II) chloride hexahydrate dissolved in 30 mL of methanol. Upon addition, the solution turned deep orange in colour. Lilac-coloured precipitate was noticed after a few minutes. The

solution was refluxed for two hours, during which time more precipitate formed. The solution was then allowed to cool before filtering to collect the lilac-coloured precipitate (1.72 g, 102%). The product is assumed to contain some impurities.

2.2.11. One Pot Synthesis of {[Ni(cyclam)]@CB[8]}Cl_2

Ni^{II}(cyclam)Cl_2 (0.0280 g, 85.9 μmol) was dissolved in 10 mL of H_2O in a 25 mL round bottom flask to yield an orange solution. To this solution was added CB[8] (0.0362g , 20.8 μmol) heterogeneously. A further 10 mL of water was added to the reaction flask before refluxing for 2 hours. As the solution was refluxed, the CB[8] completely dissolved and the colour changed from orange to yellow. After two hours, the solution was allowed to cool to room temperature slowly. Pale yellow crystals precipitated out of solution, yielding 0.102 g (40.0%).

2.2.12. Inclusion complex of {[Cu(cyclam)]$(OH_2)_2$@CB[8]} $(NO_3)_2 \cdot 17H_2O$

This complex was prepared in a similar manner to that of {[Ni(cyclam)]@CB[8]}$(NO_3)_2$, according to the method of Kim *et al.*[46] To an aqueous solution of cyclam@CB[8] • 4 HCl (0.147 g, 0.0776 mmol) was added 9.7 equivalents of $Cu^{II}(NO_3)_2 \cdot 3H_2O$ (0.182 g, 0.754 mmol). Refluxing for two hours resulted in a colour change from pale green to deep purple. Large purple crystals of {[Cu(cyclam)]$(OH_2)_2$@CB[8]}$(NO_3)_2$ were obtained upon slow evaporation of the solvent at room temperature.

2.2.13. $Ni^{II}(tacn)_2(ClO_4)_2$

$Ni^{II}(tacn)_2(ClO_4)_2$ was synthesized according to a standard literature method.[50] Nonane (1,4,7-triazacyclononane trihydrochloride) (0.478 g, 2.00 mmol) was dissolved in 40 mL of H_2O to yield a colourless solution. $Ni(ClO_4)_2 \cdot 6H_2O$ (0.366 g, 1.00 mmol) was added to the solution heterogeneously with stirring. When the $Ni(ClO_4)_2 \cdot 6H_2O$ had dissolved, aqueous 0.4 M NaOH was added dropwise until the solution reached a pH of 9. The solution was then refluxed for 2 hours. Excess solvent was removed *via* rotary evaporation, and the solution was stored at 5 °C for 12 hours. The lilac crystals were collected *via* vacuum filtration and washed with ice cold water to yield 0.191 g (20.0%).

2.2.14. Inclusion complex of $\{[Ni(tacn)_2]@CB[8]\}(ClO_4)_2$

The inclusion complex of $\{[Ni(tacn)_2]@CB[8]\}(ClO_4)_2$ was prepared in a manner similar to that outlined in section 2.2.11. $Ni(tacn)_2(ClO_4)_2$ (0.111 g, 0.216 mmol) was dissolved in water (15 mL) to yield a pink solution. Cucurbit[8]uril (0.103 g, 0.0610 mmol) was added to the solution heterogeneously. The solution was then allowed to reflux for 24 hours. After 24 hours, the solution was examined and was found to contain a pale pink precipitate. Approximately 75 mL of deionized water was added to the round bottom flask and the solution was allowed to reflux for another twelve hours. After twelve hours, the precipitate had completely dissolved to yield a clear pink solution. Slow cooling to room temperature produced feather-like pale pink crystals. The crystals were collected, giving a yield of 0.0553 g (41.3 %).

2.2.15. Hexaaquacobalt(III)

Aqueous solutions containing hexaaquacobalt(III) were prepared *via* the multi-step procedure highlighted by Jordan *et al.*[51]

Step 1: Synthesis of hexaamminecobalt(III) chloride

Hexaamminecobalt (III) chloride was prepared according to a standard literature method.[52] To 10 mL of H_2O was added 6.05 g (0.113 mol) of ammonium chloride. The solution was heated and allowed to stir until the ammonium chloride dissolved. At this point, $CoCl_2 \cdot 6H_2O$ (9.07 g, 52.1 mmol) was added to the solution; with addition, the solution turned bright indigo blue. Upon complete dissolution of the $CoCl_2 \cdot 6H_2O$, the solution was poured into an erlenmeyer flask containing activated charcoal (~1 gram). Concentrated ammonia (20 mL) was then added to the solution, changing the colour to deep reddish orange. The solution was then placed in an ice bath to cool.

When cool, 20 mL of 6% H_2O_2 were added dropwise with stirring, and the solution was heated at 60 °C for 20 minutes; with heating, the pinkish colour of the solution turned decidedly orange. The solution was allowed to cool once more, first to room temperature, and then in an ice bath. With cooling, orange crystals precipitated from solution. The precipitate and the charcoal were collected *via* vacuum filtration and then dissolved in 83 mL of a boiling 0.45 M HCl solution. After fifteen minutes, the orange crystals had completely dissolved, leaving only the charcoal. The charcoal was removed from the solution *via* hot filtration, and 10 mL of concentrated HCl were added to the orange filtrate to precipitate orange crystals of hexaamminecobalt (III) chloride. After cooling in an ice bath, the orange crystals were collected and allowed to dry on the vacuum line, yielding 7.62 grams (55.0%).

Note: This synthesis was attempted using bone charcoal, but the yield was decidedly lower (15.6%) due to the formation of the pentaamminecobalt (III) chloride species.

Step 2: Synthesis of a Solution containing $Co(CO_3)_3^{3-}$

Jordan's method[51] was followed in the preparation of a solution containing the anionic species $Co(CO_3)_3^{3-}$. Sodium hydrogen carbonate (75.8 g, 0.902 mol) was added to 250 mL of H_2O in a 1000 mL Erlenmeyer flask. The heterogeneous solution was allowed to stir while $Co(NO_3)_2 \cdot 6H_2O$ (2.90 g , 9.96 mmol) was added; upon addition, the solution turned lilac in colour. A diluted solution of 30% H_2O_2 (2 mL of 30% H_2O_2 in 250 mL H_2O) was then added dropwise over a one hour time period. During addition, the solution turned colour from lilac to deep emerald green. After complete addition of the H_2O_2 solution, 500 mL of H_2O were added to bring the solution to a total volume of one litre. The solution was allowed to stir for 12 hours to completely dissolve the excess carbonate.

Step 3: Synthesis of $[Co(NH_3)_6][Co(CO_3)_3]$

Following Jordan's method,[51] $[Co(NH_3)_6][Co(CO_3)_3]$ was prepared by dissolving 3.59 g (13.4 mmol) of $[Co(NH_3)_6]Cl_3$ in 200 mL of H_2O to give a bright orange solution. This solution was then added to the solution of $Co(CO_3)_3^{3-}$ prepared above. Stirring for 1 hour and subsequent cooling in an ice bath in the fridge (24 hours) produced emerald green crystals, which were then filtered and washed with water to yield 2.54 grams of product. The yield, calculated in reference to $Co(NO_3)_2 \cdot 6H_2O$, was 63.7%.

Step 4: Synthesis of Hexaaquacobalt (III)

Hexaaquacobalt (III) was prepared according to Jordan's method.[51] A 15 mL solution of 4M $HClO_4$ was allowed to stir in a 50 mL Erlenmeyer flask while immersed in an ice bath. To this solution was added $[Co(NH_3)_6][Co(CO_3)_3]$ (0.600 g, 1.50 mmol). With addition, the formation of carbon dioxide gas was noted. After ~ 2 hours, yellow precipitate corresponding to the formation of $[Co(NH_3)_6](ClO_4)_3$ had formed. To separate the blue supernatant hexaaquacobalt (III) solution, the mixture was centrifuged and the liquid decanted into a vial. The vial was fitted with a septum and the solution purged with nitrogen for 30 minutes before it was stored at -12 °C.

2.3. Kinetics

2.3.1. Preparation of Stock Solutions:

Stock solutions of $[Ni^{II}(cyclam)]$@CB[8], $HClO_4$, $LiClO_4$, hexaaquacobalt (III), hydroquinone, catechol, and $Ni^{II}(cyclam)$ were prepared using doubly distilled deionized water. The $HClO_4$ and hexaaquacobalt(III) stock solutions were analyzed for precise $[HClO_4]$ by titration against a 0.0100 M standardized solution of sodium hydroxide, using phenolphthalein as the indicator. Solutions of $LiClO_4$ were passed through an ion exchange column before being monitored for precise $[HCLO_4]$ by the same method.

Stock solutions containing hexaaquacobalt(III) were analyzed for Co(III) concentration spectrophometrically by measuring the absorbance at 605 nm and using the reported extinction coefficient ($\varepsilon_{605} = 35.3\ L \cdot mol^{-1} \cdot cm^{-1}$).[53]

2.3.2. Experimental Design and Technique

All kinetic measurements were performed on a double mixing KinetAsyst SF-61DX2 stopped-flow system. Temperature was controlled to ± 0.05°C using a Lauda model RM6 refrigerated recirculating water bath. A schematic of the double mixing unit of the instrument is given in Figure 2.1.[54]

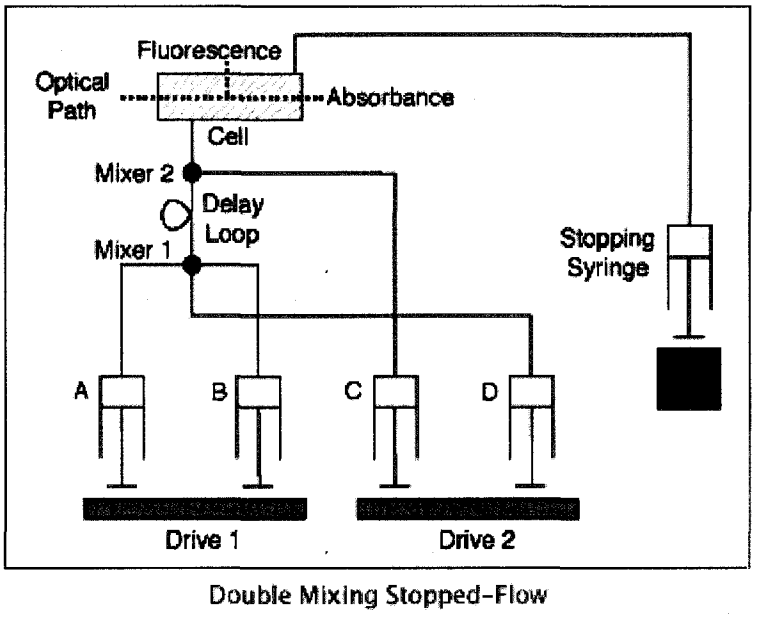

Figure 2.1. Schematic showing double mixing unit of a stopped-flow spectrometer. Figure reproduced with permission from reference 54.

The reactions relevant to this work were monitored *via* single mixing stopped-flow kinetics. In this mode, only drive 2 is used. Reservoir C is filled with reactant A, while reservoir D is filled with reactant B. High pressure forces the reactants into a mixing chamber, where they are rapidly mixed and then allowed to flow into an observation cell. The reaction is abruptly stopped when the reactant flow forces a stopping syringe against a stop-block. The action of the stopping syringe against the stop-block initiates the acquisition of data. A monochromator allows the experimenter to

choose the wavelength at which the absorbance changes are monitored. Light of the chosen wavelength passes through the reactants in the observation cell; an optical fibre carries transmitted light to a photomultiplier tube, where it is intensified and fitted to an absorbance *versus* time curve by HiTech's "KinetAsyst" software. Fig P software was also used in the kinetic fitting of data.

2.3.3. Oxidation of [Ni(cyclam)]@CB[8] by Hexaaquacobalt(III)

The oxidation of [Ni(cyclam)]@CB[8] by hexaaquacobalt(III) was performed under pseudo-first-order conditions with the concentration of the oxidant (hexaaquacobalt(III)) being held in at least a 10-fold excess. The reaction was performed at five different concentrations of hexaaquacobalt(III) (0.0002 M – 0.0010 M) at five different temperatures (288 – 308 K) with a constant concentration of [Ni(cyclam)]@CB[8] (1.40×10^{-5} M). It is important to note that the mixing of the reagents in the stopped-flow unit results in a two-fold dilution of each species. Each kinetic run was repeated until five runs were obtained with results differing by no more than 10%; reported k_{obs} values reflect the averages of these runs. Due to the potential decomposition of the hexaaquacobalt(III) species, particularly at low acidities, the reactions were performed quickly, and the stock solutions of hexaaquacobalt(III) were stored at -12 °C until just before needed. Ionic strength was kept constant at 1.00 M by adding $HClO_4$.

The reaction was tested for acid dependence by varying the concentration of acid (0.200 – 0.800 M) and performing the same reaction with a fixed concentration of hexaaquacobalt(III) (1.00×10^{-3} M) and [Ni(cyclam)]@CB[8] (1.00×10^{-5} M) at five

different temperatures. Ionic strength was kept at a constant 1.00 M by adding appropriate amounts of $LiClO_4$.

2.3.4. Oxidation of Benzenediols and Ni^{II}(cyclam)Cl_2

Oxidation of benzene-1,4-diol (hydroquinone), benzene-1,2-diol (catechol) and Ni^{II}(cyclam)Cl_2 by [Ni^{III}(cyclam)]@CB[8] was performed under pseudo-first-order conditions by using an excess (>100-fold) of the reducing agent. The oxidation conditions were simplified due to the fact that a stoichiometric deficiency of hexaaquacobalt(III) species generates the relatively stable [Ni^{III}(cyclam)]@CB[8]} *in situ*; storage of the oxidant at -12 °C and time considerations are therefore unnecessary.

The observed rate constants (k_{obs}) were collected for five reductant concentrations (0.002 M – 0.006 M), at five different temperatures (284 – 297 K), and at a constant acidity of 1.00 M. The concentration of the oxidant [Ni^{III}(cyclam)]@CB[8] was kept at a constant 1.30×10^{-5} M. Reported k_{obs} values are average values for five runs with rate constants differing by no more than 10%. The oxidant, [Ni^{III}(cyclam)]@CB[8], was generated *in situ* by the addition of a stoichiometric deficiency of hexaaquacobalt(III) (1.30×10^{-5} M) to [Ni^{II}(cyclam)]@CB[8] (1.31×10^{-5} M). It should be noted that the mixing of the reagents in the stopped-flow unit results in a two-fold dilution of each species.

2.4. Other Analytical Methods

^1H NMR were collected on a Bruker Avance 300 MHz NMR spectrometer; ^{13}C NMR were collected at the Atlantic Region Magnetic Resonance Centre on a 500 MHz

NMR spectrometer. Elemental analysis was performed at Guelph Chemical Laboratories Ltd. Electrospray ionization mass spectroscopy data was acquired using a thermo UHPLC/MS at the National Research Centre. UV-visible spectra were measured on a Cary 50 Bio UV-vis spectrophotometer. X-ray crystal structure determination was performed by Andreas Decken at the University of New Brunswick on a Bruker AXS P4/SMART 1000 diffractometer. For details regarding the methodology of structure determination, please refer to the Appendix.

Chapter 3 – Results & Discussion

Pendant Arm Macrocyclic Complexes

3.1 Synthesis of Copper Pendant Arm Macrocyclic Complexes

Several cyclam derivatives incorporating bulky pendent arms have been previously synthesized by Haines and Zhang (see Figure 3.1).[49] Ligands L^2 – L^3 were used as previously synthesized; L^1 was synthesized again according to the scheme outlined by Haines and Zhang (see Scheme 3.1).

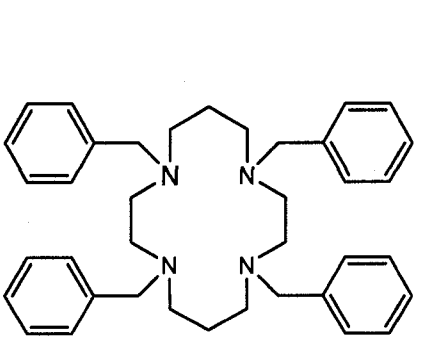

L^1

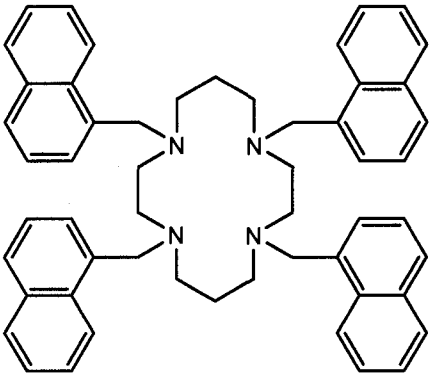

L^2

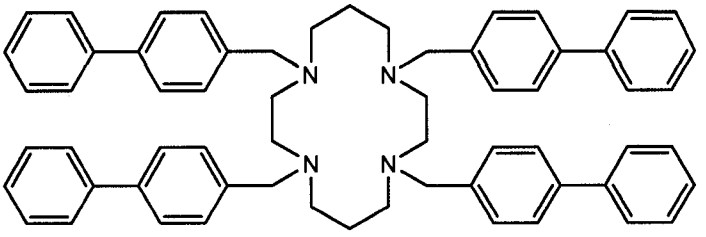

L^3

Figure 3.1. Bulky pendant arm macrocycles previously synthesized by Haines and Zhang.

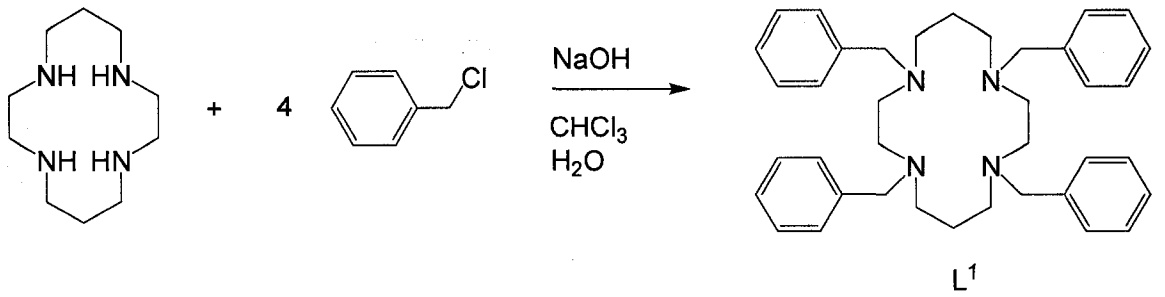

Scheme 3.1. Reaction scheme representing synthesis of L^1.

It was thought that these might act as sterically bulky ligands, which, when complexed to a redox active metal centre, may force the electron transfer reaction to occur over a larger distance and at slower rates. It is of key interest to this present work, therefore, to complex these bulky ligands with redox-active metal centres such as copper and nickel. Experiments showed a facile complexation of the ligands ($L^1 - L^3$) with copper to form the corresponding metal complexes, according to Scheme 3.2.

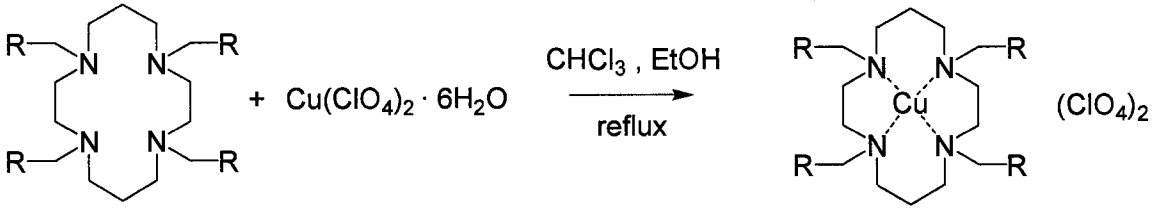

Scheme 3.2. Reaction scheme representing synthesis of metallated pendant arm cyclam complexes (R = phenyl, anthracene, or 4-biphenyl)

3.2. Characterization

Copper complexes of L^1-L^3 were characterized by elemental analysis. Complexes CuL^1 and CuL^3 were further characterized by their X-ray crystallographic structures.

3.2.1. CHN Analysis

Excellent agreement was found between the calculated percentages of carbon, hydrogen, and nitrogen for CuL^1, CuL^2, and CuL^3 (See Table 3.1) and those determined by elemental analysis.

Complex	%	Analysis Found	Calculated
CuL^1	C	55.12	55.44
	N	6.08	5.88
	H	6.58	6.81
CuL^2	C	63.57	63.87
	N	5.07	4.76
	H	5.88	5.52
CuL^3	C	66.08	66.04
	N	6.00	5.72
	H	5.27	4.97

Table 3.1. CHN analysis data for CuL^1, CuL^2 and CuL^3.

3.2.2. X-ray Crystallography

Crystal structures of CuL^1 and CuL^3 are reported below. (The crystals of CuL^2 were too small for X-ray diffraction analysis.) As fully discussed in section 4.1.2, cyclam can adopt one of five different isomeric structures, designated as trans-I – trans-V.[55] The cyclam rings in CuL^1 and CuL^2 are found in the trans-I configuration, with the substituents orientated above the plane of the macrocyclic rings. This finding is in agreement with literature data for tetra-substituted cyclam derivatives.[56]

3.2.2.1 [(L^1)Cu(NCMe)](ClO_4)$_2$ • 3 MeCN: ***CuL^1***

X-ray quality emerald green single crystals of CuL^1 were grown *via* diffusion of diethyl ether into a concentrated acetonitrile solution of $[Cu^{II}(L^1)](ClO_4)_2$. An ORTEP depiction of the copper complex is shown in Figure 3.2, and relevant bond distances and bond angles are given in Table 3.2. Refinement details and other crystallographic data are presented in Table 3.3. The overall geometry of the copper centre is square pyramidal, with a solvent molecule, acetonitrile, taking up the axial position. This structure has been previously reported by Lindoy *et al.*[29]

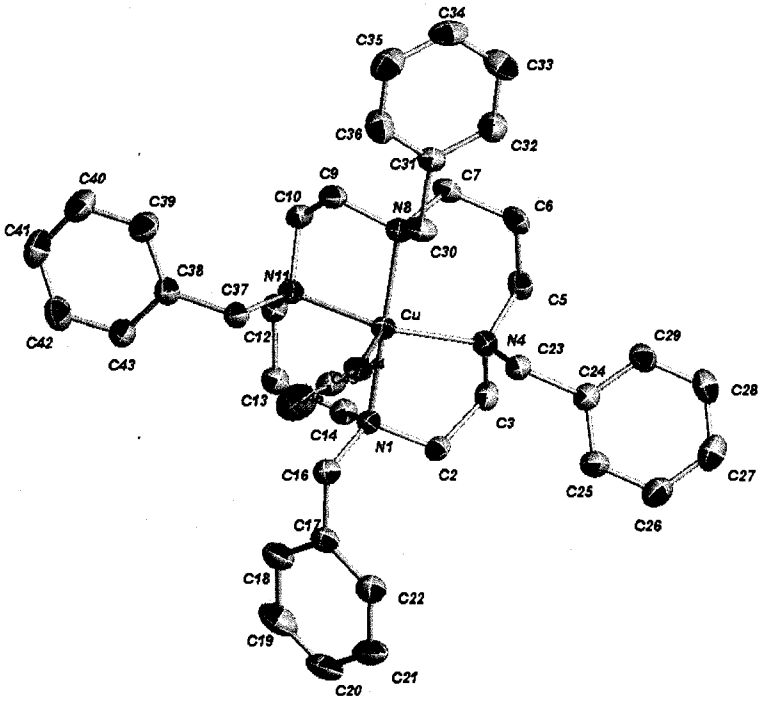

Figure 3.2. ORTEP representation of CuL^1. Hydrogens omitted for clarity.

	Lengths		Angles		Angles
Cu-N(44)	2.194(2)	N(4)-Cu-N(11)	150.69(7)	N(8)-Cu-N(1)	176.94(7)
Cu-N(1)	2.158(2)	N(4)-Cu-N(8)	93.37(7)	N(4)-Cu-N(44)	108.32(7)
Cu-N(4)	2.092(2)	N(11)-Cu-N(8)	85.92(7)	N(11)-Cu-N(44)	100.98(8)
Cu-N(8)	2.131(2)	N(4)-Cu-N(1)	85.87(7)	N(8)-Cu-N(44)	91.78(7)
Cu-N(11)	2.103(2)	N(11)-Cu-N(1)	93.29(7)	N(1)-Cu-N(44)	91.27(7)

Table 3.2. Selected bond distances (Å) and bond angles (°) for CuL^1

Empirical formula	$C_{46}H_{60}Cl_2CuN_8O_8$
Formula weight	987.46
***a, b, c* (Å); ß (°)**	32.557(16), 9.871(4), 29.733(13); 93.579(12)
V, Å^3	9537(8)
Z	8
D_{calc}, Mg m^{-3}	1.375
Absorption coefficient, mm^{-1}	0.631
***T*, K**	173 ± 1
Theta Range for Data Collection (°)	1.25 to 27.50
Crystal system	Monoclinic
Space group	C2/c
Total reflections	31988
Independent reflections	10700 [R(int) = 0.0464]
Parameters	571
Final R indices [I>2sigma(I)][a]	R1 = 0.0435, wR2 = 0.1011

R indices (all data)[a]	R1 = 0.0743, wR2 = 0.1074
Goodness-of-fit on F^2	1.000

[a] $R1 = \Sigma \| F_o | - | F_c \| / \Sigma | F_o |$; $wR2 = (\Sigma[w(F_o^2-F_c^2)^2]/\Sigma[F_o^4])^{1/2}$

Table 3.3. X-ray crystallographic data for CuL^1.

3.2.2.2. [(L^3)Cu(NCMe)](ClO_4)$_2$ • MeCN: ***CuL^3***

X-ray quality green single crystals of CuL^3 were grown *via* diffusion of diethyl ether into a concentrated acetonitrile solution of $[Cu^{II}(L^3)](ClO_4)_2$. An ORTEP depiction of the copper complex is shown in Figure 3.3, and relevant bond distances and bond angles are given in Table 3.4. Refinement details and other crystallographic data are presented in Table 3.5. The overall geometry of copper centre is square pyramidal, with a solvent molecule, acetonitrile, taking up the axial position.

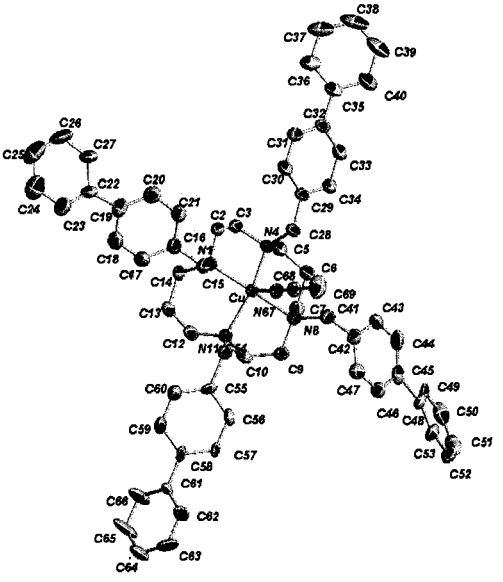

Figure 3.3. ORTEP representation of CuL^3. Hydrogens omitted for clarity.

	Lengths		Angles		Angles
Cu-N(67)	2.178(3)	N(4)-Cu-N(11)	151.17(10)	N(1)-Cu-N(8)	176.74(10)
Cu-N(1)	2.130(3)	N(4)-Cu-N(1)	85.92(11)	N(4)-Cu-N(67)	104.46(10)
Cu-N(4)	2.095(3)	N(11)-Cu-N(1)	93.24(10)	N(11)-Cu-N(67)	104.36(11)
Cu-N(8)	2.163(3)	N(4)-Cu-N(8)	93.46(11)	N(1)-Cu-N(67)	93.15(10)
Cu-N(11)	2.097(3)	N(11)-Cu-N(8)	85.76(10)	N(8)-Cu-N(67)	90.10(10)

Table 3.4. Selected bond distances (Å) and bond angles (°) for CuL^3.

Empirical formula	$C_{66}H_{70}Cl_2CuN_6O_8$
Formula weight	1209.72
***a, b, c* (Å); ß (°)**	13.3972(14), 16.8602(18), 16.8745(18); 66.626(2)
V, Å^3	2988.6(5)
Z	8
D_{calc}, Mg m^{-3}	1.344
Absorption coefficient, mm^{-1}	0.516
***T*, K**	198 ± 1
Theta Range for Data Collection (°)	1.45 to 27.49
Crystal system	Triclinic
Space group	P-1
Total reflections	20875
Independent reflections	12960 [R(int) = 0.0284]
Parameters	840

Final R indices [I>2sigma(I)][a]	R1 = 0.0533, wR2 = 0.1225
R indices (all data)[a]	R1 = 0.1103, wR2 = 0.1534
Goodness-of-fit on F^2	1.028

[a] $R1 = \Sigma \| |F_o| - |F_c| | / \Sigma |F_o|$; $wR2 = (\Sigma[w(F_o^2-F_c^2)^2]/\Sigma[F_o^4])^{1/2}$

Table 3.5. X-ray crystallographic data for CuL^3.

3.3. Attempted Synthesis of Nickel Pendant Arm Macrocyclic Complexes

Addition of $L^1 - L^3$ to nickel (II) perchlorate, using the same method as for the copper complexes mentioned above, resulted in the formation of the yellow square planar nickel complexes in solution. However, the complexes were unstable, and decomposition to nickel hydroxide occurred upon removal of the solvent.

At first glance, these results seem surprising; after all, the nickel(II) cation, with its radius of 83 pm, is similar in size to that of the copper(II) cation (87 pm). However, the coordination geometries of these two metal centres are remarkably different. Nickel, a d^8 metal, prefers a square planar or octahedral environment. Copper, a d^9 metal, is more flexible in its coordination geometries, being commonly found in octahedral, tetragonally distorted octahedral, square pyramidal, square planar, and trigonal bipyramidal geometries.[56]

It can be imagined that the bulky pendant arms coordinated to the nitrogen donor atoms of the cyclam backbone introduce steric interference to the complexing metal centre. Because copper is able to take up so many different coordination geometries, the square pyramidal complex, with a solvent acetonitrile molecule in the axial coordination site is quickly formed as both the kinetic and thermodynamic product. Nickel, however, is most stable in a square planar or octahedral environment, in which the nickel centre is

positioned directly in the plane formed by the four nitrogen donor atoms. Due to the steric hindrance of the bulky pendant arms, the nickel can not penetrate to the plane of the macrocycle, and is thus held by weak coordination in unstable coordination geometry (most likely square pyramidal). The instability of nickel species in a coordination environment other than square planar or octahedral is thought to be responsible for the inability to isolate this complex in the solid state.

Similar findings have been reported previously by the Lindoy group[29] who in 2003, synthesized a series of similar pendant arm macrocycles based on cyclam (See Figure 3.3), with the L^5 ligand being identical to the L^1 ligand synthesized in this work. The group reported the successful synthesis of copper complexes with $L^1 - L^5$; however, the nickel complex of L^5 could not be isolated in the solid state, in agreement with the findings of this present work.

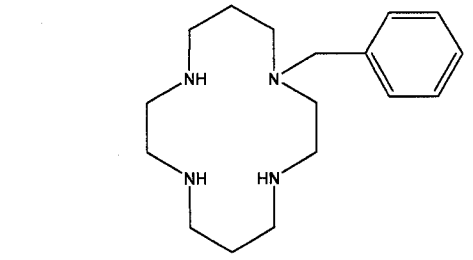

L^1

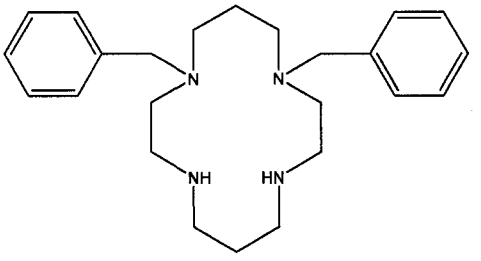

L^2

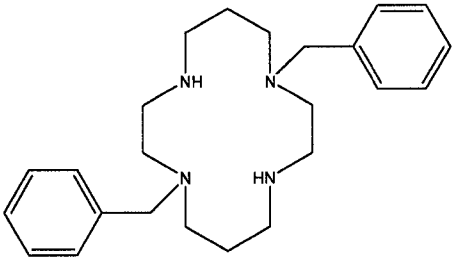

L^3

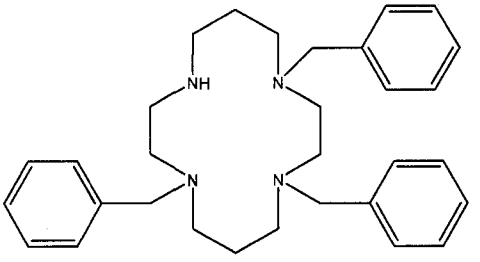

L^4

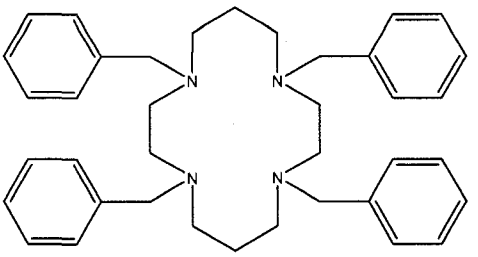

L^5

Figure 3.3. N-benzylated complexes of cyclam synthesized by Lindoy *et al.*[29]

3.4. Hindrances to Future Work and Consequent Redirection

Though the copper complexes of $L_1 - L_3$ were synthesized successfully, studies of electron transfer reactions using these sterically bulky systems were severely hampered by the extremely poor solubility of these complexes in water. In fact, the copper complexes were found to dissolve in only one solvent – acetonitrile. Since non-aqueous solvent systems could damage the stopped-flow instrument, kinetic studies involving these systems were not possible. It was assumed that the nickel complexes would have similar solubility; therefore, further attempts to isolate the nickel complexes were abandoned.

Although the pendant arm macrocyclic complexes are interesting from a synthetic point of view, they are not useful as probes for determining the effect of steric bulk on the rate of electron transfer, which is a key focus of this project. Fortunately, a second method of enforcing long-distance electron transfer reactions using the host molecule cucurbit[8]uril is available. This approach will be discussed in Chapter 4.

Chapter 4 – Results & Discussion

Cucurbit[8]uril Inclusion Complexes

4.1. Synthesis of Cucurbit[8]uril Inclusion Complexes

Since the metallated pendant arm complexes were not suitable for kinetic studies, a new method for including a redox active metal centre within a sterically bulky system reminiscent of metalloenzymes was necessary. Such a method presented itself with reports of the large host molecule, cucurbit[8]uril, which was capable of forming inclusion complexes with metal macrocycles.[46,47] The steric bulk of the cucurbit[8]uril ring would effectively isolate the redox-active metal centre, and the steric effects on electron transfer rates could be monitored *via* stopped-flow spectrophotometry. Also a key objective in this part of the project was to modify the reported literature method for the synthesis of these complexes, as the current procedure precludes the introduction of certain macrocyclic complexes into the cavity of cucurbit[8]uril.

4.1.1. Literature Method for the Synthesis of Macrocyclic Inclusion Complexes with Cucurbit[8]uril

The synthesis of supramolecular complexes involving the inclusion of metal macrocycles within the cavity of cucurbit[8]uril began in 2001 with reports by Kim *et al.*[46] of the inclusion compounds {[Cu(cyclam)]@CB[8]}$(NO_3)_2$ and {[Cu(cyclen)]@CB[8]}$(NO_3)_2$. Reports of a related inclusion compound, {[Ni(cyclam)]@CB[8]}$(NO_3)_2$ followed soon after by the Fedin group.[47] The synthetic methodology for these inclusion complexes was composed of two consecutive steps (see

Scheme 4.1). Step one involved the reaction of CB[8] with protonated cyclam to form the inclusion complex cyclam@CB[8] • 4 HCl. Step two involved metallation of the inclusion complex by reaction with an excess of alkali metal salt.

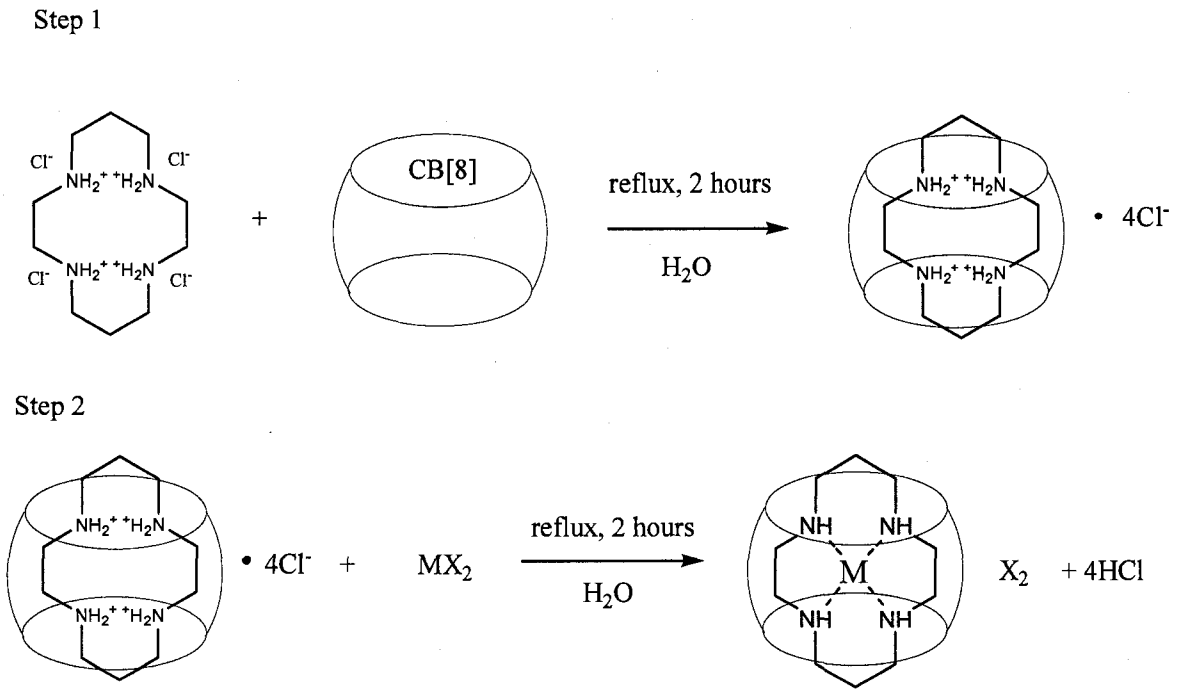

Scheme 4.1. Schematic showing Kim's two-step method for the synthesis of inclusion complexes with cucurbit[8]uril.

Direct synthesis through the addition of pre-metallated cyclen to an aqueous solution of CB[8] was attempted by Kim *et al.* for the $[Cu(cyclen)](NO_3)_2$ system; however, it was stated that attempts to do so "failed even under forcing conditions."[46] The reasoning for the failed reaction was given as the increased rigidity of the cyclen ring when complexed to a metal centre. Presumably, the ring had to be able to bend and twist in order to orient itself within the cucurbituril ring. There is no record of an attempt to directly include a metallated macrocycle with a larger ring-size within cucurbit[8]uril.

Presumably, it was supposed that if the smaller cyclen ring could not be included while complexed to a metal centre, inclusion of the larger 14-membered metalated cyclam ring would also be impossible.

The synthesis of {[Ni(cyclam)]@CB[8]}$(NO_3)_2$ *via* Kim's two step method was repeated and a crystal structure was obtained. Though the crystal structure was not suitable for publication, it clearly showed Ni^{II}(cyclam) included within the cavity of CB[8]. As alluded to earlier, this two-step synthetic method is rather limiting; many macrocycles are unstable when not complexed to a metal centre. Of particular interest to this work is the inclusion of a well-studied outer-sphere oxidant – $Ni(tacn)_2$ (see Figure 4.1) into the cavity of CB[8].

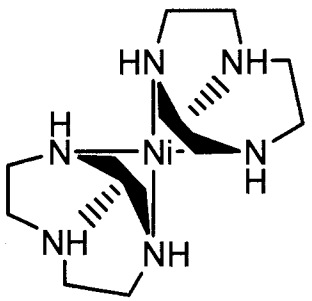

Figure 4.1. Structural representation of $Ni^{II}(tacn)_2$

This macrocyclic complex is composed of two 1,4,7-triazacyclononane (tacn) ligands coordinated to a nickel centre; inclusion of such a species *via* a two-step method would be very difficult, if not impossible. For this reason, a one-pot synthesis of [Ni(cyclam)]@CB[8]Cl_2 was developed in this work, and is reported below.

4.1.2. "One Pot" Synthesis of {[Ni(cyclam)]@CB[8]}Cl_2

The direct, one-pot reaction of an excess of Ni(cyclam)Cl_2 with cucurbit[8]uril (see Scheme 4.2) was found to yield yellow crystals that were identical to those obtained by the two-step method proposed by the Kim group.[46] See section 4.3.2 for crystallography details.

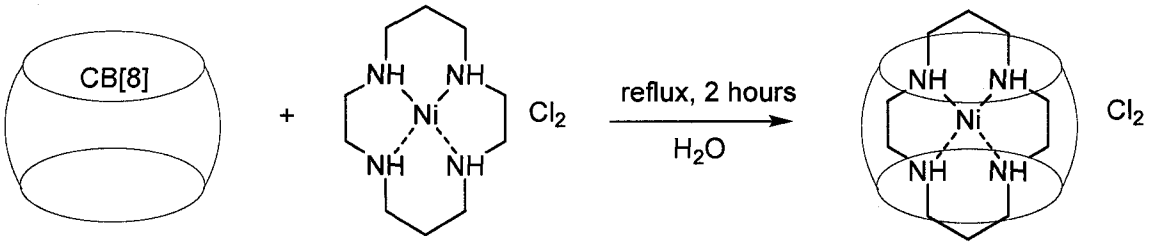

Scheme 4.2. Schematic showing direct "one-pot" synthesis of [Ni(cyclam)]@CB[8]} Cl_2

Why was it impossible to directly include the metallated cyclen complex within the cavity of cucurbit[8]uril? The answer most probably lies in the geometry of Cu^{II}(cyclen). It has long been established that the smaller cavity size of the twelve-membered cyclen ring as compared to that of the fourteen-membered cyclam ring prevents the copper atom from residing in the plane of the nitrogen donor atoms; rather, it is located 0.5 Å above the plane, so that the complex takes up a square pyramidal geometry.[25] This orientation of the copper centre makes it inherently less stable. It can be imagined that the bending and twisting of the macrocycle during complexation with cucurbit[8]uril induces strain on the macrocyclic complex; if the metal is situated above the cavity of the macrocycle, it is likely that this strain could cause the dissociation of the metal centre from the cyclen ring. Additional experimentation would be necessary to substantiate this proposed de-metallation.

It is of great interest that the inclusion of square planar nickel cyclam within the cavity of cucurbit[8]uril can be accomplished *via* a one-pot, direct method, contrary to literature reports. This is a significant and exciting contribution to the host-guest chemistry of metallated macrocycles. Synthesis following the two-step method is viable but time-consuming. Cucurbit[8]uril is a precious reagent; performing the reaction in a single step reduces the chance of product loss through transferal from one reaction flask to another. Furthermore, and most importantly, a direct, one-step synthesis provides new opportunities for the inclusion of macrocycles that are unstable when not complexed to a metal centre, such as the previously mentioned $Ni^{II}(tacn)_2$ macrocycle.

4.1.3. Synthesis of {[Ni(tacn)$_2$]@CB[8]}(ClO$_4$)$_2$

Synthesis of the inclusion complex $\{[Ni(tacn)_2]@CB[8]\}(ClO_4)_2$ was attempted according to Scheme 4.3. Crystals were grown *via* slow evaporation from hot aqueous solution; however, the crystals were not suitable for X-ray diffraction. The compound was characterized in solution by electrospray ionization mass spectroscopy (refer to Section 4.2.2); however, without a crystal structure it is difficult to assess the identity of the product in the solid state.

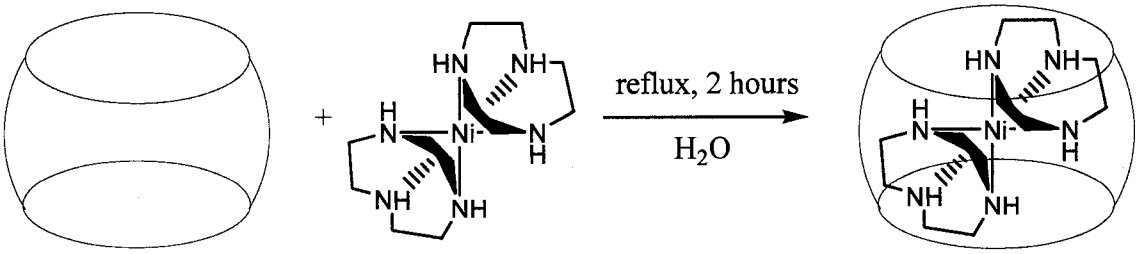

Scheme 4.3. Schematic representing synthesis of $\{[Ni(tacn)_2]@CB[8]\}(ClO_4)_2$

4.1.4. *Synthesis of (R,S,R,S){[Cu(cyclam)$(OH_2)_2$]@CB[8]} $(NO_3)_2 \cdot 17H_2O$ – Copper^{II}cyclam in the Trans-I Configuration*

Though the synthesis of {[Cu(cyclam)$(OH_2)_2$]@CB[8]}$(NO_3)_2$ was reported by the Kim group in 2001,[46] a crystal structure of this complex has not been deposited on the Cambridge Structural Database. It was of interest, therefore, to synthesize this compound and to report its crystal structure. The synthesis of the inclusion complex, [Cu(cyclam)$(OH_2)_2$]@CB[8] is illustrated schematically below and has been described previously (see Section 2.2.12). Large X-ray quality single crystals were attained *via* slow evaporation of the solvent (water) over a period of four days. Refer to Section 4.3.3 for crystallography details.

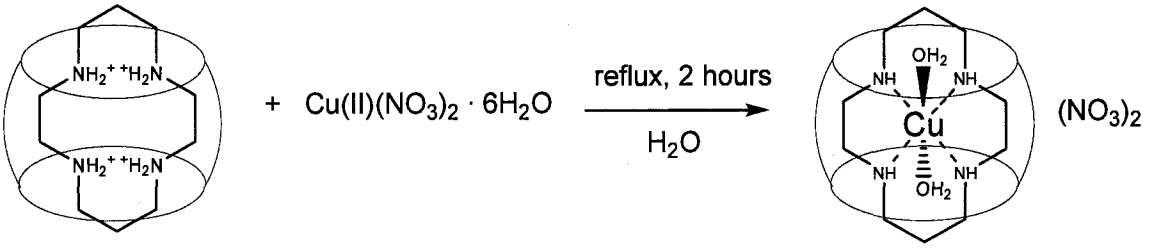

Scheme 4.4. Schematic illustrating synthesis of {[Cu(cyclam)$(OH_2)_2$]@CB[8]}

The [Cu(cyclam)$(OH_2)_2$]@CB[8] inclusion complex exhibits several interesting features. The crystal packing shows only one third of the cucurbit[8]uril molecules to be occupied by copper(II) cyclam macrocycles. This incomplete occupancy persists even though the cucurbit[8]uril is refluxed with a six-fold excess of protonated cyclam and copper salt. A water molecule coordinates to each axial position, so that the copper centre is found in a tetragonally distorted octahedral environment. Most striking is the fact that the copper(II)cyclam macrocycle takes up the unusual *trans*-I conformation. A second point of interest is that, while the nickel cyclam guest is fully included in the

[Ni(cyclam)]@CB[8] system, the copper cyclam guest is found to be partially extruded from the host cavity in the solid state. This may be due to the steric constraints of the *trans*-I conformation.

In 1965, Bosnich, Poon, and Tobe announced the synthesis of a variety of cobalt complexes with the [then] newly discovered macrocyclic ligand 1,4,8,11-tetraazacyclotetradecane (cyclam). In order to characterize the stereochemistry of these newly synthesized complexes, a naming scheme for the five possible configurational isomers of cyclam was introduced (see Figure 4.3).[55] This scheme, in which the positive signs are indicative of hydrogens orientated above the plane of the cyclam ring and the negative signs are indicative of hydrogens orientated below the plane of the cyclam ring, has remained valid and functional to the present day.[57] The various configurations can be denoted either by the designations trans-I to trans-V, respectively, or by the R/S designations of the tetrahedral, asymmetric nitrogen centres.

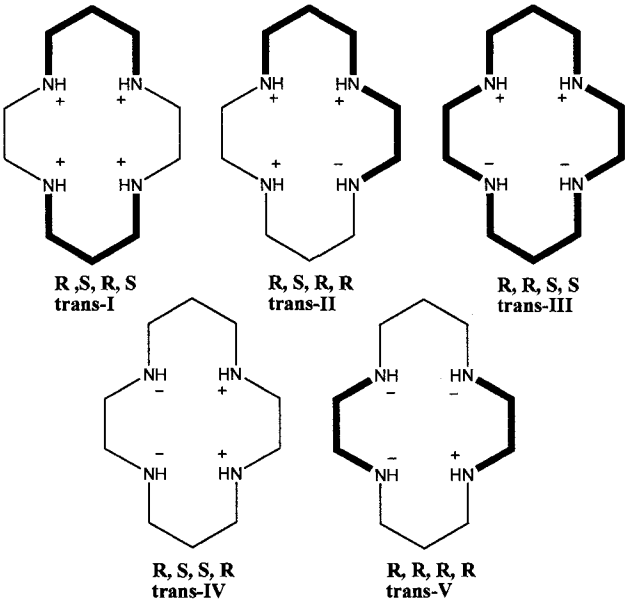

Figure 4.3. Configurational isomers of cyclam and their designations. Figure adapted from reference 62.

As postulated by Bosnich, Poon, and Tobe,[55] the most stable conformation for the free, uncomplexed cyclam ligand is the trans-III isomer. This isomer respresents a conformation in which the hydrogens on the nitrogen donor atoms undergo minimal steric clashes. In 1965, Bosnich *et al.* found that nickel cyclam with two axial chloride atoms is also found in the trans-III conformation.[58] By 1976, it was well-accepted that the trans-III configuration was the most stable isomer of metallated cyclam complexes.[59] This is to be expected, as the trans-III conformer allows the hexameric rings to be in their most stable chair configuration, while the pentameric rings assume the stable gauche form.

Configurational isomers other than the trans-III form have been reported; however, these involve metal complexes of *substituted* cyclam derivatives. As the first example of this phenomenon, Barefield *et al.* reported the structure of a nickel complex of N-tetramethylcyclam, Ni^{II}(TMC), in which the four methyl substituents are orientated above the plane of the cyclam ring, resulting in the trans-I configuration.[59,60,61,] It was believed that the trans-I configuration was formed as a result of the inability of tertiary amines to undergo isomerization.

To this day, the elucidation of rare configurational isomers of metal cyclam-based complexes has remained a topic of considerable interest. A trans-IV nickel complex of a substituted cyclam derivative was announced in 2007 by Soneta *et al.*[27] Much research has been applied to the isolation of trans-I nickel cyclam in solid state and its isomerization to the trans-III form by oxidation under acidic conditions.[57]

In 1999, Zimmer *et al.* undertook a cluster analysis of the copper complexes involving cyclam and its derivatives; all of the structures deposited on the Cambridge

Structural Database were included in this study.[56] As reported earlier by Hancock *et al.*[25], Zimmer found that Cu^{II}(cyclam) exists only in the stable trans-III form. Copper complexes of 1,4,8,11-substituted cyclam were commonly found in the trans-I form, and as a general rule, octahedral complexes are more commonly found in the trans-III form than in the trans-I form. Of the octahedral complexes studied, 90.2% were found to take up the trans-III form. This trend had also been noticed earlier in a similar study involving Ni^{II}(cyclam) configurational isomers.[62] It was postulated that substituents (which were always present in complexes of trans-I configurations) would sterically clash with the species (solvent molecules or substituents) occupying the axial positons as shown in Figure 4.4; therefore, an octahedral geometry is the least favoured geometry for trans-I configurational isomers.

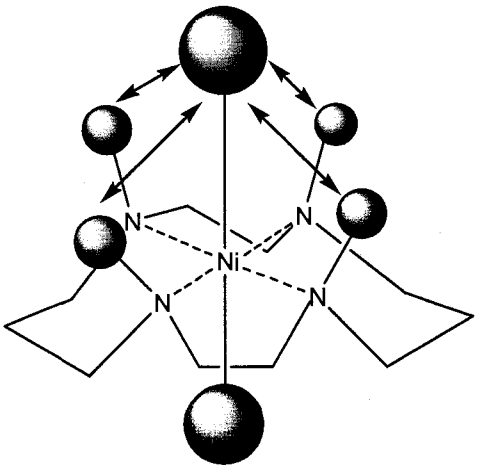

Figure 4.4. Illustration of the steric repulsion present in the trans-I configuration of an octahedral N-substituted nickel macrocycle. Figure adapted from reference 62.

The crystal structure of [Cu(cyclam)$(OH_2)_2$]@CB[8], then, is the first documented structure of an unsubstituted copper^{II} cyclam complex in the trans-I configuration. This

is an exciting and significant result. Furthermore, the copper atom is found in a tetragonally distorted octahedral environment, which for copper, a d^9 metal, is not unusual. What is unusual is the fact that the trans-I configuration persists even though octahedral complexes in trans-I configurations are exceedingly rare, as discussed above. Presumably, the octahedral geometry is allowed due to the fact that there are no substituents present to sterically hinder the coordination of axial ligands.

In contrast, the crystal structure of protonated cyclam within CB[8] and that of Ni^{II}(cyclam) within CB[8] (See Sections 4.2.1 and 4.2.2) show both the free cyclam ligand and the metallated nickel complex in the expected trans-III configuration. Could the unexpected trans-I configuration of the [Cu(cyclam)$(OH_2)_2$]@CB[8] lend insight to the mechanism of metal complexation?

Since the discovery of the macrocyclic effect, much research has been devoted to the elucidation of the mechanism of ligand complexation with the metal center.[63,64,65,66] It has been generally accepted that a step-wise mechanism is followed, in which the nitrogen donor atoms of the cyclic ligand coordinate to the metal centre one at a time, with concomitant desolvation of the metal centre (See Scheme 4.4).[66]

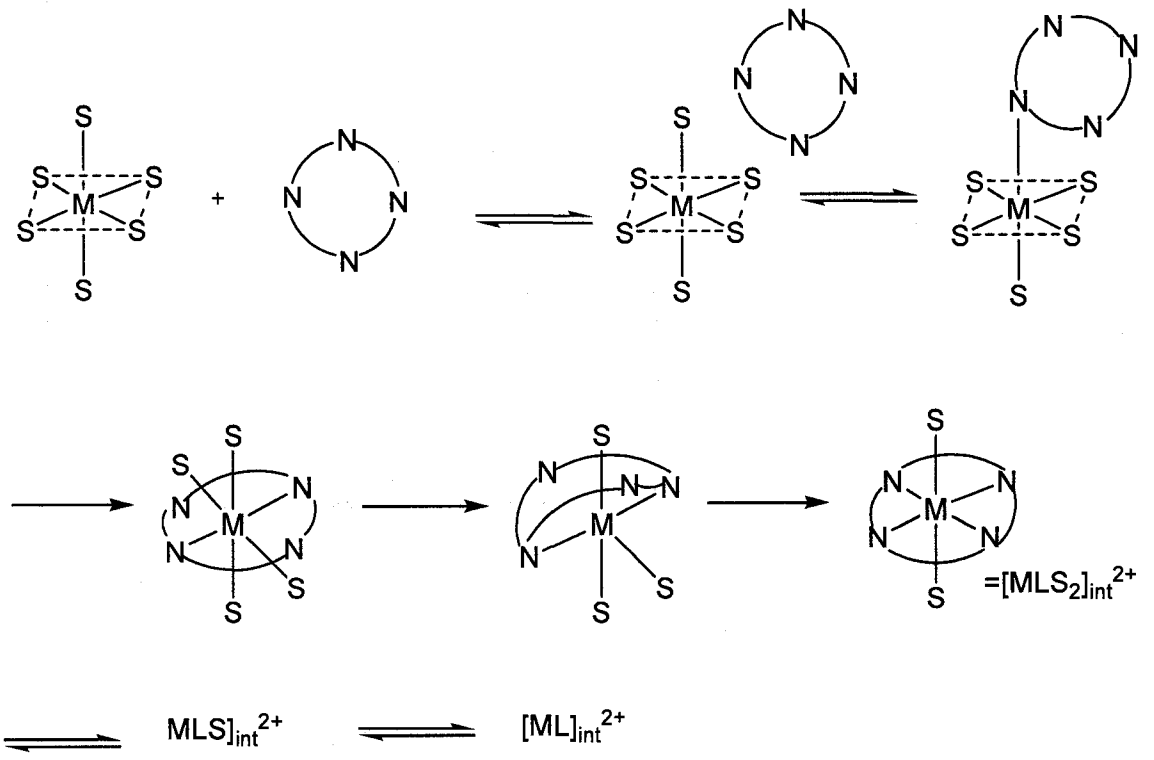

Scheme 4.4. Schematic showing the stepwise coordination of a cyclic ligand to metal centre. Figure adapted from reference 66.

The formation of metal macrocyclic complexes has been described as consisting of two major kinetic pathways, k_1 and k_2, where k_1 is a second-order rate constant corresponding to the fast formation of an intermediate species and k_2 is a first order rate constant corresponding to the slow rearrangement of the intermediate species to its most favoured configurational isomer (see Scheme 4.5).[66]

$$M^{2+} + L \underset{\text{fast}}{\overset{k_1(M^{-1}s^{-1})}{\rightleftharpoons}} [ML]_{int}$$

$$[ML]_{int} \underset{\text{slow}}{\overset{k_2\,(s^{-1})}{\rightleftharpoons}} [ML]$$

Scheme 4.5. Schematic showing the two major kinetic pathways involved in the formation of metal macrocyclic complexes.

Kim's two-step method for inserting metal macrocycles within the cavity of cucurbit[8]uril provides a view into metal complexation within a unique environment. Given the steric contraints of the cucurbit[8]uril ring, it seems unlikely that a step-wise mechanism of metal complexation is followed. It is tempting to think that the metal coordinates to the cyclam ring in one step. However, the fact that Cu^{II}(cyclam) is found in the trans-I configuration within the cucurbit[8]uril ring, while the uncomplexed cyclam macrocycle is found in the trans-III configuration lends support to the step-wise coordination of the metal centre to the cucurbit[8]uril ring. Further experimentation (such as encapsulating Cu^{II}(cyclam) within cucurbit[8]uril *via* the direct one-pot method) would be necessary to further substantiate this claim. Why the encapsulated Cu^{II}(cyclam) prefers the trans-I configuration while the encapsulated Ni^{II}(cyclam) prefers the trans-III configuration is unknown at this time.

4.2. Characterization

Cyclam and cucurbit[8]uril were characterized *via* NMR spectroscopy. The inclusion complexes [Ni(tacn)$_2$]@CB[8] and [Ni(cyclam)]@CB[8] were characterized in solution *via* electrospray ionization mass spectroscopy. X-ray crystal structures of the

cucurbit[8]uril inclusion complexes – cyclam@CB[8], [Ni(cyclam)]@CB[8], and [Cu(cyclam)]@CB[8] – were obtained and further confirmed the successful synthesis of cyclam and cucurbit[8]uril.

4.2.1. NMR Spectroscopy

The identity of cyclam (see Figure 4.5) was initially confirmed through ^{1}H NMR spectroscopy. The NMR data has been summarized in Table 4.1.

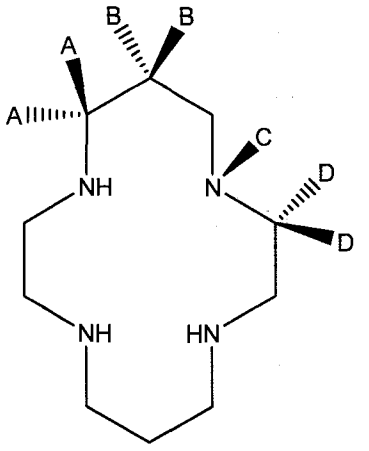

Figure 4.5. Structural representation of cyclam. Non-equivalent hydrogens labeled A-D.

Solvent	Proton	Chemical Shift (ppm)/ Multiplicity/Number of Protons
DCl	Proton A	2.59 / triplet / 8H
	Proton B	1.53 / quintet / 4H
	Proton C	n/a (exchanges with deuterium)
	Proton D	2.85 / singlet / 8H

Table 4.1. ^{1}H NMR data for cyclam (300 MHz)

The identity of cucurbit[8]uril (See Figure 4.5) was also confirmed *via* ^{1}H and ^{13}C NMR spectroscopy. The NMR data has been tabulated and compared to the literature data for cucurbit[8]uril[67] in Table 4.2 and Table 4.3, respectively.

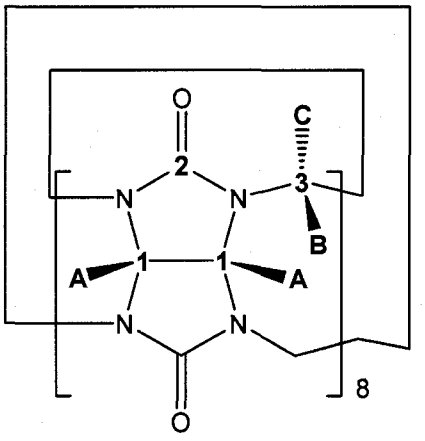

Figure 4.6. Structural representation of cucurbit[8]uril; carbons labeled 1- 3; protons labeled A-C

Solvent	**Proton**	**Chemical Shift (ppm) / Multiplicity/ Number of Protons**
D_2O/~0.2M CsCl	A	5.59 / singlet / 16 protons
	B	5.70 / doublet / 16 protons
	C	4.30 / doublet / 16 protons
Solvent	**Carbon**	**Chemical Shift (ppm)**
D_2O/~0.2M CsCl	1	51.5
	2	156.5
	3	70.3

Table 4.2. NMR data (^{1}H and ^{13}C) for synthesized CB[8] (500 MHz)

Solvent	Proton	Chemical Shift (ppm) / Multplicity/ Number of Protons
D_2O/0.2M CsCl	A	5.61 / singlet / 16 protons
	B	5.80 / doublet / 16 protons
	C	4.30 / doublet / 16 protons
Solvent	**Carbon**	**Chemical Shift (ppm)**
D_2O/0.2M CsCl	1	53.26
	2	157.65
	3	72.08

Table 4.3. Literature values for ^{1}H and ^{13}C NMR of cucurbit[8]uril (300 MHz)

4.2.2. Electrospray Ionization Mass Spectroscopy

The inclusion complexes [Ni(cyclam)]@CB[8] and [Ni(tacn)$_2$]@CB[8] were characterized in aqueous solution *via* electropspray ionization mass spectroscopy. The spectrum for [Ni(cyclam)]@CB[8] shows the most intense ion peak (m/z) of 794.13, which correlates very well with the expected m/z value for the species {CB[8] + Ni(cyclam)}$^{2+}$ (794.68). The spectrum for [Ni(tacn)$_2$]@CB[8] shows the most intense ion peak (*m/z*) of 822.58, which is consistent with the expected m/z value for the {CB[8] + Ni(tacn)$_2$}$^{2+}$species (823.23).

4.2.3. X-Ray Crystallography

The X-ray crystal structures of cyclam@CB[8], {[Ni(cyclam)]@CB[8]}Cl_2 and {[Cu(cyclam)]@CB[8]}$(NO_3)_2$ are reported below. {[Cu(cyclam)]@CB[8]}$(NO_3)_2$ was synthesized according to the two-step method proposed by the Kim group,[46] while {[Ni(cyclam)]@CB[8]}Cl_2 was synthesized according to a direct, one-step method.

4.2.3.1. $C_{48}H_{48}N_{32}O_{16}$, $[C_{10}H_{26}N_4][Cl]_2 \bullet 9\ H_2O$: ***Cyclam@CB[8] • 2HCl***

X-ray quality large colourless crystals of cyclam@CB[8] • 2HCl were obtained *via* slow evaporation from a saturated aqueous solution over a period of one month. ORTEP depictions of cyclam encapsulated within cucurbit[8]uril are shown in Figure 4.7, and refinement details are presented in Table 4.4. Three of the cyclam methylene groups are disordered and were refined isotropically. The cyclam ring is found in the trans-III configuration, which has long been recognized as the most stable configurational isomer of cyclam.[55] The cyclam macrocycle is fully encapsulated within the cucurbit[8]uril ring. This crystal structure has previously been reported by the Kim group.[46]

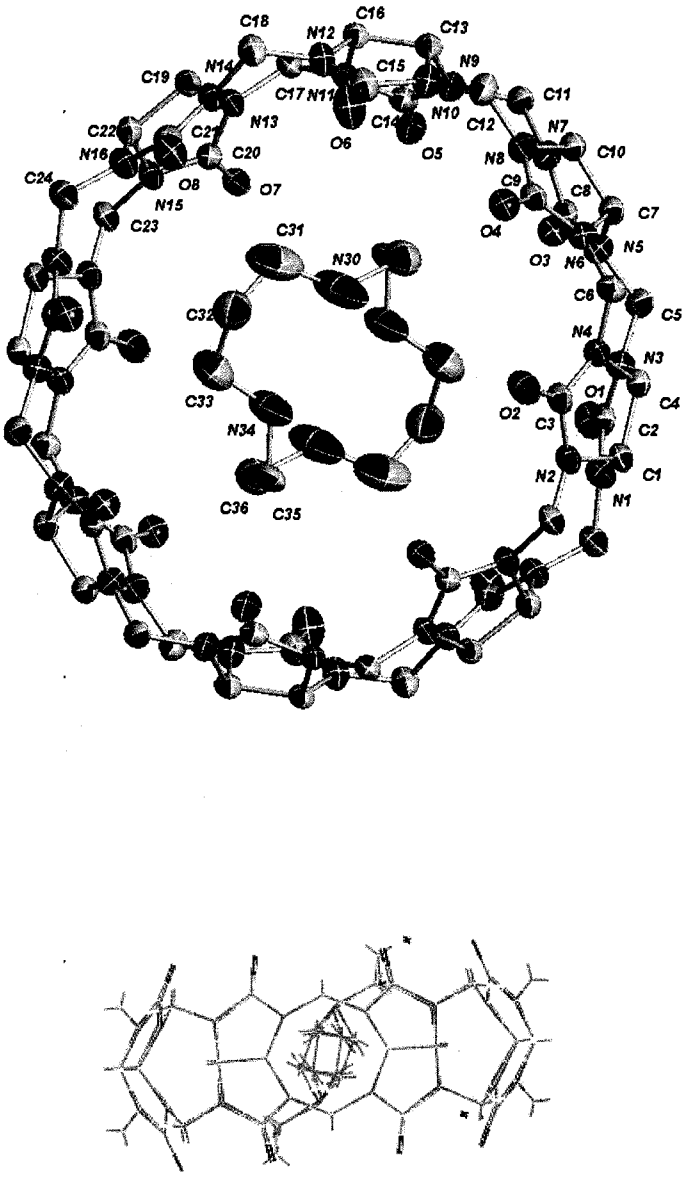

Figure 4.7. ORTEP depictions of cyclam@CB[8]. Hydrogens omitted for clarity. (Above = top view; below = side view). Side view shows cyclam in stable trans-III configuration.

Empirical formula	$C_{58}H_{92}Cl_2N_{36}O_{25}$
Formula weight	1764.58
***a, b, c* (Å); ß (°)**	29.284(4), 29.284(4), 26.383(8); 90
V, Å^3	19594(7)
Z	9
D_{calc}, Mg m^{-3}	1.346
Absorption coefficient, mm^{-1}	0.165
***T*, K**	173 ± 1
Theta range for data collection (°)	1.11 to 27.50
Crystal system	Rhombohedral
Space group	R-3
Total reflections	45729
Independent reflections	9872 [R(int) = 0.0464]
Parameters	529
Final R indices [I>2sigma(I)][a]	R1 = 0.0572, wR2 = 0.1675
R indices (all data)[a]	R1 = 0.0926, wR2 = 0.1827
Goodness-of-fit on F^2	1.078

[a] $R1 = \Sigma \| \|F_o\| - \|F_c\| \| / \Sigma \|F_o\|$; $wR2 = (\Sigma[w(F_o^2-F_c^2)^2]/\Sigma[F_o^4])^{1/2}$

Table 4.4. X-ray crystallographic data for cyclam@CB[8].

4.2.3.2. $[Ni(C_{10}H_{24}N_4)][Cl]_2(C_{48}H_{48}N_{32}O_{16}) \bullet 10\ H_2O$: ***{[Ni(cyclam)]@CB[8]}Cl_2***

X-ray quality bright yellow single crystals of {[Ni(cyclam)]@CB[8]}Cl_2 were obtained *via* slow evaporation from a saturated aqueous solution. ORTEP depictions of the nickel cyclam complex encapsulated within cucurbit[8]uril are shown in Figure 4.8, and relevant bond distances and bond angles are given in Table 4.5. Refinement details and other crystallographic data are presented in Table 4.6. The Ni^{II}(cyclam) species is fully encapsulated within the cucurbit[8]uril ring, and the cyclam ring adopts the trans-III configuration, with the nickel centre being found in square planar geometry. This configurational isomer has been shown previously to be the most stable configuration for an unsubstituted Ni^{II}cyclam macrocycle.[59] The inclusion complex {[Ni(cyclam])@CB[8]}Cl_2 has been previously reported by the Kim group.[46]

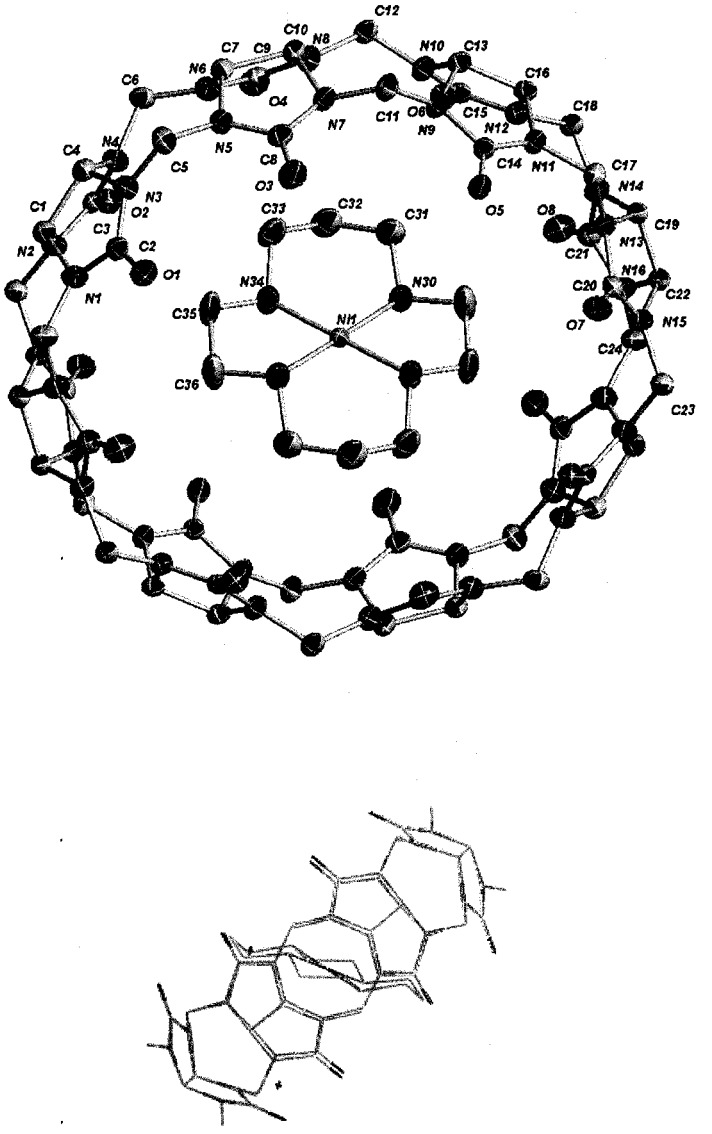

Figure 4.8. ORTEP depictions of [Ni(cyclam)]@CB[8]. Hydrogens omitted for clarity. (Above = top view; below = side view). Side view shows cyclam in stable trans-III configuration.

	Lengths		Angles
Ni(1)-N(34)#1	1.9242(19)	N(34)#1-Ni(1)-N(34)	180.0
Ni(1)-N(34)	1.9242(19)	N(34)#1-Ni(1)-N(30)	86.76(8)
Ni(1)-N(30)#1	1.9248(19)	N(34)#1-Ni(1)-N(30)	93.24(8)
Ni(1)-N(30)	1.9248(19)	N(34)-Ni(1)-N(30)	93.24(8)
		N(34)-Ni(1)-N(30)#1	93.24(8)
		N(30)-Ni(1)-N(30)#1	180.0

Table 4.5. Selected bond distances (Å) and bond angles (°) for {[Ni(cyclam)]@CB[8]}Cl_2.

Empirical formula	$C_{58}H_{92}Cl_2N_{36}NiO_{26}$
Formula weight	1839.29
***a, b, c* (Å); ß (°)**	29.096(3), 29.096(3), 26.470(6); 90
V, Å^3	19407(5)
Z	9
D_{calc}, Mg m^{-3}	1.416
Absorption coefficient, mm^{-1}	0.380
***T*, K**	173 ± 1
2θ range (°)	1.40 to 27.49
Crystal system	Rhombohedral
Space group	R-3
Total reflections	45519
Independent reflections	9807 [R(int) = 0.0269]

Parameters	514
Final R indices [I>2sigma(I)][a]	R1 = 0.0498, wR2 = 0.1523
R indices (all data)[a]	R1 = 0.0561, wR2 = 0.1574
Goodness-of-fit on F^2	1.119

[a] $R1 = \Sigma \| |F_o| - |F_c| | / \Sigma |F_o|$; $wR2 = (\Sigma[w(F_o^2-F_c^2)^2]/\Sigma[F_o^4])^{1/2}$

Table 4.6. X-ray crystallographic data for {Ni(cyclam)]@CB[8]}Cl_2

4.2.3.3. $[(C_{48}H_{48}N_{32}O_{16})(C_{10}H_{26.6}CuN_4O_{1.30})][(NO_3)_2] \bullet 0.5(C_{48}H_{48}N_{32}O_{16}) \bullet 17(H_2O)$: ***{[Cu(cyclam)]@CB[8]}$(NO_3)_2$***

X-ray quality purple single crystals of Cu^{II}(cyclam) encapsulated within cucurbit[8]uril were obtained *via* slow evaporation from a saturated aqueous solution. ORTEP depictions of the copper cyclam complex is shown in Figure 4.9, and relevant bond distances and bond angles are given in Table 4.7. Refinement details and other crystallographic data are presented in Table 4.8. The Cu^{II}(cyclam) species is partially extruded from the cavity of cucurbit[8]uril, and the lattice structure shows only 1/2 of the cucurbit[8]uril molecules to be occupied by Cu^{II}(cyclam) macrocycles. In addition, the cyclam ring takes up the very unusual trans-I configuration, a phenomenon which is discussed in more detail in Section 4.1.4. The copper centre is found in a tetragonally distorted octahedral geometry, with two water molecules occupying the axial positions (Cu—N bonds = 2.00 Å; Cu—O bonds = 2.380 Å and 2.758 Å).

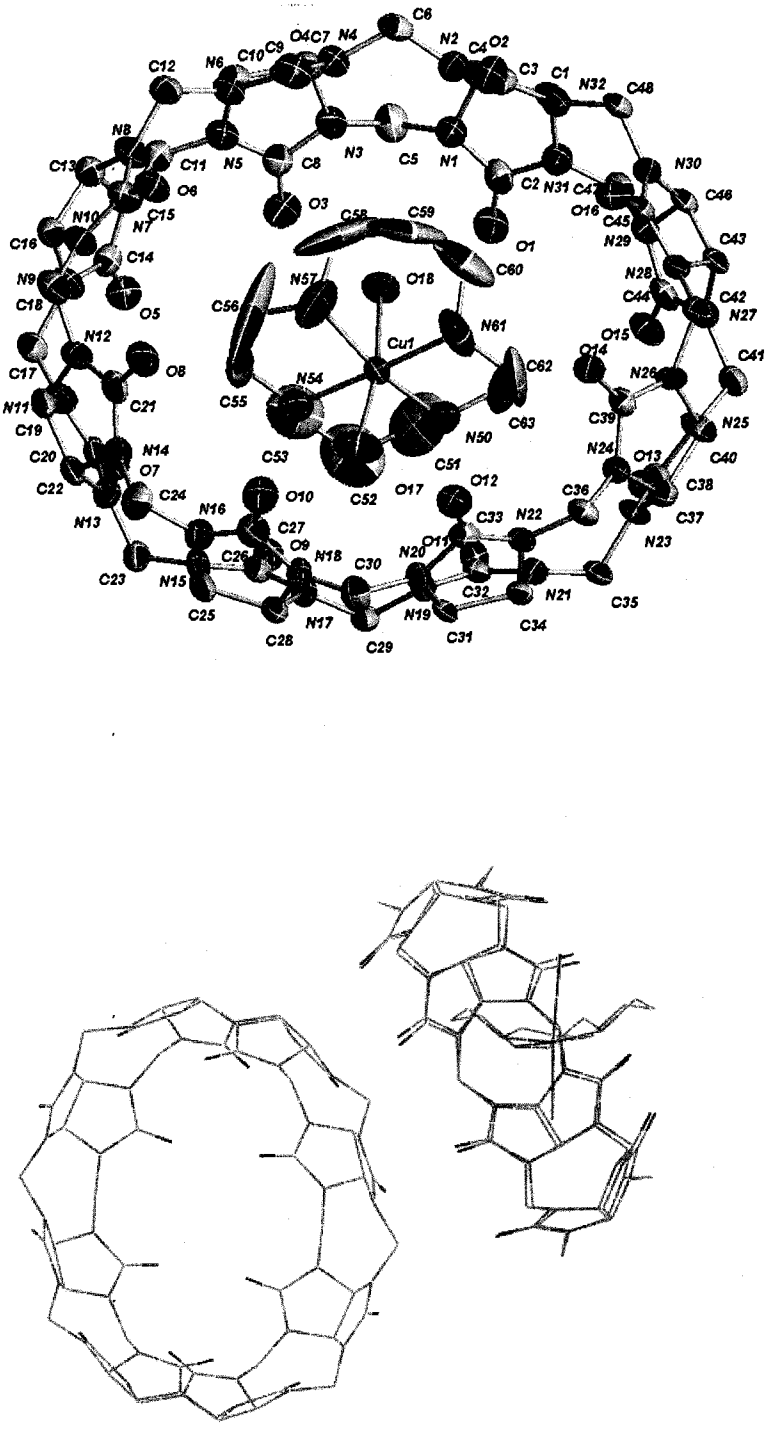

Figure 4.9. ORTEP depictions of [Ni(cyclam)]@CB[8]. Hydrogens omitted for clarity. (Above = top view; below = side view). Side view shows cyclam in the trans-I configuration, as well as an uncomplexed cucurbit[8]uril molecule in the crystal lattice.

	Length		Angle
Cu(1)-N(50	1.996(5)	N(50)-Cu(1)-N(61)	86.5(2)
Cu(1)-N(61)	2.006(5)	N(50)-Cu(1)-N(57)	166.4(2)
Cu(1)-N(57)	2.007(5)	N(61)-Cu(1)-N(57)	91.9(2)
Cu(1)-N(54)	2.018(4)	N(50)-Cu(1)-N(54)	94.8(2)
Cu(1)-O(17)	2.380(4)	N(61)-Cu(1)-N(54)	178.4(2)
Cu(1)-O(18)	2.758(12)	N(57)-Cu(1)-N(54)	86.67(19)
		N(50)-Cu(1)-O(17)	103.80(17)
		N(61)-Cu(1)-O(17)	90.51(18)

Table 4.7. Selected bond distances (Å) and bond angles (°) for {[Cu(cyclam)]@CB[8]}$(NO_3)_2$

Empirical formula	$C_{82}H_{33.15}CuN_{54}O_{48.30}$
Formula weight	2711.3
***a, b, c* (Å); ß (°)**	14.968(2), 24.109(3), 35.614(5); 101.882(2)
V, Å^3	12576(3)
Z	4
D_{calc}, Mg m^{-3}	1.432
Absorption coefficient, mm^{-1}	0.281
***T*, K**	198 ± 1
Theta Range for Data Collection (°)	1.03 to 27.50
Crystal system	Monoclinic
Space group	P2(1)/c

Total reflections	84649
Independent reflections	28159 [R(int) = 0.0538]
Parameters	1514
Final R indices [I>2sigma(I)][a]	R1 = 0.0817, wR2 = 0.2403
R indices (all data)[a]	R1 = 0.1357, wR2 = 0.2586
Goodness-of-fit on F^2	1.076

[a] $R1 = \Sigma \| |F_o| - |F_c| | / \Sigma |F_o|$; $wR2 = (\Sigma[w(F_o^2-F_c^2)^2]/\Sigma[F_o^4])^{1/2}$

Table 4.8. X-ray crystallographic data for {[Cu(cyclam)]@CB[8]}$(NO_3)_2$

4.3. Kinetics

As previously mentioned, the primary focus of this work is to study electron transfer reactions in sterically bulky synthetic systems that model more complicated biological systems. The cucurbituril inclusion complexes synthesized above provide prime candidates for such a study. Although free CB[8] is virtually insoluble in aqueous solutions, when complexed with positively charged metal macrocycles, the resulting inclusion complexes are water soluble at low concentrations. Therefore, as opposed to the copper macrocyclic compounds discussed in Chapter 3, these complexes are beautifully suited for kinetic analysis *via* stopped-flow spectrophotometry. Though it would have been of interest to use the previously unreported $[Ni^{II}(tacn)_2]$@CB[8] complex for these studies, a crystal structure could not be obtained for this compound. The incomplete occupancy of Cu^{II}cyclam in CB[8] also excluded it from kinetic analysis. For these reasons, {[Ni(cyclam)]@CB[8]}$(NO_3)_2$ was chosen as the subject of kinetic studies.

4.3.1. Oxidation of {[Ni(cyclam)]@CB[8]}$(NO_3)_2$

Since it was desirable to use the inclusion complex as an oxidant, selection of an appropriate oxidant for transforming Ni^{II}(cyclam) to Ni^{III}(cyclam) was first required. The redox potential of [Ni^{II}(cyclam)]@CB[8] has not yet been reported; however, due to the fact that the unencapsulated metal macrocycle, Ni^{II}(cyclam), has a rather high redox potential ($E° = 0.97$ V *versus* the standard hydrogen electrode),[68] it was thought that a strong oxidizing agent would be necessary. For this reason, sodium peroxodisulfate was initially chosen. The oxidation proceeded slowly, as expected with peroxodisulfate (due to the homolytic cleavage of the peroxo bond in the peroxodisulfate anion); however, there was some evidence of radical attack. This evidence presented itself as an indent on the absorbance *versus* time curve. This behaviour is not unprecedented. It is well-known that free radicals can attack organic compounds;[69] indeed, it has been reported that sodium peroxodisulfate reacts with the cucurbit[n]urils to form hydroxylated derivatives.[70] Because of this behaviour, oxidation of {Ni(cyclam)@CB[8] *via* sodium peroxodisulfate was abandoned.

Nickel^{II} bis(1,4,7-triazacyclononane), more commonly referred to as $[Ni^{II}(tacn)_2]^{2+}$, is a commonly used oxidant, especially when an outer sphere redox mechanism is desired. Coordinatively saturated with an electron count of d^8, $[Ni^{II}(tacn)_2]^{2+}$ is relatively inert and will not form a bridged species that could otherwise lead to an inner sphere oxidation mechanism. In addition, the electrochemical potential of the Ni^{II}/Ni^{III} species is relatively high, at +0.95 V *versus* the normal hydrogen electrode.[71]

Since it was desirable to use $Ni^{II}(tacn)_2$ as the oxidant, it was necessary to first oxidize this species. To do this, a strong oxidizing agent was required. Hexaaquacobalt(III) perchlorate is one such oxidant (E° for $Co(OH_2)_6^{3+}$ / $Co(OH_2)_6^{2+}$ = 1.86 V *versus* the standard hydrogen electrode);[72] it has been used as an oxidant in several kinetic studies.[72,73] The use of hexaaquacobalt(III) perchlorate has been made even more convenient in recent years by a report detailing a facile route to its synthesis.[51] Upon oxidation with hexaaquacobalt(III), $[Ni^{III}(tacn)_2]^{3+}$ was found to smoothly oxidize $[Ni^{II}(cyclam)]$@CB[8] to $[Ni^{III}(cyclam)]$@CB[8], showing an increase in absorbance within the region 250 – 340 nm corresponding to the formation of the oxidized $[Ni^{III}(cyclam)]$@CB[8] species. However, at high concentrations of the $[Ni^{III}(tacn)_2]^{3+}$ species, the absorbance change was masked by the intense color of the oxidant. High concentrations of the $[Ni^{III}(tacn)_2]^{3+}$ were necessary; the difficulty and cost of synthesizing $[Ni^{II}(cyclam)]$@CB[8] eliminated the possibility of using it as the reagent to be held in large excess.

Because of these difficulties, it was thought that hexaquacobalt(III) perchlorate might be used to oxidize $[Ni^{II}(cyclam)]$@CB[8] to $[Ni^{III}(cyclam)]$@CB[8]} directly, and a split cell experiment in the UV-visible spectrometer showed $[Ni^{II}(cyclam)]$@CB[8] to undergo clean oxidation upon reaction with excess oxidant. Though hexaaquacobalt(III) is also intensely coloured, it absorbs in a different region of the spectrum than the oxidized Ni(III) species. A full kinetic study of the oxidation of $[Ni^{II}(cyclam)]$@CB[8] was performed, and the results are given below.

4.3.1.1. Oxidation of {[Ni(cyclam)]@CB[8]}$(NO_3)_2$ by hexaaquacobalt(III)

Pseudo-first-order kinetics are observed upon reacting {[Ni(cyclam)]@CB[8]}$(NO_3)_2$ with excess oxidant, hexaaquacobalt(III). The absorbance change corresponding to the formation of the oxidized Ni(III) species and the reduced Co(II) species is pictured in Figure 4.8.

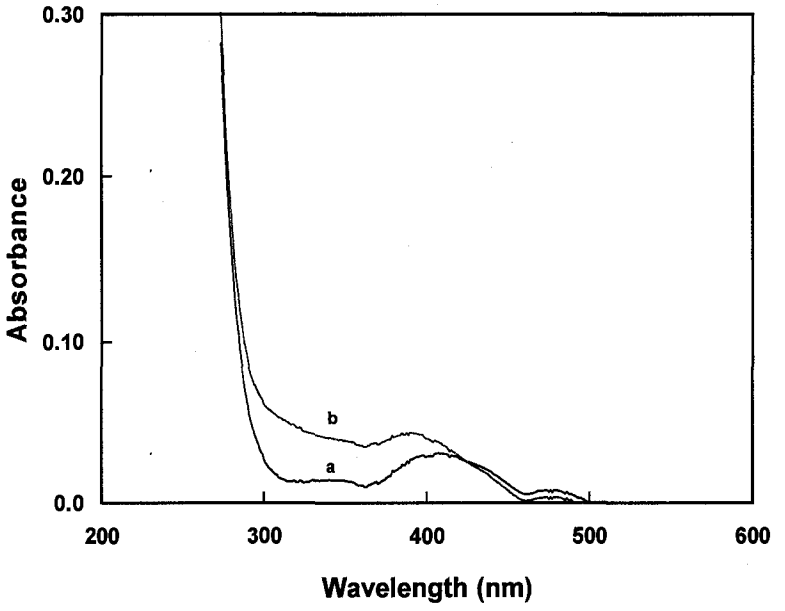

Figure 4.8. Spectral change for oxidation of {[Ni(cyclam)]@CB[8]}$(NO_3)_2$ by [Co^{III}] (a = spectral curve before mixing; b = spectral curve after mixing)

From the spectrophotometric data, an optimal wavelength of 350 nm was chosen for the measurement of absorbance *versus* time on the stopped flow spectrophotometer. This wavelength corresponds to a large spectral change, as well as being a wavelength at which the Xenon lamp in the stopped-flow spectrophotometer emits sufficient light. Reaction of [Ni^{II}(cyclam)]@CB[8] with excess oxidant gave an exponential absorbance

versus time curve, showing the reaction to be first order with respect to the $[Ni^{II}(cyclam)@CB[8]$ inclusion complex (Figure 4.9).

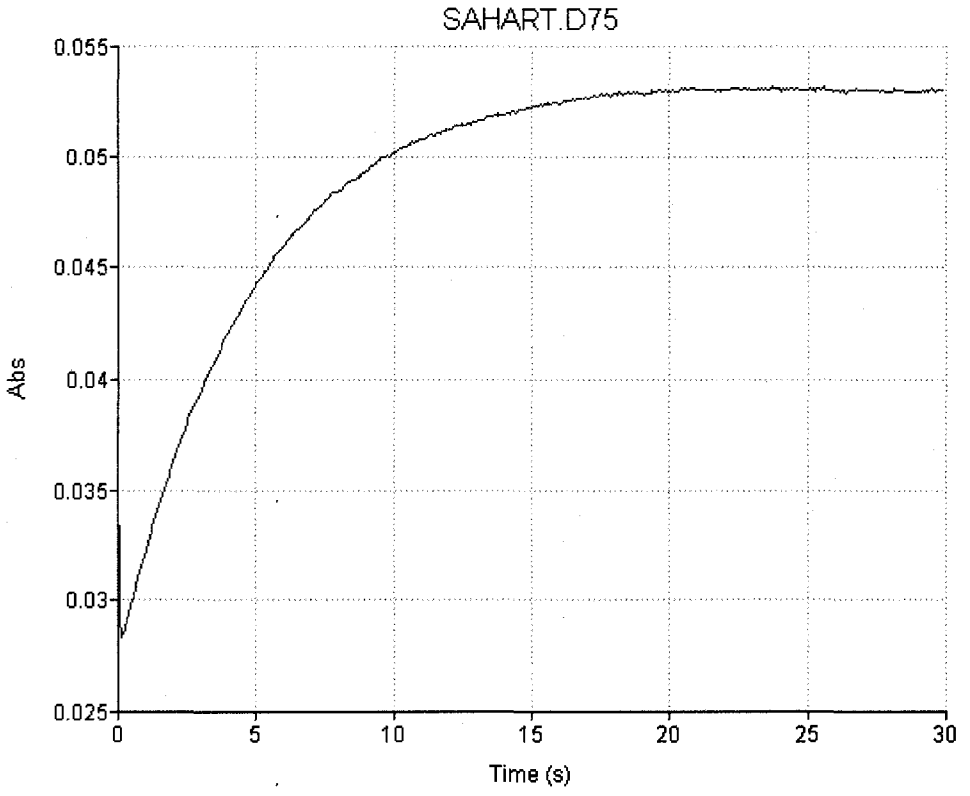

Figure 4.9. Spectrophotometric curve showing first order dependence on Ni(II) species for reduction of hexaaquacobalt(III)

In order to determine the dependence of the reaction on the oxidizing agent, as well as the effect of temperature on the rate, the reaction was performed with varying concentrations of Co(III) and at varying temperatures. For these experiments, the ionic strength and acid concentration was adjusted with $HClO_4$ to a constant 1.00 M. The values of k_{obs} for the oxidation of $[Ni^{II}(cyclam)]@CB[8]$ at five different Co(III) concentrations and at five different temperatures are listed in the Table 4.9.

Temperature (K)	10^{-4} x [hexaaquacobalt(III)] (M)	k_{obs} (s^{-1})
288	2.05	0.03426 ± 0.00004
	4.11	0.0747 ± 0.0001
	6.16	0.1116 ± 0.0001
	8.22	0.1614 ± 0.0001
	10.3	0.2064 ± 0.0001
293	2.05	0.06590 ± 0.0001
	4.11	0.1272 ± 0.0001
	6.16	0.2175 ± 0.0001
	8.22	0.2868 ± 0.0002
	10.3	0.3597 ± 0.0003
299	2.05	0.1038 ± 0.0001
	4.11	0.2367 ± 0.0002
	6.16	0.352 ± 0.001
	8.22	0.521 ± 0.001
	10.3	0.642 ± 0.001
303	2.05	0.1642 ± 0.0002
	4.11	0.355 ± 0.001
	6.16	0.580 ± 0.001
	8.22	0.748 ± 0.001
	10.3	0.962 ± 0.001
308	2.05	0.266 ± 0.001
	4.11	0.598 ± 0.002
	6.16	0.873 ± 0.004
	8.22	1.237 ± 0.004
	10.3	1.482 ± 0.003

Table 4.9. Observed rate constants for the pseudo-first-order oxidation of $[Ni^{II}(cyclam)]$@CB[8] by varying concentrations of hexaaquacobalt(III), at five different temperatures. Ionic strength and acidity constant at 1.00 M ($HClO_4$).

A plot of k_{obs} *versus* [Co(III)] at five different temperatures is given below (Figure 4.10). The observed rate constants are directly related to [Co(III)] and temperature, as an increase in either of these factors results in an increased oxidation rate. From the linearity of the lines (r^2 values ranging from 0.995 to 0.998), it can be assumed that the oxidation reaction is first-order with respect to the concentration of Co(III).

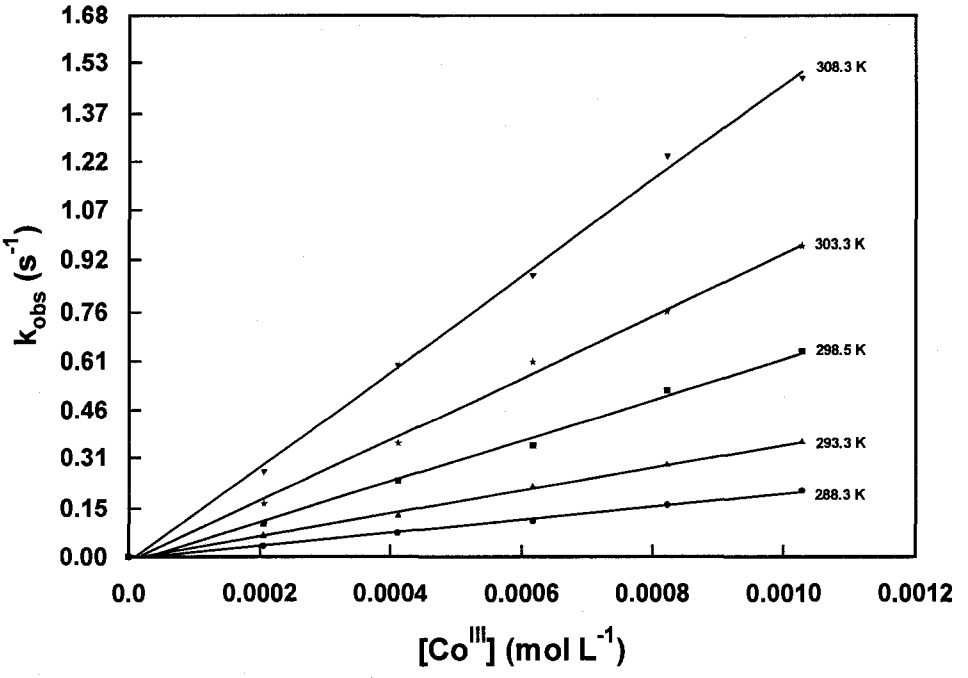

Figure 4.10. Plot of observed rate constant (k_{obs}) *versus* [Co(III)] for the oxidation of [Ni^{II}(cyclam)]@CB[8]} by Co(III) at five different temperatures. Ionic strength and acidity constant at 1.00 M ($HClO_4$).

Having established that the redox reaction follows a simple second order rate law, exhibiting first order dependence on both the oxidizing and the reducing agent, the experiment was repeated with varying acid concentrations in order to assess acid dependence. Temperature dependence was also studied by varying the temperature at which the reaction was performed. Concentrations of hexaaquacobalt(III) and [Ni^{II}(cyclam)]@CB[8] were kept constant at 1.00×10^{-3} M and 1.00×10^{-5} M, respectively. The data acquired from this experiment have been tabulated (Table 4.10) and graphically represented (Figure 4.11).

Temperature (K)					
	283	288	293	298	303
$[H^+]$ (M)	k_{obs} (s^{-1})				
0.200	0.416 ± 0.001	0.740 ± 0.002	1.432 ± 0.004	2.60 ± 0.01	3.98 ± 0.02
0.400	0.2088 ± 0.0002	0.400 ± 0.001	0.762 ± 0.002	1.319 ± 0.004	2.190 ± 0.007
0.600	0.1474 ± 0.0002	0.2746 ± 0.001	0.507 ± .001	0.843 ± 0.001	1.405 ± 0.003
0.800	0.1118 ± 0.001	0.2255 ± 0.002	0.390 ± 0.001	0.713 ± 0.001	1.073 ± 0.002

Table 4.10. Observed rate constants for the pseudo-first-order oxidation of $[Ni^{II}(cyclam)]$@CB[8] at varying concentrations of $HClO_4$, at five different temperatures. Concentration of $[Ni^{II}(cyclam)]$@CB[8] and Co(III) constant at 1.00 x 10^{-5} M and 1.00 x 10^{-3} M, respectively.

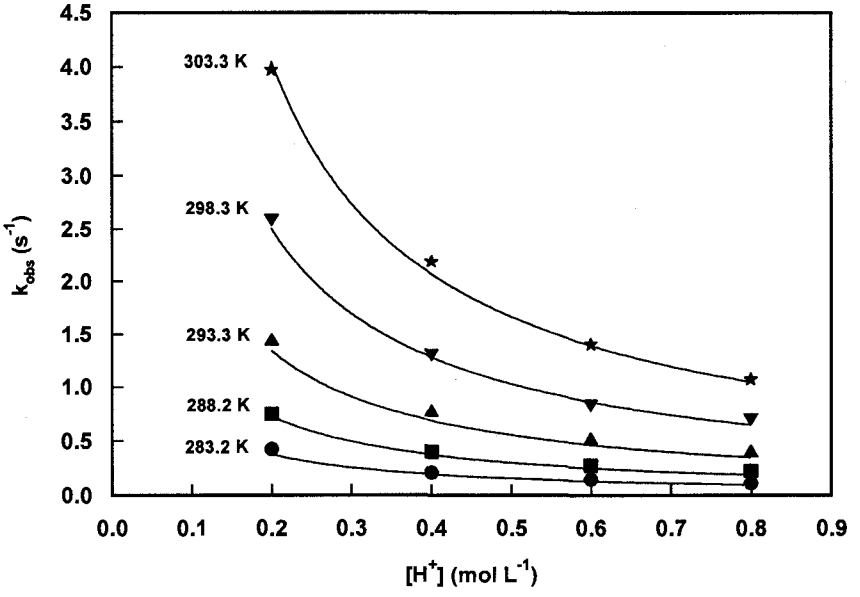

Figure 4.11. Observed rate constants for the pseudo-first-order oxidation of $[Ni^{II}(cyclam)]$@CB[8] at varying concentrations of $HClO_4$, and at five different temperatures. Concentration of $[Ni^{II}(cyclam)]$@CB[8] and Co(III) constant at 1.00 x 10^{-5} M and 1.00 x 10^{-3} M, respectively.

The data clearly show pronounced acid and temperature dependencies, with the observed rate constant varying inversely with acid concentration and directly with temperature. From the kinetic data acquired above, it is possible to deduce the mechanism of the reaction, as well as the acid dependent rate law.

4.3.1.2. Mechanism and Acid Dependent Rate Law

As mentioned above, the oxidation reaction exhibited a dependence upon acid concentration. This is not unexpected; it is well-known that hexaaquacobalt (III) hydrolyzes in aqueous solution as per the following reaction:

$$Co(OH_2)_6^{3+} \underset{}{\overset{K_a}{\rightleftharpoons}} Co(OH_2)_5(OH)^{2+} + H^+ \qquad \textbf{Reaction 4.1}$$

Therefore, two possible pathways exist for the oxidation of $Ni^{II}L@CB[8]$, where L = 1,4,8,11-tetraazaycyclotetradecane (cyclam) (See Scheme 4.6). The first pathway (indicated by k_1) involves oxidation by the protonated hexaaquacobalt species, whereas the second pathway (indicated by k_2) involves oxidation by the mono-deprotonated pentaaquacobalt hydroxo cobalt species, represented hereafter as $Co(OH)^{2+}$.

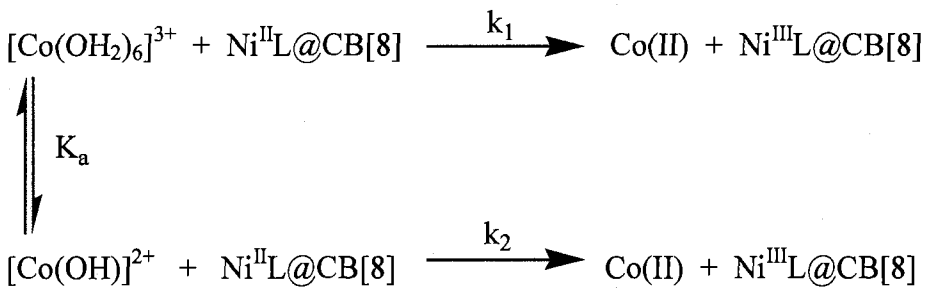

Scheme 4.6. Proposed reaction mechanism for the oxidation of $[Ni^{II}(cyclam)]@CB[8]$ by Co(III)

The formal rate law for the above mechanism can be derived as follows:

$$\text{Rate} = \frac{d[Ni^{III}L@CB(8)]}{dt}$$

$$= k_1[Co(OH_2)_6^{3+}][Ni^{II}L@CB(8)] + k_2[Co(OH)^{2+}][Ni^{II}L@CB(8)]$$

$$= (k_1[Co(OH_2)_6^{3+}] + k_2[Co(OH)^{2+}])[Ni^{II}L@CB(8)] \qquad \textbf{Equation 4.1}$$

Solving this rate law would be impossible because it involves two unknown concentrations, that of $[Co(OH_2)_6^{3+}]$ and $[Co(OH)^{2+}]$. However, an expression for each of these species can be derived from the equilibrium given in Reaction 4.1 and the Law of Mass Balance. The equilibrium indicated by Reaction 4.1 can be expressed as follows:

$$K_a = \frac{[Co(OH)^{2+}][H^+]}{[Co(OH_2)_6^{3+}]} \qquad \textbf{Equation 4.2}$$

Furthermore, the Law of Mass Balance states that the total concentration of $[Co(OH_2)_6^{3+}]$ is equal to the sum of the concentrations of $[Co(OH_2)_6^{3+}]$ and $[Co(OH)^{2+}]$, as per Equation 4.3.

$$[Co(OH_2)_6^{3+}]_{total} = [Co(OH_2)_6^{3+}] + [Co(OH)^{2+}] \qquad \textbf{Equation 4.3}$$

Using Equations 4.2 and 4.3, the values for the unknown concentrations can be calculated as follows:

$$[Co(OH)^{2+}] = (K_a / K_a + [H^+])\,[Co(OH_2)_6^{3+}]_{total} \qquad \textbf{Equation 4.4}$$

$$[Co(OH_2)_6^{3+}] = ([H^+] / [H^+] + K_a)\,[Co(OH_2)_6^{3+}]_{total} \qquad \textbf{Equation 4.5}$$

The derived values for $[Co(OH)^{2+}]$ and $[Co(OH_2)_6^{3+}]$ can then be substituted into the rate law depicted in Equation 4.1 to yield the following rate law involving only known concentrations of $[Co(OH_2)_6^{3+}]_{total}$, $[H^+]$, and $[Ni^{II}L@CB(8)]$:

$$\text{Rate} = \frac{k_1[H^+] + k_2K_a}{[H^+] + K_a}\,[Ni^{II}L@CB(8)]\,[Co(OH_2)_6^{3+}]_{total} \qquad \textbf{Equation 4.6}$$

The reaction was studied by monitoring the growth in the absorbance peak due to the oxidation of the $[Ni^{II}L]@CB[8]$ species to the $[Ni^{III}L]@CB[8]$ species. The concentration of this reactant was kept constant throughout the experiment, with only the concentration of the excess reagent, $[Co(OH_2)_6^{3+}]_{total}$, being changed. Therefore, the experimental rate at which the reaction proceeds can be described by:

$$\text{Rate} = k_{obs}[\,Ni^{II}L@CB(8)]$$

$$\text{with } k_{obs} = \frac{k_1[H+] + k_2K_a}{[H+] + K_a}\,[Co(OH_2)_6^{3+}]_{total} \qquad \textbf{Equation 4.7}$$

At the acid concentrations used in this study, $[H^+] \gg K_a$, and the above equation simplifies to the following:

$$k_{obs} = k_1 + \frac{k_2 K_a}{[H^+]} [Co(OH_2)_6^{3+}]_{total} \qquad \textbf{Equation 4.8}$$

or, equivalently,

$$\frac{k_{obs}}{[Co(OH_2)_6^{3+}]_{total}} = \frac{k_2 K_a}{[H^+]} + \frac{k_1}{[Co(OH_2)_6^{3+}]_{total}} \qquad \textbf{Equation 4.9}$$

A plot of $k_{obs}/[Co(OH_2)_6^{3+}]_{total}$ *versus* the reciprocal of the acid concentration ($1/[H^+]$) gives a straight line plot which negates the possibility of the reaction following the k_1 pathway described in Scheme 4.6, as the y intercepts are zero within experimental error (See Figure 4.12).

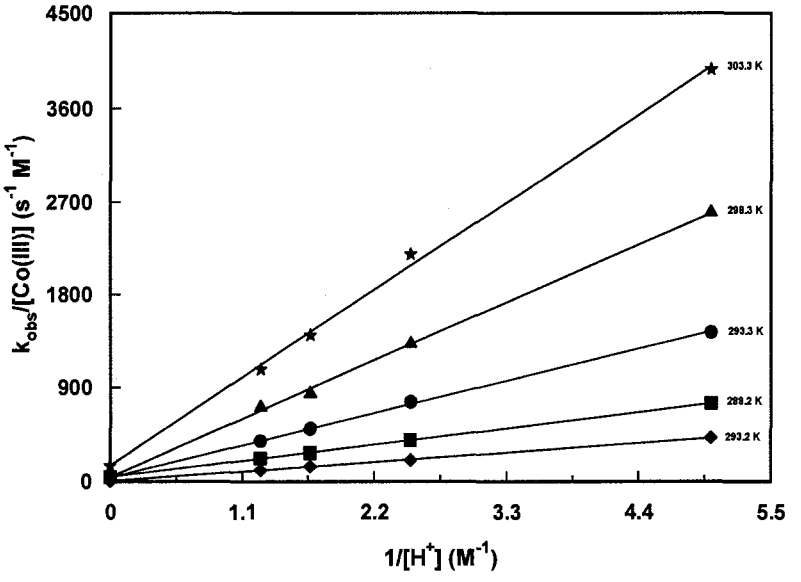

Figure 4.12. Plot of $k_{obs}/[Co(III)]$ *versus* $1/[H^+]$ at five different temperatures, showing a negligible k_1 oxidation pathway.

Therefore, the monodeprotonated $Co(OH)^{2+}$ species is the sole active oxidant and the proposed mechanism for the oxidation reaction is as follows:

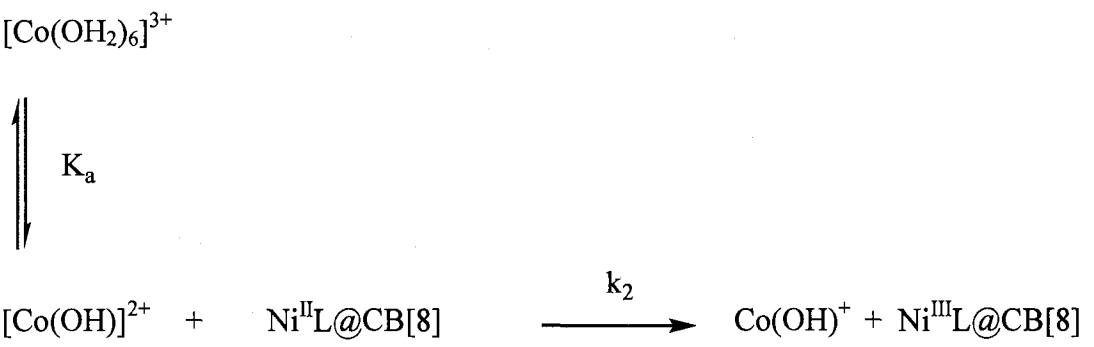

Scheme 4.7. Proposed reaction mechanism for the oxidation of $[Ni^{II}L]@CB[8]$.

This mechanism is not unexpected, as the authors of an earlier study on the oxidation of Ni^{II}cyclam by hexaaquacobalt(III) perchlorate reported similar findings.[53] With the possibility of the reaction following the k_1 pathway eliminated, the rate law can be simplified, as shown in the following equation:

$$\text{Rate} = k_2[Co(OH)^{2+}][Ni^{II}L@CB(8)]$$

$$= k_{obs}[Ni^{II}L@CB(8)]$$

$$\text{Where } k_{obs} = \frac{k_2K_a}{[H^+]+K_a}[Co(OH_2)_6{}^{3+}]_{total} \qquad \textbf{Equation 4.10}$$

As previously mentioned, the conditions of the experiment ($[H^+] \gg K_a$) allow for a further simplification: $k_{obs} = \frac{k_2K_a}{[H^+]}[Co(OH_2)_6{}^{3+}]_{total}$ **Equation 4.11**

The composite rates (k_2K_a) can therefore be determined from the plot of $k_{obs}/[Co(OH_2)_6^{3+}]_{total}$ *versus* $1/[H^+]$ (see Figure 4.12), which gives a straight line plot with a slope of k_2K_a. The composite values are listed in Table 4.12, and are valuable as a direct comparison to previous literature[53] (which also reports rate constants as composite values).

Temperature (K)	**k_2K_a (s^{-1})**
283	82.9 ± 0.9
288	140 ± 1
293	279 ± 4
298	509 ± 9
303	770 ± 20

Table 4.12. Composite values (k_2K_a) for oxidation of $[Ni^{II}(cyclam)]$@CB[8] by $[Co(OH)]^{2+}$.

An Eyring plot of the above data (Figure 4.15) gives composite activation parameters for the oxidation of $[Ni^{II}(cyclam)]$@CB[8] by $[Co(OH)]^{2+}$, with an enthalpy change ($\Delta H\dagger$) of 77 ± 3 kJ/mol and an entropy change ($\Delta S\dagger$) of 67 ± 1 J/K mol.

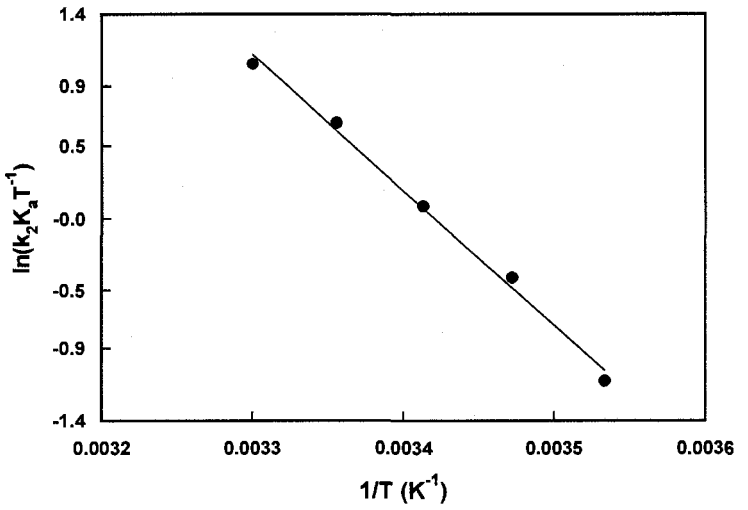

Figure 4.13. Eyring plot of composite rates (k_2K_a) for oxidation of $[Ni^{II}(cyclam)]$@CB[8] by $[Co(OH)]^{2+}$

Alternatively, a non-linearized plot of k_{obs} *versus* acid concentration can be generated (see Figure 4.14 and the data curve-fit to the following equation, with the factor of 0.001 arising from the concentration of $Co(OH_2)_6^{3+}$ (0.001 M).

$$y = 0.001 \frac{A * K_a}{x + K_a} \qquad \textbf{Equation 4.12}$$

where $y = k_{obs}$

$A = k_2$

K_a = acid dissocation constant for hexaaquacobalt (III)

$x = [H^+]$

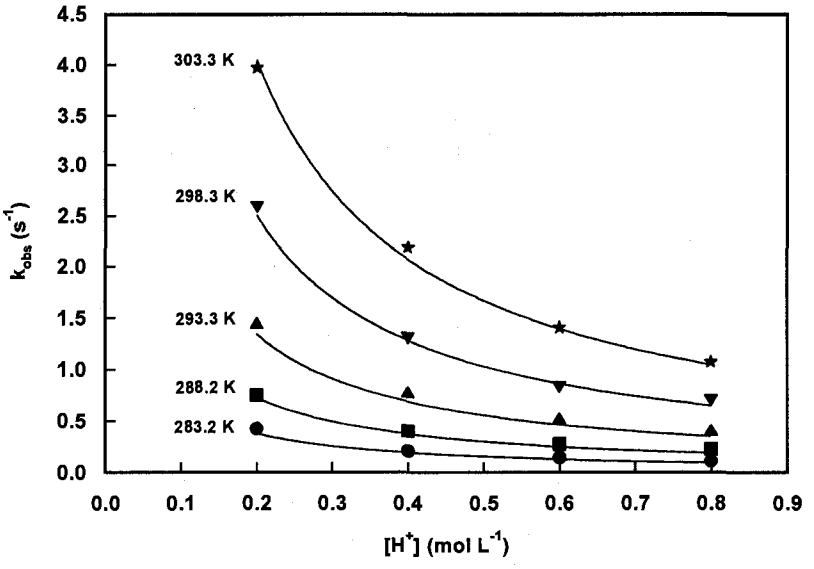

Figure 4.14. Observed rate constants for the pseudo-first-order oxidation of [Ni^{II}(cyclam)]@CB[8] at varying concentrations of $HClO_4$, and at five different temperatures. Concentration of [Ni^{II}(cyclam)]@CB[8] and Co(III) constant at 1.00×10^{-5} M and 1.00×10^{-3} M, respectively.

In order to curve-fit the data, it is necessary to have a value for the acid dissociation constant of hexaaquacobalt(III) (K_a). Historically, this value has been the subject of much debate. Difficulty in synthesizing the Co^{III} species, instability of the species at low acidities, oligomerization at high concentrations, and oxidation of water in aqueous solution have all contributed to a number of differing results for K_a.[74,75,76,77,78,79] The work of R. B. Jordan has shed much light on the uncertainty surrounding hexaaquacobalt(III). In 2002, the Jordan group published a facile synthesis for this oxidant,[51] and in 2006, a reliable value for the acid dissociation constant, $K_a = 1.4 \times 10^{-3}$, was reported.[72]

Substituting this value for K_a into Equation 4.10, the data can be curve-fit using Fig P software to determine the values of k_2 at five different temperatures. These values have been reported in Table 4.11. However, it is important to note that the second order

rate constants have been generated using the assumption that the value for K_a changes very little over the studied temperature range. This is not unreasonable; the K_a value at 279 K has been reported to be 0.001, while the value at 298 varies very little, at 0.0014.[72]

Temperature (K)	10^5 x k_2 ($M^{-1}s^{-1}$)
283	0.610 ± 0.034
288	1.11 ± 0.06
293	2.10 ± 0.11
298	3.75 ± 0.21
303	5.86 ± 0.33

Table 4.11. Rate constants, k_2, for the oxidation of $[Ni^{II}(cyclam)]$@CB[8] by $[Co(OH)]^{2+}$ at five different temperatures.

An Eyring plot of the above data (Figure 4.15) gives activation parameters for the oxidation of $[Ni^{II}(cyclam)]$@CB[8] by $[Co(OH)]^{2+}$ (oxidation *via* the k_2 pathway), with an enthalpy change ($\Delta H\dagger$) of 77 ± 4 kJ/mol and an entropy change ($\Delta S\dagger$) of 120 ± 10 J/K mol.

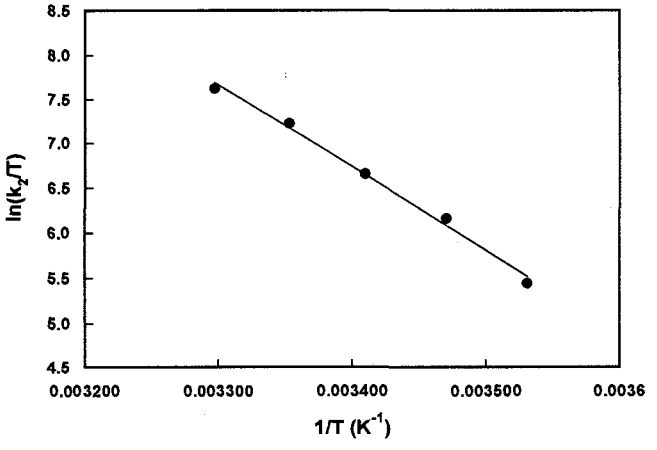

Figure 4.15. Eyring plot of k_2 values for oxidation of $[Ni^{II}(cyclam)]$@CB[8] by $[Co(OH)]^{2+}$

A discussion of activation parameters will be facilitated by defining two theories for the structure of the oxidized [Ni^{III}(cyclam)]@CB[8] species. Previous work[80] has shown that free oxidized Ni^{III}(cyclam) is most commonly found in a tetragonally distorted square planar geometry with two coordinated water molecules in the axial positions. Within the cucurbit[8]uril ring, transformation to the nickel(III) species with concomitant coordination of the axial water molecules can be imagined to be sterically unfavourable. As a further point of interest, it is noted that the chloride ligands in the inclusion complex [Ni(cyclam)]@CB[8] are not found to be coordinated to the nickel centre, (see Section 4.2.2 for X-ray crystal structure) as would be expected for free Ni(cyclam). If the chloride ligands are too large and sterically bulky to coordinate to the axial positions of Ni(cyclam) when it is encapsulated by cucurbit[8]uril, it is reasonable to expect that the larger water molecules will also not be coordinated to the nickel centre in the encapsulated Ni^{III}(cyclam) complex.

As an alternative, it is possible that the nickel centre is in the correct position within the cucurbit[8]uril ring to coordinate to two of the nitrogen atoms making up the glycoluril units of the cucurbit[8]uril ring (See Figure 4.16). This postulation is supported by an ESR spectrum with splitting patterns indicative of nitrogen atoms in the axial positions (unpublished work).[81] Also, it is known that in the presence of sulfate anions, a tetragonally distorted Ni(III) species with a coordinated sulfate anion is formed preferentially to the diaqua complex.[82]

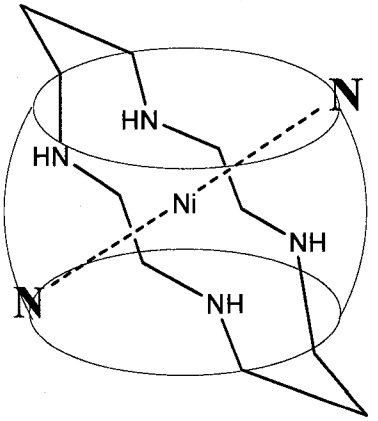

Figure 4.16. Figure showing tetragonally distorted Ni^{III} with axial coordination to the cucurbit[8]uril ring nitrogens

The activation enthalpy ($\Delta H\dagger$) and entropy ($\Delta S\dagger$) for this reaction is within the range expected from an outer sphere oxidation of Ni^{II}(cyclam) by hexaaquacobalt (III).[53] The positive enthalpy value implies that energy is absorbed in the transition from the initial state to the activated complex. Positive entropy values are indicative of transition states that are less ordered than the corresponding initial states. The positive entropy values can be explained in light of the two proposed structures of the $[Ni^{III}(cyclam)]$@CB[8] species.

In the first proposal, where the oxidized Ni^{III} species is a tetragonally distorted diaaqua complex, the positive activation entropy can be understood in terms of the solvent shell surrounding the $[Ni^{II}(cyclam)]$@CB[8] complex. The solvent is an acidic aqueous solution, and as such, exists in a highly ordered state with the water molecules solvating the positively charged hydrogen ions of the acid. Upon oxidation of the nickel centre to the 3^+ state, two of these solvating water molecules coordinate to the metal centre, disrupting the organized solvent shell. In addition, the inclusion of the two water

molecules into the sphere of cucurbit[8]uril increases the randomness, and thus the entropy, of the system.

The second proposal, where the oxidized Ni^{III} species is coordinated to two of the cucurbit[8]uril ring nitrogens, also supports the positive entropy values, and is also explained in terms of solvent effects. Upon coordination to the nitrogens of the glycoluril units, it is possible that the ring deforms – taking on a more oblong shape. Such ellipsoidal distortion has already been reported for certain cucurbit[8]uril inclusion complexes.[48] If this is indeed the case, it is possible that several water molecules present in the cavity of cucurbit[8]uril may be extruded from the cavity. Addition of free water molecules to the organized solvent system will increase the randomness of the solvent shell, resulting in positive activation entropy values.

4.3.1.3. Mode of Electron Transfer – Inner-Sphere or Outer-Sphere?

As mentioned in Section 1.1.1, there are two major modes of electron transfer in redox active metal complexes – outer-sphere and inner-sphere. Analyses of inner-sphere electron transfer reactions are complicated due to bond breaking/forming; therefore, outer sphere reactions are more desirable. That the oxidation of square planar Ni^{II}cyclam encapsulated within cucurbit[8]uril takes place *via* an outer-sphere redox mechanism is not immediately apparent. Although square planar d^8 nickel is relatively inert, the nickel cation is coordinatively unsaturated with vacant axial coordination sites. In addition, the hexaquacobalt(III) ion in its monodeprotonated form has a hydroxy species that could act as a bridging ligand, yielding the following intermediate:

$[(H_2O)_5Co—(OH)—Ni(cyclam)]$

However, it has been previously shown[53] that redox reactions with hexaaquacobalt(III) as the oxidant fall into two major categories – those with composite rate values (k_2K_h) less than 100 (thought to proceed *via* an inner-sphere mechanism) and those with composite rate values of greater than 1000 (thought to proceed *via* an outer-sphere mechanism).

In a study[53] involving the oxidation of free Ni^{II}cyclam by hexaaquacobalt(III), it was determined that the mechanism was outer-sphere in character. The composite rate (k_2K_a) was found to be 970 s^{-1}. The lower rate constant, as compared to rate constants of other reductants with hexaaquacobalt(III) (ascorbic acid and hydroquinone being 1480 s^{-1} and 1280 s^{-1}, respectively) is attributed to either the high redox potential of Ni^{II}cyclam or to the electrostatic repulsion between two positively charged reactants. It is quite reasonable to expect that the oxidation of encapsulated Ni^{II}cyclam will also follow an outer-sphere mechanism, as the cucurbit[8]uril ring makes the coordination of a bridging ligand even more unlikely to occur.

4.3.1.4. Effect of Steric Bulk on Reaction Rates and Activation Parameters

Of key importance to this body of work is the investigation into the effect of steric encumbrance on the rates of electron transfer. In the $[Ni^{II}(cyclam)]$@CB[8] /$[Co(OH)]^{2+}$ system described above, the steric bulk is provided by the cucurbit[8]uril ring, which surrounds the reductant and prevents the close approach of the oxidizing agent. It would be of great interest to compare the rates of oxidation of the free Ni^{II}cyclam system with that of the sterically hindered $[Ni^{II}(cyclam)]$@CB[8] system.

As alluded to earlier, the oxidation of Ni^{II}(cyclam) by hexaaquacobalt(III) was performed by Brodovitch and McAuley almost thirty years ago.[53] The mechanism of oxidation reported by Brodovitch and McAuley is identical to the postulated mechanism in this work, with the mono-deprotonated $[Co(OH)]^{2+}$ species being the active oxidant. Although direct comparison is hindered by the fact that McAuley's studies were performed at an ionic strength of 1.5 M as compared to this study at an ionic strength of 1.0 M, general conclusions can be drawn. McAuley reported a composite value (k_3K_a) of 970 ± 30 s^{-1} for the oxidation of Ni^{II}(cyclam) by Co(III) at 25.0°C. Under similar conditions (25.0 °C), the composite value for the oxidation of [Ni^{II} (cyclam)]@CB[8] by Co(III) was found to be 509 ± 9 s^{-1}. Using the hydrolysis constant reported by Sisley and Jordan (1.4 x 10^{-3} M),[72] the respective values for the k_2 pathway are (6.93 ± 0.12) x $10^5 M^{-1}s^{-1}$ for the unencapsulated Ni^{II}(cyclam) and (3.64 ± 0.06) x 10^5 M^{-1} s^{-1} for the encapsulated Ni^{II}(cyclam). The rate constant is therefore decreased by a factor of 1.9 (see Table 4.9).

Oxidant	Reductant	k_2 ($M^{-1}s^{-1}$)
Hexaaquacobalt(III)	[Ni^{II}(cyclam)]@CB[8]	(3.64 ± 0.06) x 10^5
Hexaaquacobalt(III)	Ni^{II}(cyclam)	(6.93 ± 0.12) x 10^5

Table 4.9. Rates (k_2) of electron exchange for oxidation of [Ni^{II}(cyclam)]@CB[8] and Ni^{II}(cyclam) by hexaaquacobalt(III).

Because the distance of closest approach of the oxidizing agent to the nickel(II) cyclam center is necessarily greater in the system including the sterically bulky CB[8], it is reasonable to expect the electron transfer to occur at a slower rate. However, there are

many factors besides sterics that come into play in an electron transfer reaction, and all factors should be taken into account.

Firstly, the rate of electron transfer reaction is influenced by the ionic strength of the medium in which the reaction occurs,[83] according to the Debye-Hückel limiting law, which states the following:

$$\log_{10}k = \log_{10}k_0 + 1.02z_Az_B\sqrt{I} \qquad \textbf{Equation 4.13}$$

Where: k = rate in real solution with known ionic strength, I

k_0 = rate in solution of infinite dilution

z_A, z_B = charges on component ions

I = ionic strength

Because the component ions in this system are like in charge, it is reasonable to expect the reaction rate to decrease with increasing ionic strength. The fact that McAuley's study was performed at an ionic strength of 1.5 M and this study was performed at an ionic strength of 1.0 M will influence the results slightly; however, the effect (ionic strengths differing by only 0.5 M) can be expected to be minimal.

Though it would seem prudent to calculate the predicted rate increase due to the change in the ionic strength using Equation 4.12, this calculation is precluded due to the fact that the equation is valid only for ionic strengths ≤ 0.01; at higher ionic strengths this equation can be taken only as a generalization.[6]

Secondly, the rate at which oxidation occurs is intrinsically related to the oxidation potential of the reductant. Reductants with higher oxidation potentials will require longer oxidation times and *vise versa*. It is interesting to note that Kim's study of a Cu^{II}(cyclen) inclusion complex showed the cucurbit[8]uril to have a stabilizing effect

on the reduced copper(I) species, lowering the reduction potential.[46] If the oxidized Ni(III) species is stabilized by the cucurbit[8]uril ring, the rate constant would understandably be faster than expected. The corollary is also true: if the Ni(II) species is stabilized by the cucurbit[8]uril ring, the rate constant of the electron transfer reaction will be lower than expected. To acquire a more accurate analysis of the steric effect of the cucurbit[8]uril species on the oxidation rate, it would be necessary to determine the oxidation potential of the $[Ni^{II/III}(cyclam)]$@CB[8] species. However, all attempts to do so have failed as a result of the extremely low solubility of the $[Ni^{II}(cyclam)$@CB[8] system in aqueous solution. (Concentrations needed for electrochemical studies are higher than those needed for kinetic studies.)

The activation parameters for the oxidation of $[Ni^{II}(cyclam)]$@CB[8] by hexaaquacobalt (III) have been calculated and can be compared to the activation parameters reported by McAuley *et al.*[53] for the oxidation of the encapsulated Ni^{II}(cyclam) (see Table 4.10). Because McAuley reported activation parameters based on the composite values of k_2K_a, it is necessary to use the composite activation parameters for direct comparison. Inspection of Table 4.10 shows the activation parameters for the encapsulated and free Ni^{II}(cyclam) system to be comparable within experimental error, which is to be expected.

Complexes	$\Delta H^{\dagger}$ from k_2K_a (kJ/mol)	$\Delta S^{\dagger}$ from k_2K_a (J/K mol)
$[Ni^{II}(cyclam)]$@CB[8]	77 ± 3	67 ± 1
Ni^{II}cyclam	69.2 ± 3.6	49 ± 30

Table 4.10. Composite (k_2K_a) activation parameters for oxidation of $[Ni^{II}(cyclam)]$@CB[8] and Ni^{II}cyclam by hexaaquacobalt(III)

4.3.2. Oxidation of benzenediols – (benzene-1,4-diol and benzene-1,2-diol) by [Ni^{III}(cyclam)]@CB[8]

Successful oxidation of the inclusion complex [Ni^{III}(cyclam)]@CB[8] allows it to be used as an outer sphere oxidant for a variety of reductants. Benzenediols are commonly used reductants as the family of compounds exhibit a wide range of oxidation potentials.[68] The reduction of the organic substrates, benzene-1,4-diol (hydroquinone) and benzene-1,2-diol (catechol) by free Ni^{III}(cyclam) has been categorized as proceeding *via* an outer-sphere mechanism in previous studies,[68, 84] and it is reasonable to expect the encapsulated Ni^{III}(cyclam) species to behave in the same way. In addition, these previous studies with free Ni^{III}(cyclam) will afford a direct comparison to the encapsulated Ni^{III}(cyclam) system. The oxidation kinetics of hydroquinone and catechol by [Ni^{III}(cyclam)]@CB[8] will be described separately in the sections below; however, the rate laws and mechanisms are believed to be similar and will be reported together in Section 4.3.2.3.

4.3.2.1. Oxidation of hydroquinone by [Ni^{III}(cyclam)]@CB[8]

Excellent pseudo-first-order kinetics are observed upon the reaction of excess hydroquinone with the oxidizing agent [Ni^{III}(cyclam)]@CB[8]. When analyzed spectrophotometrically, the spectrum shows a decrease in the absorbance, corresponding to the disappearance of [Ni^{III}(cyclam)]@CB[8] (Figure 4.17). The wavelength of 370 nm was chosen as the optimum wavelength at which to monitor the reaction. This wavelength corresponds to a large spectral change, as well as being a wavelength at which the Xenon lamp in the stopped-flow spectrophotometer emits sufficient light.

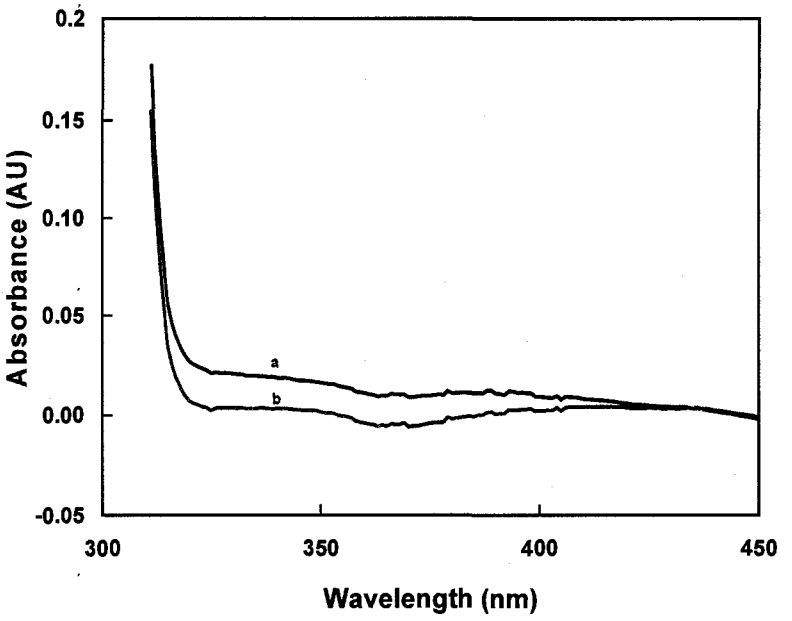

Figure 4.17. Spectral change for oxidation of hydroquinone by [Ni^{III}(cyclam)]@CB[8] (a = spectral curve before mixing; b = spectral curve after mixing)

The oxidation reaction proceeds according to the following scheme:

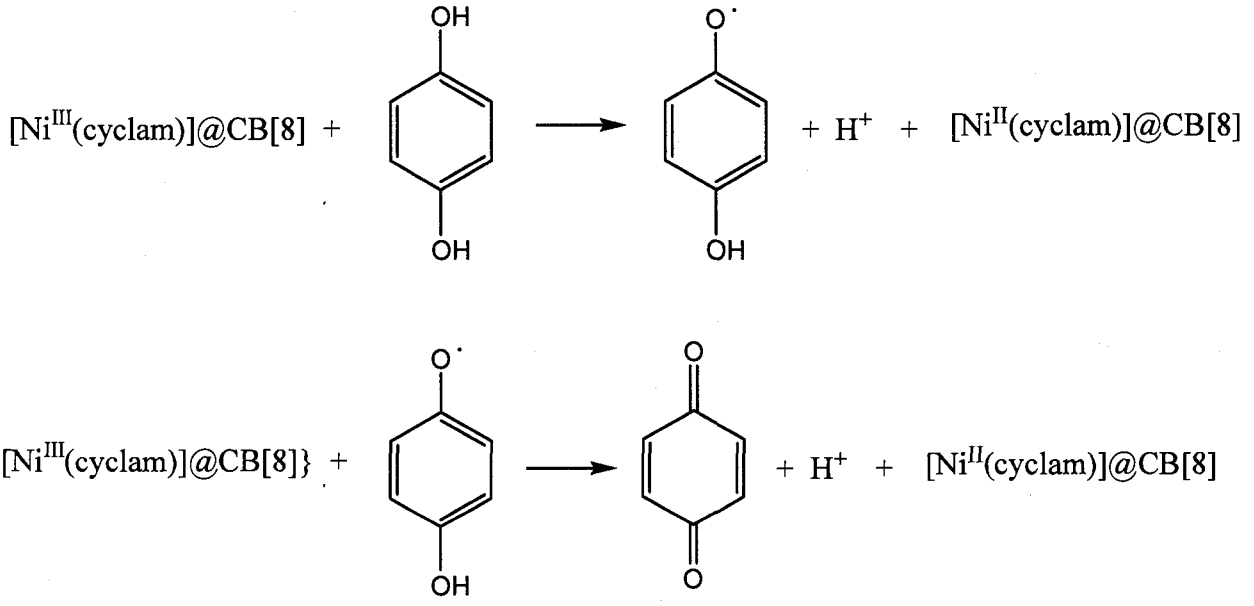

Scheme 4.8. Schematic representing oxidation of hydroquinone by [Ni^{III}(cyclam)]@CB[8]

Measurement of absorbance *versus* time on the stopped flow spectrophotometer showed an exponential absorbance change *versus* time (Figure 4.17), indicating a first order reaction with respect to the Ni(III) species.

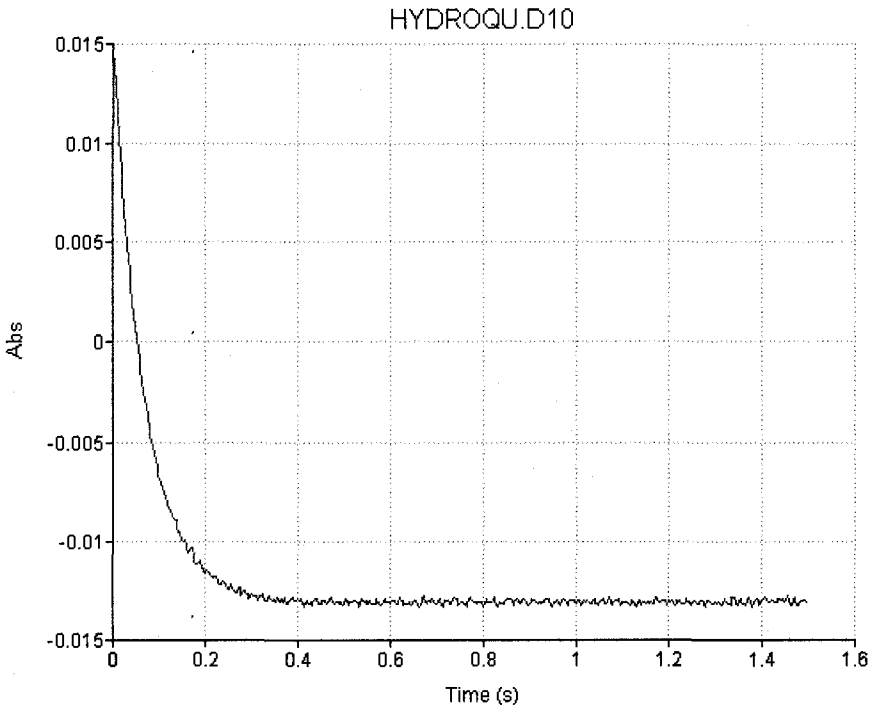

Figure 4.18. Spectrophotometric curve showing first order dependence on Ni(III) species for oxidation of hydroquinone

To determine the dependency of the reaction on the concentration of the reducing agent (hydroquinone), as well as to study the temperature dependence of the reaction, the absorbance change was monitored repeatedly at varying temperatures and at varying hydroquinone concentrations. For these experiments, the ionic strength and acidity was adjusted with $HClO_4$ to a constant 1.00 M.

The k_{obs} values for the oxidation of hydroquinone at five different hydroquinone concentrations and at five different temperatures are listed in Table 4.11 and illustrated graphically in Figure 4.19.

Temperature (K)	10^{-3} x hydroquinone (M)	k_{obs} (s^{-1})
288	2.00	8.85 ± 0.03
	3.00	12.96 ± 0.06
	4.00	16.82 ± 0.04
	5.00	20.38 ± 0.06
	6.00	24.21 ± 0.08
290	2.00	10.27 ± 0.04
	3.00	14.75 ± 0.06
	4.00	18.7 ± 0.5
	5.00	22.9 ± 0.1
	6.00	27.2 ± 0.2
293	2.00	12.42 ± 0.03
	3.00	18.25 ± 0.05
	4.00	23.55 ± 0.08
	5.00	29.0 ± 0.1
	6.00	33.4 ± 0.1
295	2.00	13.88 ± 0.06
	3.00	20.09 ± 0.08
	4.00	25.52 ± 0.08
	5.00	31.6 ± 0.2
	6.00	37.1 ± 0.3
297	2.00	15.2 ± 0.1
	3.00	22.1 ± 0.3
	4.00	29.7 ± 0.3

Table 4.11. Observed rate constants for the pseudo-first-order oxidation of hydroquinone by [Ni^{III}(cyclam)]@CB[8] at varying concentrations of hydroquinone and at varying temperatures. Ionic strength and acidity constant at 1.00 M ($HClO_4$).

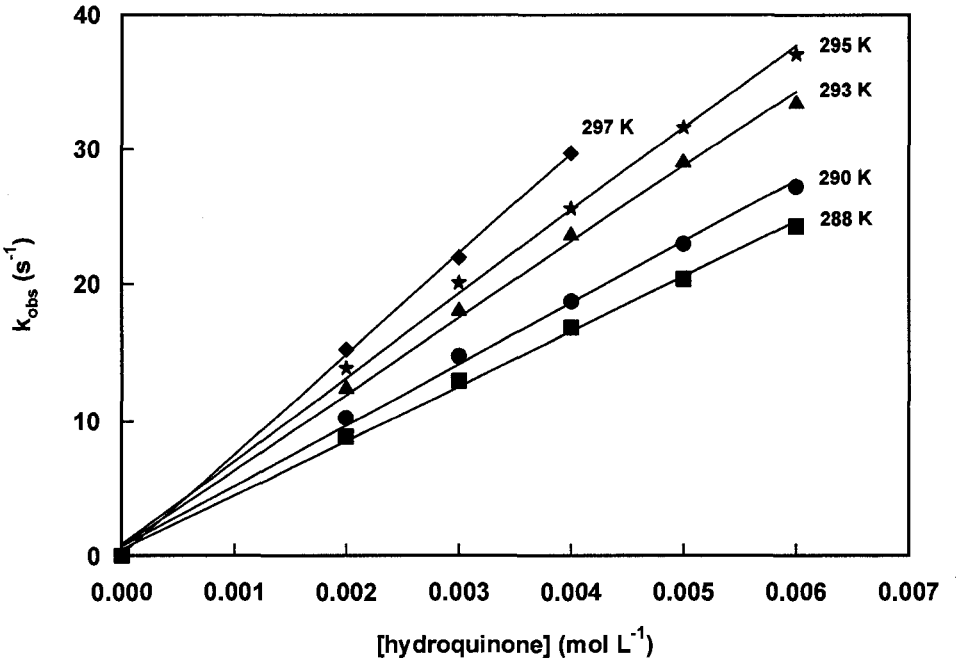

Figure 4.19. Plot of observed rate constants (k_{obs}) *versus* [hydroquinone] for the oxidation of hydroquinone by [Ni^{III}(cyclam)]@CB[8] at five different temperatures. Ionic strength and acidity constant at 1.00 M ($HClO_4$).

From the above plot, it is obvious that the reaction rate is directly proportional to the temperature at which the reaction is performed and to the concentration of the reducing agent, hydroquinone. The linearity of the data (r^2 values ranging from 0.997 to 0.999) shows the oxidation reaction to be first-order with respect to the concentration of hydroquinone. Therefore, it can be deduced that the reaction exhibits simple second order behavior, with first order dependence on each of the reactants.

4.3.2.2. Oxidation of Catechol by [Ni^{III}(cyclam)]@CB[8]

Pseudo-first-order kinetics were also observed in the oxidation of catechol by [Ni^{III}(cyclam)]@CB[8]. In order to ensure pseudo-first-order conditions, catechol was held in a large excess over the oxidant, [Ni^{III}(cyclam)]@CB[8]. The reaction was first analyzed spectrophometrically in order to determine the optimum wavelength at which to monitor the absorbance change with time. As apparent from the spectrum below (Figure 4.20), the absorbance decreases as the reaction proceeds, corresponding to the disappearance of the Ni(III) species. The greatest absorbance change is seen at a wavelength of ~310 nanometers; however, due to the fact that the Xenon lamp in the stopped-flow instrument emits very little light at this low wavelength, a wavelength of 350 was chosen as the ideal wavelength at which to monitor the reaction.

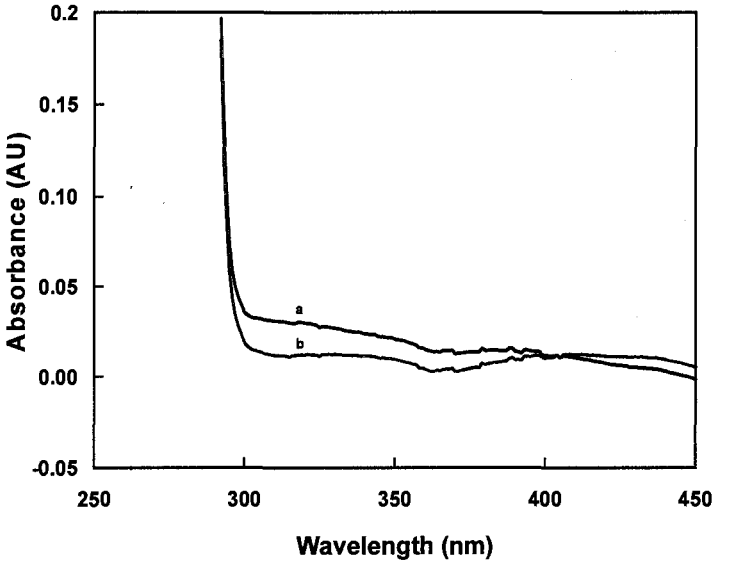

Figure 4.20. Spectral change for oxidation of catechol by [Ni^{III}(cyclam)]@CB[8] (a = spectral curve before mixing; b = spectral curve after mixing)

The oxidation reaction proceeds according to the following scheme:

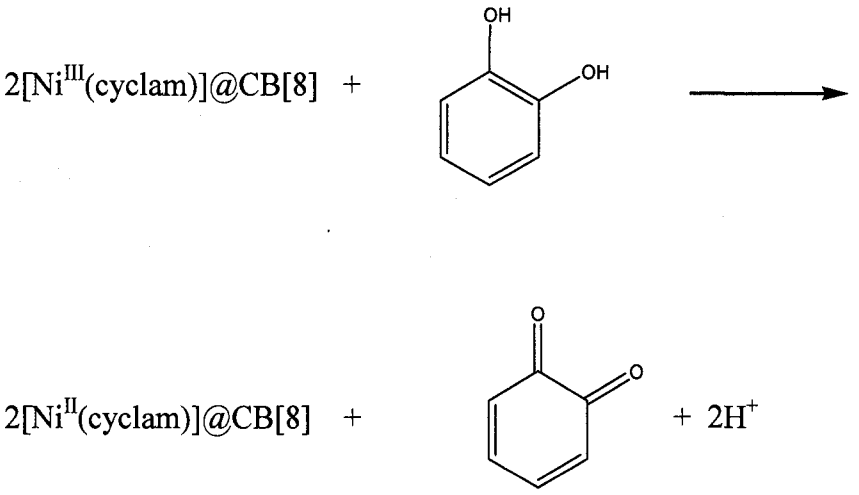

Scheme 4.9. Schematic representing the oxidation of catechol by $[Ni^{III}(cyclam)]@CB[8]$.

When monitored on the stopped flow spectrophotometer, the oxidation of catechol by $[Ni^{III}(cyclam)]@CB[8]$ shows an exponential absorbance change *versus* time. This exponential trace (Figure 4.21) shows the reaction to first order with respect to the oxidant, $[Ni^{III}(cyclam)]@CB[8]$

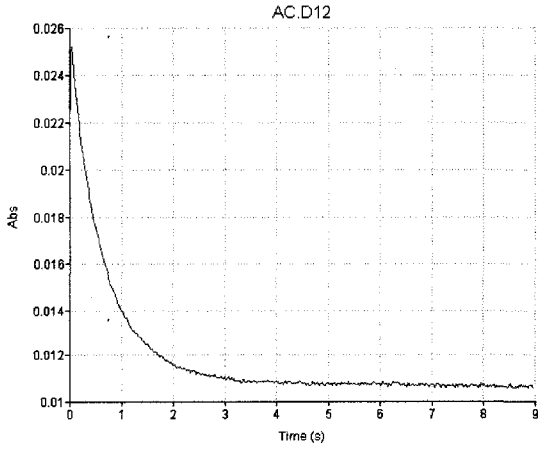

Figure 4.21. Spectrophotometric curve showing first order dependence on Ni(III) species for oxidation of catechol.

To determine the dependency of the reaction on the concentration of the reducing agent, as well as on temperature, the reaction was studied at five difference concentrations of catechol, and at five different temperatures. For these experiments, the ionic strength/acid concentration was kept constant at 1.00 M using standardized perchloric acid. The observed rate constants (k_{obs}) for the above experiments have been tabulated in Table 4.12 and illustrated graphically in Figure 4. 22.

Temperature (K)	10^{-3} x catechol (M)	k_{obs} (s^{-1})
284	2.00	0.595 ± 0.002
	3.00	0.924 ± 0.004
	4.00	1.263 ± 0.006
	5.00	1.648 ± 0.006
	6.00	2.018 ± 0.007
287	2.00	0.685 ± 0.002
	3.00	1.084 ± 0.004
	4.00	1.446 ± 0.005
	5.00	1.876 ± 0.006
	6.00	2.347 ± 0.009
290	2.00	0.833 ± 0.003
	3.00	1.258 ± 0.005
	4.00	1.710 ± 0.006
	5.00	2.188 ± 0.009
	6.00	2.71 ± 0.01
293	2.00	0.966 ± 0.003
	3.00	1.458 ± 0.004
	4.00	1.977 ± 0.006
	5.00	2.498 ± 0.009
	6.00	3.08 ± 0.01
296	2.00	1.162 ± 0.004
	3.00	1.728 ± 0.008
	4.00	2.388 ± 0.008
	5.00	3.03 ± 0.01
	6.00	3.71 ± 0.02

Table 4.12. Observed rate constants for the pseudo-first-order oxidation of catechol by $[Ni^{III}(cyclam)]$@CB[8] at varying concentrations of catechol and varying temperatures. Acidity and ionic strength constant at 1.00 M ($HClO_4$).

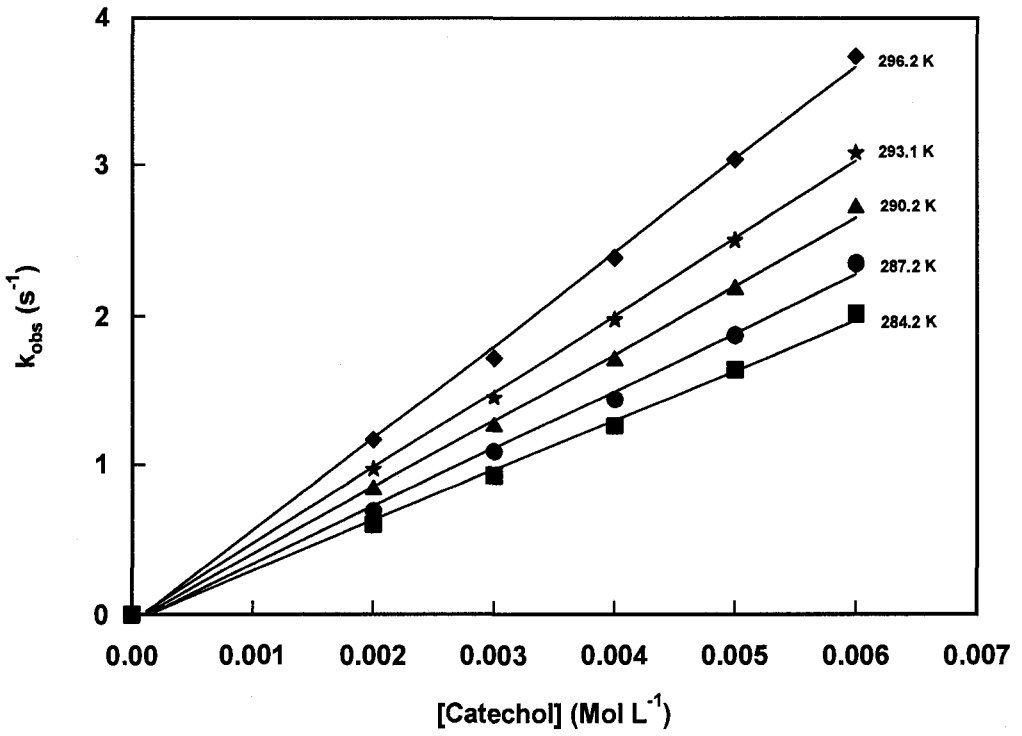

Figure 4.22. Plot of observed rate constant (k_{obs}) *versus* [catechol] for the oxidation of catechol by [Ni^{III}(cyclam)]@CB[8] at five different temperatures. Acidity and ionic strength constant at 1.00 M ($HClO_4$).

It is apparent from the above plot that the rate of reaction is directly proportional to both the concentration of the reducing agent and the temperature at which the reaction is performed. The linearity of the data (r^2 values ranging from 0.996 to 0.999) shows the oxidation reaction to be first-order with respect to the concentration of catechol. Therefore, it can be deduced that the reaction exhibits simple second order behavior overall.

4.3.2.3. Mechanisms and Reaction Rates for Oxidation of Hydroquinone and Catechol by [Ni^{III}(cyclam)]@CB[8]

Previous work[68, 84] has shown the oxidation of hydroquinone and catechol by an outer-sphere oxidant to follow a two step mechanism involving the formation of a radical species according to Scheme 4.10, where H_2Q represents hydroquinone or catechol, $HQ^{\cdot}$ the semi-quinone radical, Q the oxidized quinone, and X the oxidant.

$$X^{III} + H_2Q \xrightarrow{k_1} X^{II} + HQ^{\cdot} + H^+$$

$$X^{III} + HQ^{\cdot} \xrightarrow{fast} X^{II} + Q + H^+$$

Scheme 4.10. Proposed mechanism for oxidation of hydroquinone and catechol *via* an outer-sphere oxidant.

In addition, it is necessary to consider the fact that hydroquinone and catechol are weakly basic, and will be protonated in acidic solution according to the following reaction:

$$H_3Q^+ \overset{K_a}{\rightleftharpoons} H^+ + H_2Q \qquad \textbf{Reaction 4.2}$$

Since the oxidation of the radical species is extremely fast, the rate of reaction is determined by the rate determining k_1 pathway; however, the weakly basic nature of benzenediols warrants the consideration of a second pathway (k_2) involving oxidation of the protonated species, H_3Q^+, as shown in Reaction 4.3.

$$X^{III} + H_3Q^+ \xrightarrow{k_2} X^{II} + HQ^{\cdot} + H^+$$ **Reaction 4.3**

The oxidation of hydroquinone and catechol by [Ni^{III}(cyclam)]@CB[8] can therefore be expected to proceed by the following mechanism, where *L* represents the cyclam ligand.

$$[Ni^{III}L]@CB[8] + H_2Q \xrightarrow{k_1} [Ni^{II}L]@CB[8] + HQ^{\cdot} + H^+$$

$$\Vert \; K_a$$

$$[Ni^{III}L]@CB[8] + H_3Q^+ \xrightarrow{k_2} [Ni^{II}L]@CB[8] + HQ^{\cdot} + H^+$$

Scheme 4.11. Proposed mechanism for the oxidation of hydroquinone and catechol by [Ni^{III}cyclam]@CB[8]

The overall reaction can be expressed as follows:

$$2\{Ni^{III}L@CB[8]\}^{3+} + H_2Q \longrightarrow 2[Ni^{II}L]^{2+} + Q + 2H^+$$ **Reaction 4.4**

The following derived rate law takes both reaction pathways into account, with the coefficient of *2* originating from the stoichiometry of the overall reaction.

$$\text{Rate} = \frac{1}{2}\frac{d[Ni^{II}L@CB(8)]}{dt} = k_{obs}[Ni^{III}L@CB(8)]$$

$$= 2k_1[H_2Q][Ni^{III}L@CB(8)] + 2k_2[H_3Q]^+[Ni^{III}L@CB(8)]$$

$$= (k_1[H_2Q] + k_2[H_3Q])^* 2[Ni^{III}L@CB(8)]$$ **Equation 4.14**

In a similar manner to that reported in section 4.3.1.2 for the derivation of the rate law associated with the oxidation of [Ni^{II}(cyclam)]@CB[8], expressions for [H_2Q] and

$[H_3Q]$ can be attained from the equilibrium expression derived from Reaction 4.8 and from the Law of Mass Balance to yield a rate law involving only the known concentrations of $[H^+]$, $[H_2Q]_{total}$, and $[Ni^{III}L@CB(8)]$.

$$\text{Rate} = 2\frac{k_1K_a + k_2[H^+]}{K_a + [H^+]}[Ni^{III}L@CB(8)]\,[H_2Q]_{total} \qquad \textbf{Equation 4.15}$$

It has been shown from previous studies involving the oxidation of benzenediols that the protonated species (H_3Q^+) does not undergo oxidation to any significant extent.[68,84] As a result, the k_2 pathway is inactive, yielding the following simplified rate law:

$$\text{Rate} = 2\frac{k_1K_a}{[H+] + K_a}[H_2Q]_{total}][Ni^{III}L@CB(8)] \qquad \textbf{Equation 4.16}$$

Since the reaction is monitored under pseudo-first-order conditions with an excess of the reductant (hydroquinone or catechol), the experimental rate law can be written as follows:

$$\text{Rate} = k_{obs}[Ni^{III}L@CB(8)] \quad \text{with}$$

$$k_{obs} = 2\frac{k_1K_a}{[H^+] + K_a}[H_2Q]_{total} \qquad \textbf{Equation 4.10}$$

Further simplification of Equation 4.10 is not possible because the condition $[H^+] \gg K_a$ does not exist. The acid dissociation constants for catechol and hydroquinone have

been previously reported as 3.3 ± 0.9 M and 4.5 ± 1.2 M, (T = 25.0 °C) respectively,[68] and are not significantly greater than the acid concentration (1.00 M) at which this study was performed. Values of k_1 for hydroquinone and catechol at 23.9 °C and 22.9 °C, respectively, can be extracted by using Equation 4.10, the reported acid dissociation constants, and graphs plotting k_{obs} *versus* $[H_2Q]_{total}$. The values of the second order rate constants, k_1, are shown in Table 4.13. It should be noted that the large errors present in these values are a direct result of the uncertainty associated with the literature values of K_a.

Oxidant	**k_1 ($M^{-1}s^{-1}$) Catechol**	**k_1 ($M^{-1}s^{-1}$) Hydroquinone**
$[Ni^{III}(cyclam)]$@CB[8]	$(4.0 \pm 2.1) \times 10^2$	$(4.5 \pm 2.3) \times 10^3$

Table 4.13. Extracted k_1 values for oxidation of catechol and hydroquinone by $[Ni^{III}cyclam]$@CB[8].

Activation parameters for the oxidation of hydroquinone and catechol by $[Ni^{III}(cyclam)]$@CB[8] *via* the k_1 pathway can not be determined directly because the values of K_a are known at one temperature only. However, Eyring plots of the composite values k_3, where $k_3 = 2\,\frac{k_1 K_a}{[H+] + K_a}$ can be drawn (see Figures 4.23 and 4.24). Enthalpy and entropy values are given in Table 4.14.

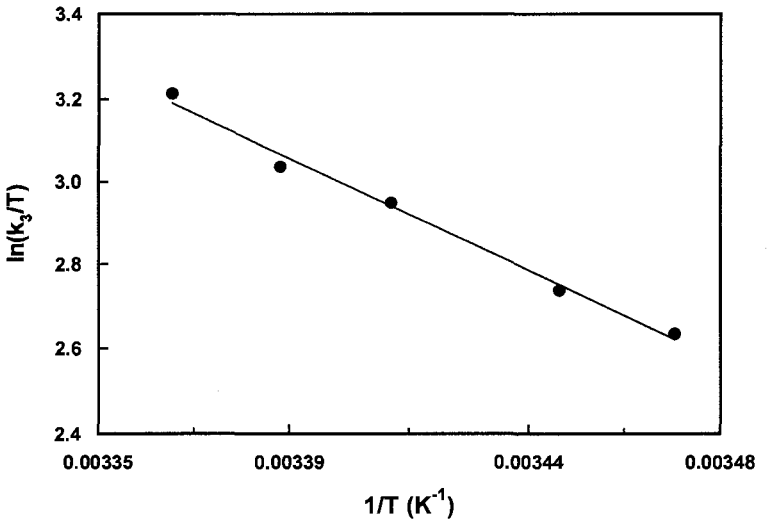

Figure 4.23. Eyring plot for the oxidation of hydroquinone by [Ni^{III}(cyclam)] @CB[8]

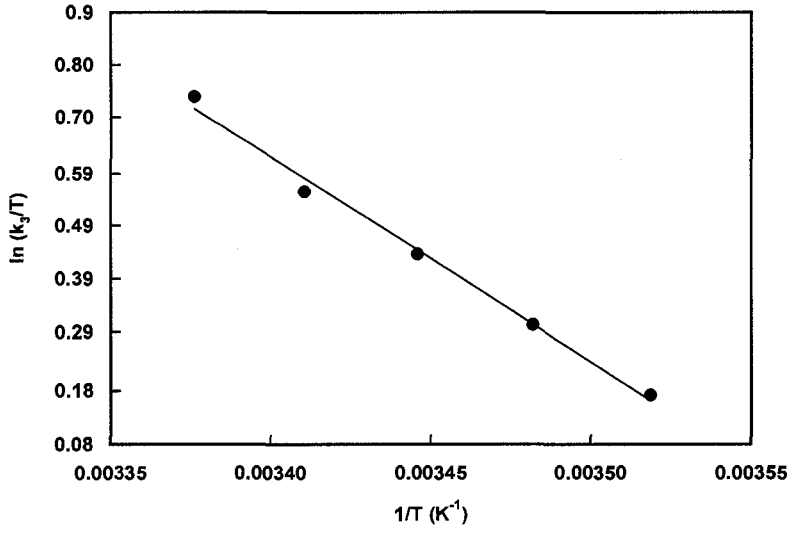

Figure 4.24. Eyring plot for oxidation of catechol by [Ni^{III}(cyclam)]@CB[8]

Reductant	$\Delta H\dagger$ from k_3 (kJ/mol)	$\Delta S\dagger$ from k_3 (J/mol)
Hydroquinone	45 ± 2	-19 ± 1
Catechol	32 ± 2	-83 ± 1

Table 4.14. Activation parameters for oxidation of hydroquinone and catechol by $\{Ni^{III}(cyclam)@CB[8]\}$.

As previously reported for the oxidation of [NiII(cyclam)]@CB[8] by hexaaquacobalt(III), the positive activation enthalpy values are indicative of an increase in energy as the reactants move from their initial states to their transition states. This energy increase is to be expected. What is surprising, however, is the negative values of the activation entropies. Negative activation entropies are indicative of increasing order in the system. This is unexpected for the following reasons:

1) If the oxidized $[Ni^{III}(cyclam)]@CB[8]$ species is coordinated to two axial water molecules (as discussed in Section 4.3.1.2), concomitant loss of these solvent molecules will take place upon reduction. These molecules will be released into an ordered acidic solvent system (H^+ ions surrounded by a network of solvating water molecules). This release of water molecules should decrease, rather than increase, the order of the system. If the oxidized $[Ni^{III}(cyclam)]@CB[8]$ species is coordinated to two nitrogens of the cucurbit[8]uril ring, reduction should cause a relaxation of the ring and the possible inclusion of free solvent molecules into its cavity. This inclusion of solvent molecules should decrease, rather than increase, the order of the system.

2) Upon oxidation, the substrate releases two protons into the solvent. Once again, this solvent system is highly ordered. The release of extra protons will disrupt this organization and should decrease, rather than increase, the order of the system.

4.3.2.4. Effect of Steric Bulk on Reaction Rates and Activation Parameters

As in the study involving the oxidation of [Ni^{II}(cyclam)@CB[8] species by hexaaquacobalt(III), it is of interest to determine if the steric bulk of the cucurbit[8]uril ring slows the rate of electron transfer. As alluded to previously, a direct comparison between the oxidation of the benzenediols with Ni^{II}(cyclam) and the oxidation of the same benzenediols with the sterically encumbered Ni^{II}(cyclam) within the cucurbit[8]uril ring is available. In 1981, the McAuley group[68] reported the oxidation rates of hydroquinone and catechol to be (1.1 ± 0.05) x 10^4 $M^{-1}s^{-1}$ and (7.3 ± 0.4) x 10^2 $M^{-1}s^{-1}$, respectively (at 25 °C). As a comparison, the oxidation rates of the same species using [Ni^{III}(cyclam)]@CB[8] as the oxidant were calculated at (4.5 ± 2.3) x 10^3 $M^{-1}s^{-1}$ (23.9 °C)and (4.0 ± 2.1) x 10^2 $M^{-1}s^{-1}$ (22.9 °C), respectively. This data has been summarized in Table 4.15.

Oxidant	**k_1 ($M^{-1}s^{-1}$) Catechol**	**k_1 ($M^{-1}s^{-1}$) Hydroquinone**
{Ni^{III}(cyclam)@CB8}	(4.0 ± 2.1) x 10^2	(4.5 ± 2.3) x 10^3
Ni^{III}cyclam	(7.3 ± 0.4) x 10^2	(1.1 ± 0.05) x 10^4

Table 4.15. Table comparing reaction rates for oxidation of catechol and hydroquinone by [Ni^{II}(cyclam)]@CB[8] and Ni^{II}(cyclam)

The data show an inhibition of the electron transfer rates of the encapsulated oxidant; the rates are decreased by a factor of 1.8 for the oxidation of catechol and 2.4 for the oxidation of hydroquinone. At first glance, it may seem as if the errors are large enough to obscure the difference between the rates; however, as becomes apparent when one compares the composite values for the rates, this error is not significant. The composite value for the oxidation of catechol by free Ni^{III}(cyclam) was reported as 569 ± 9 $M^{-1}s^{-1}$. This value can be directly compared to the composite value determined in this work for the [Ni^{III}(cyclam)]CB[8] species (308 ± 13 $M^{-1}s^{-1}$), in which the error is significantly smaller due to the fact that the composite rate is derived solely from the slope of the k_{obs} *versus* [H_2Q] plots. It is safe to assume, therefore, that the presence of the cucurbit[8]uril ring decreases the oxidation rates by an approximate factor of 2.

As previously mentioned, the steric encumbrance of the cucurbit[8]uril ring should prevent the close approach of the reductant, forcing the electron transfer to occur over greater distances. The decreased rate constants, therefore, are justified.

However, sterics may not be the only factor affecting the rate constants. As noted previously (See Section 4.3.1.3), there is reason to believe that the cucurbit[8]uril ring may stabilize the Ni(cyclam) species. Whether the reaction rate is decreased or increased by this stabilization depends on whether the Ni^{II}(cyclam) or Ni^{III}(cyclam) species is stabilized. Elucidation of the redox potential of the [$Ni^{II/III}$(cyclam)]@CB[8] species would determine the extent of this stabilization effect on the reaction rates; however, the limited solubility of this compound in aqueous solutions precluded this measurement.

Activation parameters for the oxidation of hydroquinone and catechol by Ni^{III}(cyclam) can not be directly compared to literature values because the literature

values of $\Delta H\dagger$ and $\Delta S\dagger$ were reported for the second order rate constants (k_1), rather than for the composite rate, k_3, as reported in this study.

4.3.3. Attempted Oxidation of $Ni^{II}(cyclam)Cl_2$ by $[Ni^{III}(cyclam)]$@CB[8]

It has been determined that free Ni^{II}(cyclam) and encapsulated Ni^{II}(cyclam) exhibit different extinction coefficients at selected wavelengths.[81] For this reason, it was of interest to see whether the oxidation of free Ni^{II}(cyclam) by the encapsulated [Ni^{III}cyclam]@CB[8] would exhibit a spectrophotometric change that could be monitored *via* stopped-flow techniques. Such a study would provide insight into the steric affect of the cucurbit[8]uril ring by comparison with the previously determined self-exchange rate for the NiL^{2+}/NiL^{3+} system (1×10^3 $M^{-1}s^{-1}$).[85] The following scheme for the oxidation reaction can be envisioned:

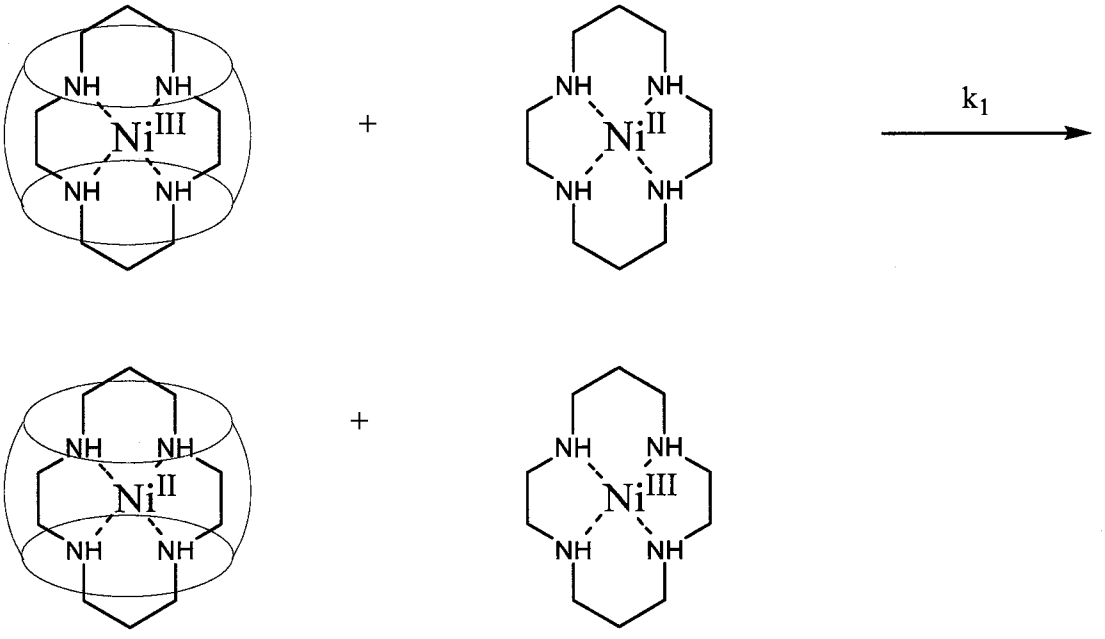

Scheme 4.12. Proposed scheme for oxidation of $Ni^{II}(cyclam)Cl_2$ by $[Ni^{III}(cyclam)]$@CB[8].

The reaction was performed under pseudo-first-order conditions, in a manner identical to that followed for the oxidation of hydroquinone and catechol. The data have been summarized below (See Figures 4.25 – 4.27).

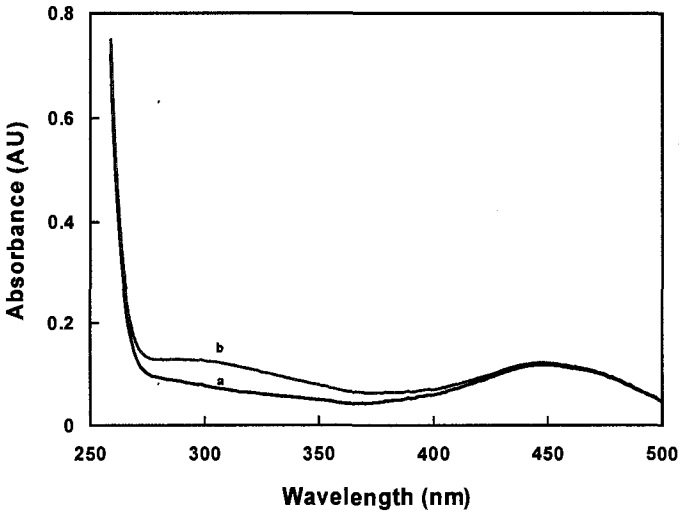

Figure 4.25. Spectral change for the oxidation of Ni^{II}(cyclam) by [Ni^{III}(cyclam)]@CB[8]. (a = spectral curve before mixing; b = spectral curve after mixing)

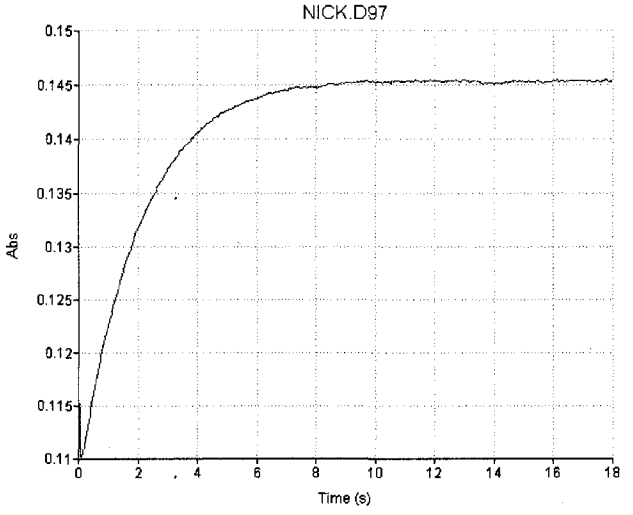

Figure 4.26. Spectrophotometric curve for oxidation of Ni^{II}(cyclam) by [Ni^{III}(cyclam)]@CB[8].

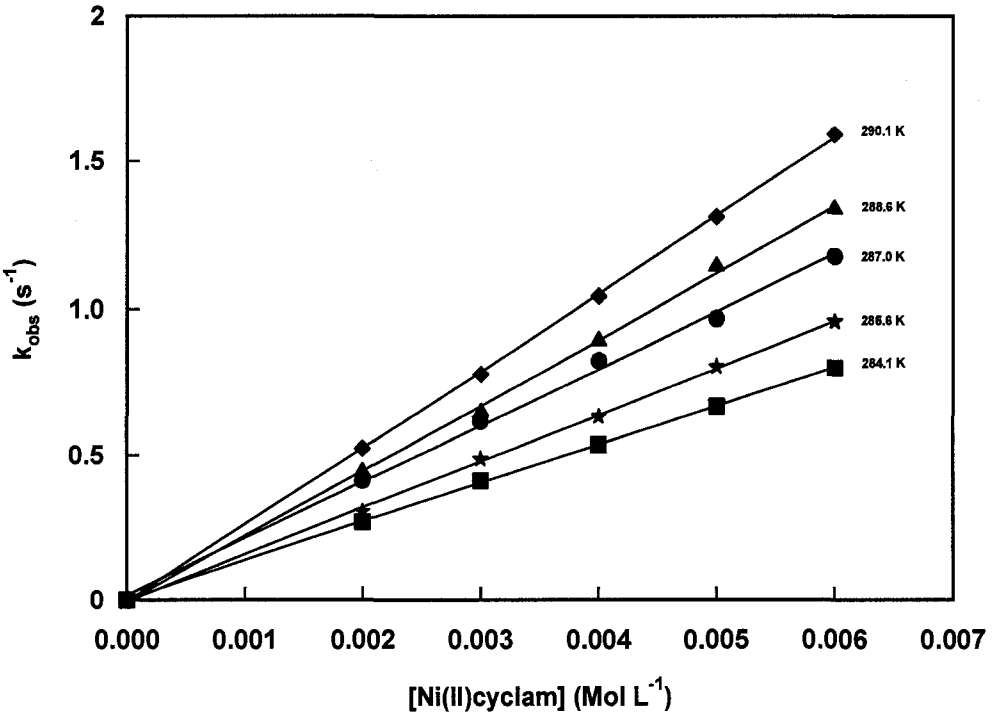

Figure 4.27. Plot of observed rate constant (k_{obs}) *versus* Ni^{II}(cyclam) for the oxidation of Ni^{II}(cyclam) by [Ni^{III}(cyclam)]@CB[8] at five different temperatures. Acidity and ionic strength constant at 1.00 M ($HClO_4$).

The above data appear to be indicative of a second order reaction with first order dependence on the oxidant and the reductant, as described by the rate law:

Rate $= k_1[Ni^{III}(cyclam)@CB(8)][Ni^{II}cyclam]$

The calculated rate constants, however, are approximately 10 times slower than the rate of self-exchange (See Table 4.16). This finding is inconsistent with previous results from this study (showing a rate decrease by a factor of ~2).

Temperature (K)	k_1 ($M^{-1}s^{-1}$)	Self – Exchange Constant ($M^{-1}s^{-1}$)
288	133 ± 1	1.0×10^3
290	161 ± 2	
293	195 ± 5	
295	225 ± 3	
297	264 ± 2	

Table 4.16. Comparison of k_1 values with self-exchange constant for Ni^{II}(cyclam)/Ni^{III}(cyclam)

Due to these inconsistencies, an alternative possibility must be considered. In solution, the free Ni^{II}(cyclam) species could exchange with the Ni^{III}(cyclam) species in the cucurbit[8]uril ring. Since the binding constant for this system is unknown, the likelihood of this exchange reaction can not be determined. Without further experimentation, it is impossible to assess whether the absorbance changes monitored are due to electron transfer reactions or to simple exchange of the included guest.

Chapter 5 – Conclusion

The key objective of this work was to design and synthesize sterically bulky redox active systems which would enforce long range electron transfer reactions. Long-range electron transfer reactions have been the subject of many studies due to the prevalence of these reactions in the biological processes of photosynthesis and respiration. As is often the case in scientific studies of this sort, the pathway of experimentation was riddled by potholes and landmarks; a survey of the problems encountered and the discoveries made is given below.

It was initially thought that bulky pendant arm macrocycles, when complexed to a metal centre, might act as steric hindrances to the close approach of a redox agent. The copper complexes of several pendant arm macrocycles were obtained; however, these complexes were not soluble in aqueous solution, and were therefore not suitable for kinetic studies. An interesting point in this phase of the project was the discovery that the nickel complexes of the same pendant arm macrocycles were formed in solution, but could not be isolated in the solid state, probably due to geometric constraints.

Due to the above mentioned problems, a different route to a sterically bulky redox active system was approached using the macrocyclic cavitand cucurbit[8]uril. In 2000, the Kim group[46] announced the inclusion of metal macrocycles within the cavity of cucurbit[8]uril *via* a two-step mehod, and the motivation for this particular project was the postulation that these inclusion complexes might provide unique systems for studying the effect of the bulky cucurbit[8]uril ring on the rate of electron transfer. It was of initial interest to synthesize new, previously unreported macrocyclic complexes by a more convenient route. This was realized with a "one-pot" synthetic route for the synthesis of

cucurbit[8]uril inclusion complexes – a route that has previously been reported as impossible. The one-step synthetic method opened the door to the inclusion of other macrocyclic complexes within cucurbit[8]uril, and the new methodology was applied to the synthesis of the inclusion compound $[Ni(tacn)_2]$@CB[8].

Of further interest was the crystal structure of the inclusion complex [Cu(cyclam)]@CB[8], which was previously unreported. The crystal structure is unique in that the cucurbit[8]uril moiety "holds" the cyclam ring in the rare trans-I configuration. This is a significant and exciting result; interest in rare configurational isomers of metal macrocyclic complexes is high,[27] and this is the first report of Cu^{II}(cyclam) in the trans-I configuration in the solid state.

It was of interest to use $[Ni(tacn)_2]$@CB[8] as an outer sphere oxidant for various reductants; however, the crystal structure of this complex could not be attained. Therefore, kinetic studies were performed for the structurally characterized [Ni(cyclam)]@CB[8] system. A full kinetic study was performed for the oxidation of [Ni(cyclam)]@CB[8] by hexaaquacobalt(III). The results of this study can be directly compared to a previous study by the McAuley group[53] on the oxidation of free Ni^{II}(cyclam) *via* hexaaquacobalt(III). Comparison of McAuley's data with the data reported in this work suggests that the steric encumbrance of the cucurbit[8]uril ring slows the rate of electron transfer by a factor of 1.9.

The oxidized $[Ni^{III}$(cyclam)]@CB[8] inclusion complex was then used to study the electron transfer reactions of various reductants, namely hydroquinone and catechol. Once again, the electron transfer rates could be directly compared to those determined in a previous study involving the free Ni^{II}(cyclam) species.[68] It would appear that the

cucurbit[8]uril ring slows the electron transfer rate by a factor of 1.8 (in the case of catechol) and 2.4 (in the case of hydroquinone).

It is to be noted that factors other than sterics may have had an impact on the rates of reaction – the most important being changes in the redox potential of the included Ni^{II}(cyclam) species due to the stabilization/destabilization effect of the cucurbit[8]uril ring. Though the redox potential of the inclusion complex would have been of great value, its determination was rendered impossible due to the poor solubility of the inclusion complex in aqueous solution. However, due to the fact that the inclusion complex was used both as the reductant and the oxidant, and the rate decreases were consistent (showing a decrease of a factor of two), it can be safely assumed that any change in the electrochemical potential of the inclusion complex must be very small. The decrease in electron transfer rates can therefore be assumed to be principally associated with the steric bulk of the cucurbit[8]uril ring.

The kinetic results generated in this work are comparable to previous studies involving the inclusion of redox active species within sterically bulky hosts, which report decreasing rate constants for the oxidation of the included species due to 1) steric hindrance and 2) changes in the oxidation potential of the inclusion complex, with the second factor playing a larger role in systems that are significantly stabilized/destabilized by the host species.[15,16,17]

This study, therefore, has successfully probed the effect of steric bulk on the rate of electron transfer reactions. As previously mentioned in the introductory remarks, one must exercise caution when directly comparing the above reported synthetic systems to

biological enzymatic systems; however, as anybody who has tried to put together a complicated puzzle will appreciate – each and every clue is important.

Literature Cited

[1] Aŝperger, S. *Chemical Kinetics and Inorganic Reaction Mechanisms;* Second Edition; Kluwer Academic/Plenum Publishers: New York, NY, 2003; pp 185 – 188.

[2] Conners, K. A. *Chemical Kinetics: The Study of Reaction Rates in Solution;* VCH Publishers, Inc.: New York, NY, 1990.

[3] Denisove, E. T.; Sarkisov, O. M.; Likhtenshtein, G. I. *Chemical Kinetics: Fundamentals and New Developments;* Elsevier: New York, NY, 2003; pp 1 – 15.

[4] Guldberg, C. M.; Waage, P. *Erdmann's Journal für Practische Chemie.* 1879, 127, 69 – 114.

[5] Laidler, K. J.; Meiser, J. H.; Sanctuary, B. C. *Physical Chemistry: Fourth Edition*; New York, US, 2003.

[6] Jordan, R. *Reaction Mechanisms of Inorganic and Organometallic Systems;* Second Edition; Oxford University Press: New York, NY, 1998; pp 291 – 322.

[7] Illey, J. N.; Moreira, R.; Rosa, E. *J. Chem. Soc. Perkin Trans.* **1987**, *2*, 1503 – 1508.

[8] Igwe, J. C.; Abia, A. A. *Int. J. Phys. Sci.* **2007**, 119 – 127.

[9] Henderson, R. A. *The Mechanisms of Reactions at Transition Metal Sites*; Oxford University Press: Oxford, England, 1993; pp 46 – 50.

[10] Davidson, V. L.; Jones, L. H. *Biochemistry.* **1996**, *35*, 8120 – 8125.

[11] Körner, M.; Tregloan, P. A.; Van Eldik, R. *Dalton Trans.* **2003**, 2710 – 2717 (and references within.)

[12] Butler, J.; Davies, D. M.; Sykes, A. G. *J. Am. Chem. Soc.* **1981,** *103*, 469 – 471.

[13] Herz, T.; Gedeck, P.; Clark, T. *J. Am. Chem. Soc.* **1999**, *121*, 1379 – 1380.

[14] Fukuzumi, S.; Yhosida, Y.; Urano, T.; Suenobu, T.; Imahori, H. *J. Am. Chem. Soc.* **2001**, *123*, 11331-11332 .

[15] Macartney, D. H.; Roszak, A. W.; Smith, K. C. *Inorg. Chim. Acta.* **1999**, *291*, 365 – 371.

[16] Wang, R.; Yuan, L.; Macartney, D. *Organometallics*, **2006**, *25*, 1820 – 1823.

[17] Yuan, L.; Macartney, D. H. *J. Phys. Chem. B.* **2007**, *111*, 6949 – 54.

[18] Lindoy, L. F. *The Chemistry of Macrocyclic Ligand Complexes*; Cambridge University Press: Cambridge, Great Britain, 1989.

[19] Curtis, F. W.; Einstein, A. C.; Willis, J. *J. Chem. Soc. A.* **1966**, 1015 – 1018.

[20] Cabbiness, D. K.; Margerum, D. W. *J. Am. Chem. Soc.* **1969**, *91*, 6540 – 6541.

[21] Hinz, F. P.; Margerum, D. W. *J. Am. Chem. Soc.* **1974**, *96*, 4993 – 4994.

[22] Van Alphen, J. *Rec. Trav. Chim.*, **1937**, *56*, 343.

[23] Stetter, H.; Mayer, K. H. *Chem. Ber.* **1961**, *94*, 1410.

[24] Barefield, E. K. *Inorg. Chem.* **1972**, *11*, 2273 – 2274.

[25] Thom, V. J.; Fox, C. C.; Boeyens, J. C. A.; Hancock, R. D. *J. Am. Chem. Soc.***1984**, *106*, 5947 – 5955.

[26] Liang, X.; Sadler, P. J. *Chem. Soc. Rev.* **2004**, *33*, 246 – 266.

[27] Ikeda, R.; Soneta, Y.; Miyamura, K. *Inorg. Chem. Comm.* **2007**, *10*, 590 – 592.

[28] Lye, P. G.; Lawrence, G. A.; Maeder, M. *J. Chem. Soc. Dalton Trans.* **2001**, 2376 – 2382.

[29] Dong, Y.; Lawrence, G. A.; Lindoy, L. F.; Turner, P. *Dalton Trans.* **2003**, 1567 – 1576.

[30] Lagona, J.; Mukhopadhyay, P.; Chakrabarti, S.; Isaacs, L. *Angew. Chem. Int. Ed.* **2005**,

44, 4844 – 4870.

[31] Behrend, R.; Meyer, E.; Rusche, F. *Justus Liebigs Ann. Chem.*, **1905**, *339*, 1-37.

[32] Freeman, W. A.; Mock, W. L.; Shih, N. –S. *J. Am. Chem. Soc.*, **1981**, *103*, 7367 – 7368.

[33] Kim, J.; Jung, I. S.; Kim, S. Y.; Lee, E.; Kang, J. K.; Sakamoto, S.; Yamaguchi, K.; Kim, K. *J. Am. Chem. Soc.* **2000**, *122*, 540 – 541.

[34] Day, A. I.; Blanch, R. J.; Arnold, A. P.; Lorenzo, S.; Lewis, G. R.; Dance, I. *Angew. Chem. Int. Ed.* **2002**, *41*, 275 – 277.

[35] Liu, S.; Zavalij, P. Y.; Isaacs, L. *J. Am. Chem. Soc.* **2005**, *127*, 16798 – 16799.

[36] Day, A.; Arnold, A. P.; Blanch, R. J.; Snushall, B. *J. Org. Chem.* **2001**, *66*, 8094 – 8100.

[37] Kim, K.; Kim, J.; Jung, I. –S.; Kim, S. –Y.; Lee, E. European Patent 1, 094, 065 B1, 2000.

[38] Jeon, Y. –M.; Whang, D.; Kim, K. *J. Am. Chem. Soc.* **1996**, *118*. 9790 – 9791.

[39] Whang, D.; Heo, J.; Park, J. Y.; Kim, K. *Angew. Chem. Int. Ed.* **1998**, *37*, 78 -80.

[40] Sindelar, V.; Cejas, M.; Raymmo, F.; Chen, W.; Parker, S.; Kaifer, A. *Chem. Eur. J.* **2005**, *11*, 7054 – 7059.

[41] Kuz'mina, L. G.; Vedernikov, A. I.; Lobova, N. A.; Howard, J. A. K.; Strelenko, Y. A.; Fedin, V. P.; Alfimov, M. V.; Gromov, S. P. *New J. Chem.* **2006**, *30*, 458 – 466.

[42] Jon, A. Y.; Ko, Y. H.; Park, S. H.;Kim, H. –J.; Kim, K. *Chem. Commun.* **2001**, 1938 – 1939.

[43] Jeon, W. S.; Kim, H. –J.; Lee, C.; Kim, K. *Chem. Commun.* **2002**, 1828 – 1829.

[44] Wheate, N. J.; Buck, D. P.; Day, A. I.; Collins, J. G. *Dalton Trans.*, **2006**, 451 – 458.

[45] Bali, M. S.; Buck, D. P.; Coe, A. J.; Day, A. I.; Collins, J. G. *Dalton Trans.* **2006**, 5337 – 5344.

[46] Kim, S. –Y.; Jung, I. –S.; Lee, E.; Kim. J.; Sakamoto, S.; Yamaguchi, K.; Kim, K. *Angew. Chem. Int. Ed.*, **2001**, *40*, 2119 – 2121.

[47] Mitkina, T. V.; Naumov, D. Y.; Gerasko, O. A.; Dolgushin, F. M.; Vicent, C.; Llusar, R.; Sokolov, M. N.; Fedin, V. P. *Izv. Akad. Nauk, Ser. Khim.* **2004**, 2412 [*Russ. Chem. Bull. Int. Ed*, **2004**, *53*, 2519 - 2524].

[48] Mitkina, T. V.; Naumov, D. Y.; Gerasko, O. A.; Karat'eva, N. V.; Fedin, V. P. *Russ. Chem. Bull. Int. Ed.* **2006**, 55, 26 – 35.

[49] Zhang, N. M. Sc. Thesis, University of Prince Edward Island, Charlottetown, PE, 2003.

[50] Rowley, J. M. Sc. Thesis, University of Prince Edward Island, Charlottetown, PE, 2004.

[51] Wangila, G.; Jordan, R. B. *Inorg. Chim. Acta.* **2003**, *343,* 347 – 350.

[52] Pass, G.; Sutcliffe, H. *Practical Inorganic Chemistry*; Halsted Press, a divison of John Wiley & Sons, Inc.: New York, NY, 1974.

[53] Brodovitch, J. C.; McAuley A. *Inorg. Chem.* **1980**, *20*, 1667 – 1670.

[54] Hi-tech Scientific – Kinetic Solutions for Solution Kinetics, URL http://www.hi-techsci.co.uk/techniques/sf-tech.html (accessed February 16, 2008).

[55] Bosnich, B.; Poon, C. K.; Tobe, M. L. *Inorg. Chem.* **1965**, *4*, 1102 – 1108.

[56] Bakaj, M.; Zimmer, M. *J. Mol. Struct.* **1999**, *508*, 59 – 72.

[57] Pierce, D. T.; Hatfield, T. L.; Billo, E. J.; Ping, Y. *Inorg. Chem.* **1997**, *3*, 2950-2955.

[58] Bosnich, B.; Mason, R.; Pauling, P. J.; Robertson, G. B.; Tobe, M. L. *Chem. Commun.*

1965, *6*. 97 – 98.

[59] Wagner, F.; Barefield, E. K. *Inorg. Chem.*, **1976**, *15*. 408 – 417.

[60] Wagner, F.; Barefield, E. K. *Inorg. Chem.* **1973**, *12*, 2435 – 2439.

[61] D'Aniello, M. J. Jr.; Mocella, M. T.; Wagner, F.; Barefield, E. K.; Paul, I. C. *J. Amer. Chem. Soc.* **1975**, *97*, 192 –194.

[62] Donnelly, M. A.; Zimmer, M. *Inorg. Chem.* **1999**, *38*.1650 – 1658.

[63] Lin, C. –T.; Roorabacher, D. B.; Cayley, G. R.; Margerum, D. W. *Inorg. Chem.* **1975**, *14*, 919 – 925.

[64] Drumhiler, J. A.; Montavon, F.; Lehn, J. M.; Taylor, R. W. *Inorg. Chem.* **1986**, *25*, 3751 – 3757.

[65] Hay, R. W.; Norman, P.R. *Inorg. Chim. Acta.* **1980**, *45*, L139 – L141.

[66] Roper, J. R.; Elias, H. *Inorg. Chem.* **1992**, *31*, 1202 – 1210.

[67] Rankin, M. Honours Chemistry Thesis, University of Prince Edward Island, Charlottetown, PE, 2000.

[68] Brodovitch, J. C.; McAuley, A.; Oswald, T. *Inorg. Chem.* **1962**, *21*, 3442 – 3447.

[69] Anipsitakis, G. P.; Dionysiou, D. D.; Gonzalez, M. A. *Environ. Sci. Technol.* **2006**, *40*, 1000 – 1007.

[70] Jon, S. Y., Selvapalam, N.; Oh, D. H.; Kang, J. -K.; Kim, S.-Y.; Jeon, Y. J.; Lee, J. W.; Kim, K. *J. Am. Chem. Soc.* **2003**, *125*, 10186 – 10187.

[71] Wieghardt, K.; Schmidt, W.; Herrman, W.; Küppers, H. –J. *Inorg. Chem.* **1983**, *22*, 2953 – 2958.

[72] Wangila, G. W.; Jordan, R.B. *Inorg. Chim. Acta.* **2005**, *358*, 3750 – 3760.

[73] Brodovitch, J. C.; McAuley, A. *Inorg. Chem.* **1981**, *20*, 1667 – 1670.

[74] Sisley, M. J.; Jordan, R. B. *Inorg. Chem.* **2006**, *45*, 10758 – 10763, and references within.

[75] Hill, J.; McAuley, A. *J. Chem. Soc. A.* 1968, 1169 – 1173.

[76] McAuely, A.; Gomwalk, U. D. *J. Chem. Soc. A.* **1969**, 977 – 980.

[77] Hill, J.; McAuley, A. *J. Chem. Soc. A.* **1968**, 2405 – 2408.

[78] Malik, M. N.; Hill, J.; McAuley, A. *J. Chem. Soc. A.* **1970**, 643 – 646.

[79] McAuley, A.; Malik, M. N. *J. Chem. Soc. A.* **1970**, 2461 – 2464.

[80] Haines, R. I.; McAuley, A. *Coord. Chem. Rev.* **1981**, *39*, 77 – 119.

[81] Mitkina, T. V., Nikolaev Institute of Inorganic Chemistry, Russian Academy of Sciences, unpublished work.

[82] Zeigerson, E.; Ginzburg, G.; Schwartz, M.; Luz, Z.; Myerstein, D. J. *J. Chem. Soc. Chem. Commun.* 1979, 241 – 243.

[83] Laidler, K. J.; Meiser, J. H.; Sanctuary, B. C. Physical Chemistry; Fourth Edition; Houghton Mifflin Company: New York, NY, 2003, pp 401 – 402.

[84] McAuley, A.; Oswald, T.; Haines, R. I. Can. J. Chem. 1982, 61, 1120 – 1125.

[85] Macartney, D. H.; McAuley, A. *Inorg. Chem.* **1983**, *22*, 2062-2066.

Appendix – X-ray Crystallography

A.1. Crystallographic Methodology for CuL[1]

Crystals of CuL^1 were grown by diethyl ether vapour diffusion into acetonitrile at 18 °C. Single crystals were coated with Paratone-N oil, mounted using a 20 micron cryo-loop and frozen in the cold nitrogen stream of the goniometer. A hemisphere of data was collected on a Bruker AXS P4/SMART 1000 diffractometer using ω and θ scans with a scan width of 0.3 ° and 30 s exposure times. The detector distance was 5 cm. The data were reduced (SAINT)[1] and corrected for absorption (SADABS).[2] The structure was solved by Patterson methods and refined by full-matrix least squares on F^2(SHELXTL)[3]. Two MeCN solvent molecules were disordered over 2 and 3 positions respectively. Refinement including the disordered solvent molecules did not lead to convergence. The solvent was modelled using disordered electron densities (Platon Squeeze)[9]. One of the ClO_4 anions was disordered over two positions and the site occupancies determined as 0.44 (O(5)-O(8)) and 0.56 (O(5')-O(8')). All non-hydrogen atoms were refined using anisotropic displacement parameters. Hydrogen atoms were included in calculated positions and refined using a riding model.

A.2. Crystallographic Methodology for CuL[3]

Crystals of CuL^3 were grown by diethyl ether vapour diffusion into acetonitrile at 18 °C. Single crystals were coated with Paratone-N oil, mounted using a 20 micron cryo-loop and frozen in the cold nitrogen stream of the goniometer. A hemisphere of data was collected on a Bruker AXS P4/SMART 1000 diffractometer using ω and θ scans with a scan width of 0.3 ° and 30 s exposure times. The detector distance was 5 cm. The data were reduced (SAINT)[1] and corrected for absorption (SADABS).[2] The structure was solved by direct methods and refined by full-matrix least squares on F^2(SHELXTL)[3]. Three of the biphenyl groups were disordered and the site occupancies determined using an isotropic model as 0.6 (C(22)–C((27)), 0.4 (C(22A)–C(27A)), 0.52 (C(48)-C(52), 0.48 C(48A)-C(52A)), 0.50 (C(55)-C(66), and 0.50 C(55A)-C(66A)) and fixed in subsequent refinement cycles. Due to the proximity of the disordered atoms, high esds were encountered for the positional parameters. Consequently, all disordered rings were refined by fitting to a pivoting, regular hexagon. All non-hydrogen atoms were refined anisotropically. Hydrogen atoms were included in calculated positions and refined using a riding model.

A.3. Crystallographic Methodology for Cyclam@CB[8]

Crystals of cyclam@CB[8] were grown by solvent evaporation (water) at 18 °C. Single crystals were coated with Paratone-N oil, mounted using a polyimide MicroMount

and frozen in the cold nitrogen stream of the goniometer. A hemisphere of data was collected on a Bruker AXS P4/SMART 1000 diffractometer using ω and θ scans with a scan width of 0.3 ° and 30 s exposure times. The detector distance was 5 cm. The data were reduced (SAINT)[1] and corrected for absorption (SADABS).[2] The structure was solved by direct methods and refined by full-matrix least squares on F^2(SHELXTL)[3]. Three of the cyclam methylene groups and chloride ion were disordered and the site occupancy determined using an isotropic model as 0.5 (C(35), C(36), C(35') and C35"), and 0.67 (Cl), 0.29 (Cl') and 0.04 (Cl") and fixed in subsequent refinement cycles. All non-hydrogen atoms were refined using anisotropic displacement parameters. Hydrogen atoms were included in calculated positions and refined using a riding model. Lattice water molecules were modelled using disordered electron densities.[9]

A.4. Crystallographic Methodology for [Ni(cyclam)]@CB[8]

Crystals of [Ni(cyclam)]@CB[8] were grown by solvent evaporation (water) at 18 °C. Single crystals were coated with Paratone-N oil, mounted using a polyimide MicroMount and frozen in the cold nitrogen stream of the goniometer. A hemisphere of data was collected on a Bruker AXS P4/SMART 1000 diffractometer using ω and θ scans with a scan width of 0.3 ° and 30 s exposure times. The detector distance was 5 cm. The data were reduced (SAINT)[1] and corrected for absorption (SADABS).[2] The structure was solved by direct methods and refined by full-matrix least squares on F^2(SHELXTL)[3]. The chlorides were disordered over two positions and the site occupancies determined using an isotropic model and fixed in subsequent refinement cycles. All non-hydrogen atoms were refined using anisotropic displacement parameters. Hydrogen atoms were included in calculated positions and refined using a riding model. Solvent molecules were modelled using disordered electron densities (SQUEEZE function in Platon)[9].

A.5. Crystallographic Methodology for [Cu(cyclam)]@CB[8]

Crystals of [Cu(cyclam)@CB[8] were grown by [Cu(cyclam)]@CB[8] were grown by solvent evaporation (water) at 18 °C. Single crystals were coated with Paratone-N oil, mounted using a polyimide MicroMount and frozen in the cold nitrogen stream of the goniometer. A hemisphere of data was collected on a Bruker AXS P4/SMART 1000 diffractometer using ω and θ scans with a scan width of 0.3 ° and 30 s exposure times. The detector distance was 5 cm. The data were reduced (SAINT)[1] and corrected for absorption (SADABS).[2] The structure was solved by direct methods and refined by full-matrix least squares on F^2(SHELXTL)[3]. The chlorides were disordered over two positions and the site occupancies determined using an isotropic model and fixed in subsequent refinement cycles. All non-hydrogen atoms were refined using anisotropic displacement parameters. Hydrogen atoms were included in calculated

positions and refined using a riding model. Solvent molecules were modelled using disordered electron densities (SQUEEZE function in Platon)[9].

NOTE: In all cases, thermal ellipsoid plots are at the 50% probability level. JPEGs are drawn at the 50% probability level. In some plots, hydrogen atoms have been omitted for clarity.

A.6 References

(1) SAINT 7.23A, 2006, Bruker AXS, Inc., Madison, Wisconsin, USA.
(2) SADABS 2004, George Sheldrick, 2004, Bruker AXS, Inc., Madison,Wisconsin, USA.
(3) SHELXTL 6.14, George Sheldrick, 2000, Bruker AXS, Inc., Madison,Wisconsin, USA.
(4) GEMINI 1.0, 1999, Bruker AXS, Inc., Madison, Wisconsin, USA.
(5) RLATT 2.72, 1999, Bruker AXS, Inc., Madison, Wisconsin, USA.
(6) SMART 5.054, 1999, Bruker AXS, Inc., Madison, Wisconsin, USA.
(7) CELL_NOW, 2005 George Sheldrick, Bruker AXS, Inc., Madison, Wisconsin, USA.
(8) ROTAX, 2001, S. Parsons and R.O. Gould, 2001, Oxford University, UK.
(9) Platon, Spek, A.L. (2003), J.Appl.Cryst. 36, 7-13